



MAX-PLANCK-INSTITUT
FÜR POLYMERFORSCHUNG

JOHANNES GUTENBERG
UNIVERSITÄT MAINZ



Light Controlled Cell-Cell Adhesions and Self-Sorting in Multicellular Structures

Dissertation

zur Erlangung des Grades

Doktor der Naturwissenschaften

Am Fachbereich Biologie

Der Johannes Gutenberg-Universität Mainz

vorgelegt von

Samaneh Rasoulinejad

Geboren in Tehran, Iran

Mainz, 2020

Date of oral examination: 02.12.2020

Declaration

I hereby declare that I wrote the dissertation submitted without any unauthorized external assistance and used only sources acknowledged in this work. All textual passages which are appropriate verbatim or paraphrased from published and unpublished texts, as well as all information obtained from oral sources, are duly indicated and listed in accordance with bibliographical rules. In carrying out this research, I complied with the rules of standard scientific practice as formulated in the statutes of Johannes Gutenberg-University Mainz to ensure standard scientific practice.

_____03.12.2020_____

Samaneh Rasoulinejad

Abstract

The self-organizing of different cell types into multicellular structures and their organization into spatiotemporally controlled patterns are both challenging and extremely powerful to understand how cells function within tissues and for bottom-up tissue engineering. In this thesis, I demonstrated how two cells types can be independently controlled with blue and red light in order to control their self-assembly and self-sorting into distinct multicellular assemblies. For this purpose, different cell-cell interactions between the same or different cell types were developed such that they were individually triggerable with different colors of light, reversible in the dark and provided non-invasive and temporal control over the cell-cell adhesions. In multicellular mixtures, upon orthogonal photoactivation each cell type self-assembled independently and cells sorted out into separate assemblies based on specific self-recognition. Moreover, this work highlights the importance of the cell-cell interactions dynamics and tuning them by pulsed light activation in the formation of kinetically and thermodynamically controlled multicellular architectures. Only if cell-cell adhesions were strong and dynamic enough compact spheroids and sorting behavior of different cell types as predicted by the differential adhesion hypothesis were observed. The here developed photoswitchable cell-cell interactions and the formed self-sorted multicellular architectures with programmable organization provide us with a powerful tool for producing tissue-like structures from multiple cell types and investigate principles that govern them.

Zusammenfassung

Die Selbstorganisation verschiedener Zelltypen zu multizellulären Strukturen und ihre Organisation in räumlich-zeitlich kontrollierten Mustern sind sowohl eine Herausforderung als auch extrem leistungsfähig, um zu verstehen, wie Zellen innerhalb von Geweben und für das Bottom-up-Tissue Engineering funktionieren. In dieser Arbeit habe ich gezeigt, dass ich nicht nur die Selbstorganisation von zwei Zelltypen zu multizellulären Architekturen mit blauem und rotem Licht unabhängig voneinander kontrollieren kann, sondern auch ihre Selbstsortierung in verschiedene Zusammensetzungen erreichen kann. Die Interaktionen waren individuell mit verschiedenen Lichtfarben auslösbar, im Dunkeln reversibel und bieten eine nicht-invasive und zeitliche Kontrolle über die Zell-Zell-Verwachsungen. Bei multizellulären Mischungen hat sich bei orthogonaler Photoaktivierung jeder Zelltyp unabhängig voneinander selbst assembliert und die Zellen auf der Grundlage einer spezifischen Selbsterkenntnis in separate Baugruppen sortiert. Darüber hinaus führt die Bedeutung dynamischer Interaktionen und die Abstimmung der Dynamik der Zell-Zell-Interaktionen durch Pulslichtaktivierung zu der kompakten Struktur und darüber hinaus zu der mehrzelligen Architektur der Strukturen der differentiellen Adhäsionshypothese. Diese selbstsortierten mehrzelligen Architekturen bieten uns ein leistungsstarkes Werkzeug zur Herstellung gewebeähnlicher Strukturen aus mehreren Zelltypen und zur Untersuchung der Prinzipien, die sie steuern.

Publications

1) Orthogonal Blue and Red Light Controlled Cell-Cell Adhesions enable Sorting-out in Multicellular Structures

Rasoulinejad S., Mueller M., Nzigou, M. B., Wegner, S. V. (2020)

ACS Synth. Biol., 9, 2076–2086 (2020), doi:10.1021/acssynbio.0c00150

2) Blue Light Switchable Cell-Cell Interactions Provide Reversible and Spatiotemporal Control Towards Bottom-Up Tissue Engineering

Yüz S. G.*, Rasoulinejad S.*, Mueller M., Wegner A. E., and Wegner, S. V

Adv. Biosyst., 3, 1800310 (2019), doi: 10.1002/adbi.201800310

3) The importance of cell-cell interaction dynamics in bottom-up tissue engineering: Concepts of colloidal self-assembly in the fabrication of multicellular architectures.

Mueller M., Rasoulinejad S., Garg S., Wegner, S. V.

Nano Lett., 20, 2257–2263 (2020), doi: 10.1021/acs.nanolett.9b04160

4) Green light lithography: a general strategy to create active protein and cell micropatterns.

Xu D., Bartelt, S. M., Rasoulinejad S., Chen F., Wegner, S. .

Mater. Horizons, 6, 1222–1229 (2019), doi: 10.1039/c9mh00170k

5) The dynamic differential adhesion hypothesis: the role of the cell-cell adhesion dynamics in cell sorting

Rasoulinejad S., Wegner, S. V. (2020), Submitted

6) Spatiotemporal control over multicellular migration using green light reversible cell-cell interactions

Nzigou, M. B, Bijonowski, B.t M., Rasoulinejad S., Mueller M., Wegner, S. V. (2020)

Accepted to *Adv. Biosyst.*

Table of contents

Declaration	iv
Abstract	vi
Publications	viii
Table of contents	ix
List of figures	xii
List of tables	xiv
List of abbreviations	xv
Chapter 1: Introduction	1
1.1 Bottom-up tissue engineering	2
1.2 Cell-sorting and self-assembly of cells	3
1.2.1 Sorting through specific cell-cell adhesions and tissue affinity	4
1.2.2 Sorting by differences in cell adhesion strength (Steinberg's Differential Adhesion Hypothesis)	6
1.2.3 Differential Interfacial Tension Hypothesis (DITH)	9
1.2.4 Differential Surface Contraction Hypothesis (DSCH)	10
1.2.5 Sorting based on differences in velocity	11
1.2.6 Leading questions in cell sorting	12
1.3 Cadherins as cell-cell adhesion molecules and their role in cell-sorting	13
1.4 Candidates for controlling cell-cell contact	15
1.4.1 Chemical modifications	15
1.4.2 Light controlled interactions	17
1.4.3 Biological modifications	17
1.5 Photoswitchable proteins	18
1.5.1 Blue light responsive receptors	19
1.5.2 Red light responsive receptors	21
Chapter 2: Materials and Methods	24

2.1	Materials.....	24
2.1.1	General laboratory equipment	24
2.1.2	Microscopes	25
2.1.3	Software	25
2.1.4	Bacteria and cell lines.....	25
2.1.5	Antibodies.....	26
2.1.6	Chemicals.....	26
2.1.7	Biochemicals	27
2.1.8	Primer sequences.....	28
2.1.9	Plasmid.....	29
2.2	Methods.....	29
2.2.1	Cloning	29
2.2.2	Preparation of stable cell lines	30
2.2.3	Flow Cytometry analysis for the detection of surface protein expression	32
2.2.4	Quantification of protein expression on the cell surfaces	32
2.2.5	Immunostaining	33
2.2.6	Quantifying protein expression on the cell surface	34
2.2.7	Light sources	34
2.2.8	Light-responsive cell-cell interactions in 2D	35
2.2.9	Light dependent aggregation in suspension cultures	36
2.2.10	Dynamics and reversibility of blue and red light-triggered cell-cell interactions.....	37
2.2.11	Reversibility in suspension cultures.....	37
2.2.12	Layer by layer tissue formation.....	38
2.2.13	Self-sorting in mixed cell populations	39
2.2.14	Colocalization analysis.....	39
2.2.15	Cell viability.....	40
2.2.16	Light toxicity for spheroids.....	40
2.2.17	Methylcellulose (MC) medium preparation	40
2.2.18	Spheroid culturing and cell staining.....	41
2.2.19	Staining and co-culture of spheroids	42

2.2.20	Statistical analysis.....	42
2.2.21	Image analysis for cell clustering.....	43
2.2.22	Microscopy and image analysis of spheroids	44
Chapter 3: Result and Discussion		45
3.1	Blue light switchable cell-cell interactions provide reversible and spatiotemporal control towards bottom-up tissue engineering	45
3.2	Orthogonal Blue and Red Light Controlled Cell-Cell Adhesions enable Sorting-out in Multicellular Structures	66
3.3	The dynamic differential adhesion hypothesis: The role of cell-cell adhesion dynamics in cell sorting	90
Chapter 4: Summary and Outlook		111
Chapter 5: Appendix.....		116
	Nucleotide and amino acid sequences, ORF	116
	Amino acid sequence.....	116
	DNA sequence 5' to 3'	117
	Amino acid sequence.....	117
	DNA sequence 5' to 3'	118
References		120
Curriculum vitae		137

List of figures

Figure 1: Schematic representation of Holtfreter description for sorting out of the cell. .	5
Figure 2: Differential adhesion hypothesis (DAH).....	8
Figure 3: Schematic representation structure of classical cadherin.....	14
Figure 4: Representation of VVD structure.....	20
Figure 5: Structure and Schematic representation of the Cph1.....	22
Figure 6: Blue-light switchable cell–cell interactions.....	50
Figure 7: Fluorescent images of the stable cell lines.....	51
Figure 8: Bright field images of co-cultured CRY2-MDA and CIBN-MDA cells.	53
Figure 9: Cell number optimization for blue light dependent cell-cell interactions..	54
Figure 10: Quantification of cell–cell interactions.	55
Figure 11: Cell viability under blue light illumination.	56
Figure 12: The Ripley’s K-function.	58
Figure 13: Reversible control of cell–cell interactions.....	60
Figure 14: Dynamics of light dependent cell–cell interactions.	62
Figure 15: Layer by layer 3D architecture.	63
Figure 16: Formation of a 3D architecture layer by layer in the dark.	64
Figure 17: Blue and red light controlled cell-cell adhesions.....	69
Figure 18: Schematic representation of Cph1 and VVD constructs in pDisplay.....	70
Figure 19: Sorting of photoswitchable protein expression on MDA-MB-231 cells.....	71
Figure 20: Protein expression on the cell surfaces.....	72
Figure 21: Blue and red light controlled cell–cell adhesions.	74

Figure 22: Quantification light triggered cell-cell interactions in 2D cell cultures.	75
Figure 23: Spectra of used light sources. A) Blue light, (B) red light and (C) far-red light.	76
Figure 24: Independent control over cell-cell interactions with blue and red light..	77
Figure 25: Light toxicity in cell aggregation experiments.	78
Figure 26: Comparison of photoswitchable protein mediated cell clustering under light	80
Figure 27: Light reversion kinetics.....	81
Figure 28: Reversibility of the photoswitchable cell-cell interactions.....	82
Figure 29: Reversibility of the photoswitchable cell-cell interactions.	83
Figure 30: Blue and red light controlled self-assembly and self-sorting.	85
Figure 31: Colocalization analysis of different cell types during self-sorting.	86
Figure 32: Blue and red light controlled self-assembly and self-sorting.	87
Figure 33: Effect of cell staining on light triggered cell-sorting.....	88
Figure 34: Bright field images of spheroid formation	95
Figure 35: MDA-MB-231 spheroid size under light illumination.	95
Figure 36: Dynamics of cell-cell adhesions.	98
Figure 37: Dynamics of cell-cell adhesions.	99
Figure 38: The toxicity of different light intensity and wavelengths.	102
Figure 39: The measurement of light effect and toxicity of cells	103
Figure 40: Cell sorting of an initially intermixed heterotypic cell suspension.	104
Figure 41: Confocal images of cell sorting	105
Figure 42: Cell sorting of an initially intermixed heterotypic cell suspension.	108
Figure 43: Confocal images of cell sorting of an initially intermixed heterotypic cell ..	109

List of tables

Table 1: Quantification of protein expression on cell surface.	73
---	----

List of abbreviations

As	<i>Avena sativa</i>
azo	azobenzene
BSA	bovine serum albumin
CAM	cell adhesion molecules
Cph1	Cyanobacterial phytochrome 1
CRY2	cryptochrome 2
DAH	differential adhesion hypothesis
DNA	desoxyribonucleic acid
DMEM	Dulbecco's modified eagle medium
DMSO	dimethyl sulfoxide
FAD	flavin adenine dinucleotide
FBS	fetal bovine serum
FMN	flavin mononucleotide
GFP	green fluorescence protein
IMB	Institute of Molecular Biology
LB	Luria-Bertani
LED	Light-emitting diode
LOV	light oxygen voltage sensing
MESF	molecules of equivalent soluble fluorochrome
OD	optical density
ORF	open reading frame
PAS	per-arnt-sim
PBS	phosphat buffered saline
PCB	Phycocyanobilin
PCR	polymerase chain reaction

List of abbreviation

PDGFR	platelet derived growth factor receptor
PGA	polyglycolic acid
PS	penicillin streptomycin
PFA	paraformaldehyde
Pfr	Far-red light absorbing phytochrome
Pr	Red light absorbing phytochrome
ssDNA	single strand desoxyribonucleic acid
synNotch	synthetic notch
TM	transmembrane
UV	ultraviolet
VVD	Vivid

Chapter 1: Introduction

The self-assembly of spatially ordered tissue-like cellular structures from cells as building blocks is a new approach to tissue engineering, names bottom-up tissue engineering.¹ To build multicellular structures, one cannot simply put the cellular units together in a solution and obtain the right arrangement of cells in a tissue; it requires precise interactions between the cells. In addition, the spatial organization of the cells into hierarchical structures is primordial to generate a functional tissue where cells work together.^{2,3} This bottom-up approach to tissue assembly parallels observations seen during embryogenesis and tissue formation, where no template or scaffold is needed and cell-cell interactions are a major driving force that determines cellular organization.⁴ The feasibility of this approach is also supported by the fact that dissociated cells from different tissues are able to self-aggregate and self-sort again into multicellular structures that resemble their tissues of origin.^{5,6}

Moving forward with bottom-up tissue engineering requires understanding how cells as the basic building blocks of tissue self-assemble into multicellular structures. Towards this goal the interactions between cellular building blocks play a central role and their control provide insight into to what extent the principles of self-assembly defined for nonliving micron sized objects apply to cells. Such knowhow would allow programing multicellular architectures with desired organization and determine the limits of multicellular structures that can be generated based on self-assembly and where further biological signals are required.⁷ This puts forward the importance of not just controlling the interactions strength between the cellular building blocks but also their dynamics.

1.1 Bottom-up tissue engineering

The larger field of tissue engineering combines biological sciences and engineering to support, develop, maintain, and produce cell-based substitutes.^{7 8} Bottom-up is one of the two approaches used to achieve tissue engineering and complements the traditionally used top-down approach.

The bottom-up approach is based on the primary production of small building blocks such as cells, cell aggregates, capsules, beads, or cell-laden structures and on following the assembly of these buildings as a unit into more complex structures.⁹⁻¹¹ The advantage of this approach is the precise control over the cell distribution and hierarchical structures, which offers the unique ability to assemble cells into structures that reflect the cellular organization found in native tissues.¹¹⁻¹⁷ The major challenge in this approach is to design building blocks that undergo self-assembly and produce well-defined patterns that mimic the structural properties of tissues.¹⁸ Hereby, the aim is to assemble a multicellular structure from modular building blocks (e.g. cells, cellular aggregates, cell sheets), which can be fused to build up to bigger and more complex structures.¹⁷ In particular for the production of cell rich tissues, controlling cell-cell interactions plays an important role to build these multicellular structures and to produce modular microtissues with desired microarchitectures.¹⁹ Using external templates it is possible to induce cell-cell interactions at the microscale such as culturing cells in sheets, seeding cells in channels, micro-molding cells in hydrogels.¹⁷ Moreover, several cell sheets have been stacked together or fused either on opposite ends to create tubular tissues or side-by-side to create layered tissues.^{20,21}

Yet, the development of scaffold-free ways towards the assembly of multicellular and modular tissues is crucial to obtain structures that mimic the *in vivo* complexity and also for bio-printing.^{22,23} In bio-printing, cells are used as ink to form 3D structures. Although having a high potential to assemble complex tissues with multiple cell types, this method

still has limitations like damaging the cells during the procedure and the lack of mechanical stability.²⁴ The self-assembly of cells is a truly scaffold-free way to tissue engineering that can be described as a spontaneous process to building-up a stable structure through the surface molecules of the cells.^{21,25} Moreover, such surface molecules can be sensitive to environmental parameters like light, pH or temperature and allow triggering the assembly in a controlled manner.^{26,27}

Bottom-up approaches in tissue engineering were developed to overcome some of the limitations in the top-down approach, the most important one being the difficulty to obtain complex tissue like structures at the microscale. Bottom-up and top-down approaches in tissue engineering are not antagonists to one another instead they complement each other's strengths and weaknesses. For example, the scaffold-free bottom-up methods not only allows to build finer structures at the micrometer scale but also reduce the extracellular mechanical stresses originating from the scaffolds.^{2,3,17,21} Moreover, this natural microenvironment allows better cell-cell communication. On the other hand, larger structures are more accessible with the top down methods and provide better mechanical stability. Despite all these, retention of the microarchitecture and cellular behavior are still a challenge as the access to nutrients and the diffusion of oxygen to all the cells in a complex structure is difficult preventing the smooth growth of the overall structure.^{11,17,28-31} The self-assembly of cells in the bottom-up approach is highly dependent on the purity of the cell solution used. Thus, cell sorting is usually employed to ensure that only the cells with the wanted cell surface markers are present in solution.

1.2 Cell-sorting and self-assembly of cells

The self-assembly of cells in a free-scaffold fashion from the bottom-up requires precise control over cell-cell adhesions. Therefore, it is of interest to investigate new adhesive mediators that would allow controlling different cell-cell interactions and produce multicellular structures through self-assembly from multiple cell types.

Previous studies have shown that the mixtures of different cell types sort analogous to the phase separation of two immiscible liquids due to differences in surface tension.³² For instance, it is common knowledge that oil and water do not mix since the lower surface tension of oil leads to its spreading over the surface of the water. When shaken together, oil and water self-organize into separated layers, and the oil being on top of the water. During phase separation, relative surface and interfacial tension determine the organization of the liquids in regards to one another. Hereby, the cohesive (interaction of particles of the same substance) and adhesive (interaction of particles of different substances) forces determine the final structure.³² The factors such as the forces between subunits and the molecular mobility given through Brownian motion define the character of liquids in this scenario.³² The organization or positioning of the cells in mixtures demonstrate similar properties to liquids. However, the subunits here consist of living cells which are mobile due to active or passive forces, driven by intracellular forces or pulled by external forces, respectively.^{33,34}

In mixtures containing two or more cell types, cells in direct contact with each other are able to differentiate each other as similar (homophilic interactions) or dissimilar (heterophilic interactions).³² In addition, the interactions between cells are also not static and dynamically change in time.^{32,35–37} Therefore, the nature of spontaneous self-sorting of cells and the pathway of this separation into groups are of great interest and several hypothesis, which make this self-sorting behavior possible are briefly described in the following sections.

1.2.1 Sorting through specific cell-cell adhesions and tissue affinity

Cell sorting and tissue reorganization depends on the selective affinity and directed migration, according to the hypothesis proposed by Townes and Holtfreter.³⁸ In 1955, Townes and Holtfreter studied different combinations of cells from the germ layers of the

early vertebrate embryo. When the tissues were first chemically dissociated into single cells and later different cell types were re-aggregated, the cells recombined according to their original arrangement and formed structures resembling their natural organization.^{38,39} Moreover, the experiments demonstrated that an overall adhesion order common to all cell types exists in the early embryo, yet over time cells show different preferences to sort out based on their origin and due to cell type-specific adhesion molecules (Figure 1). This leads to the general conclusion that according to their types and the developmental stages, cells can show different levels of attraction or avoidance, and this phenomenon results in mutual attachment or separation between cell populations. Based on this hypothesis, embryos rely on differential cell affinity to sort out germ layers during embryo development.

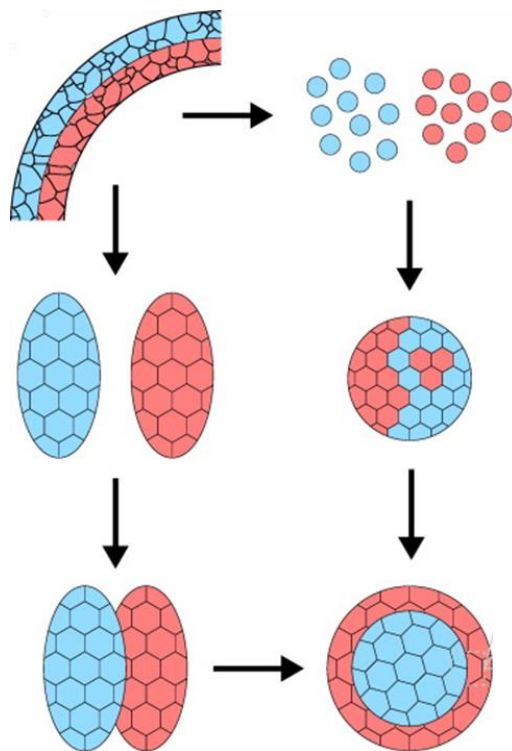


Figure 1: Schematic representation of Holfreter description for sorting out of the cell. Ectoderm (blue) and mesoderm (red) combination, cells re-aggregate and formed the same tissue arrays no matter as dissociated cells (right path) or explants cells (lower path). This figure is adapted from Rudolf *et al.* 2017.³⁸

Townes and Holtfret also suggested that cells show the same kind of 'original' movement *in vitro* as they would do *in vivo*. The natural cell migration, leads to sorting and the stratification into the usual layer structures. Furthermore, with tissue segregations sorting is completed, and with directed movement and selective cell adhesion, it is maintained.³⁹

1.2.2 Sorting by differences in cell adhesion strength (Steinberg's differential adhesion hypothesis)

The simplicity of the differential adhesion hypothesis (DAH) has provided an important theoretical framework for the scaffold free approaches in cell aggregation in the context of bottom-up tissue engineering. The Townes and Holtfret's observations led to the proposal of the DAH by Steinberg as a model to predict cell-sorting.⁴⁰ The DAH proposes that the differences in the adhesion energies between cells, which come from the identity of diverse adhesion molecules on cell surface and their expression levels, cause cells to sort out in order to reduce their interfacial free energy.⁴¹⁻⁴³

The DAH requires three key conditions to be fulfilled for cell sorting to take place in heterologous tissue. three key conditions.³³ First, the system consists of two discrete cell types as units and the interactions between these are considered. Second, the units can move freely within the system, which means they are not spatially fixed. Third, the units can adhere and create a unified whole to reduce the interfacial energy and maximize the strength of adhesive interactions.³³ In this description, cell-cell adhesions are defined as the relative work of adhesion and based on the proportion of work of adhesion between different cell populations, the final cell sorting can be determined (Figure 2A). In a binary mixture of cells consists of A and B cells and form cell-cell adhesions through surface molecules, the adhesion work between A cells is defined as W_a , the adhesion work between B cells is defined as W_b , and the adhesion work between A cells and B cells is

defined as W_{ab} . Depending on the relative value of the adhesion works, three possible arrangements of cells in the mixture have been theoretically predicted and experimentally confirmed.

i) The A cells and B cells will remain intermixed if W_{ab} is bigger than the average of the two work of adhesion, $W_{ab} > (W_a + W_b)/2$ (Figure 2B).

ii) More adhesive A cells will be enveloped by the less adhesive B cells if $(W_a + W_b)/2 > W_{ab} > W_b$ (Figure 2C).

iii) The A cells and B cells will form self-isolated domains if W_a is bigger or equal to W_b and W_b is bigger than W_{ab} , $(W_a \geq W_b > W_{ab})$ (Figure 2D).^{41,43}

The DAH has been supported by numerous experimental studies, some of which will be described in the following sections. To assess the role of cell adhesion molecules in tissue organization, cells designed to express adhesion molecules in different amounts are used. The arrangement of cells in a binary mixture due to the repeated exchange of the weaker adhesive interactions for stronger ones was shown by Duguay *et al.* using transfected L-cell in 3D spheroid cultures (Figure 2B-D).⁴³ In this study, two populations of L-cell (stained in red and green), which expressed the same amount of N-cadherin were mixed in equal proportions and finally formed a homogeneously intermixed spheroid of these two cell types (Figure 2B). When the N-cadherin expression was reduced by half for one cell population compare to other population, the two cell types segregated and the less adhesive cell type enveloped the other (Figure 2C). Aggregates containing equal numbers of L-cells expressing B-cad (green) and R-cad (red) segregated to produce mounds of R-cad-expressing cells partially capping a B-cad-expressing mass (Figure 2D). As demonstrated in these examples, the sorting can be driven by homophilic interactions, i.e. the binding between same type of adhesion molecules as well as heterophilic interactions, i.e. the binding between different types of adhesion molecules.

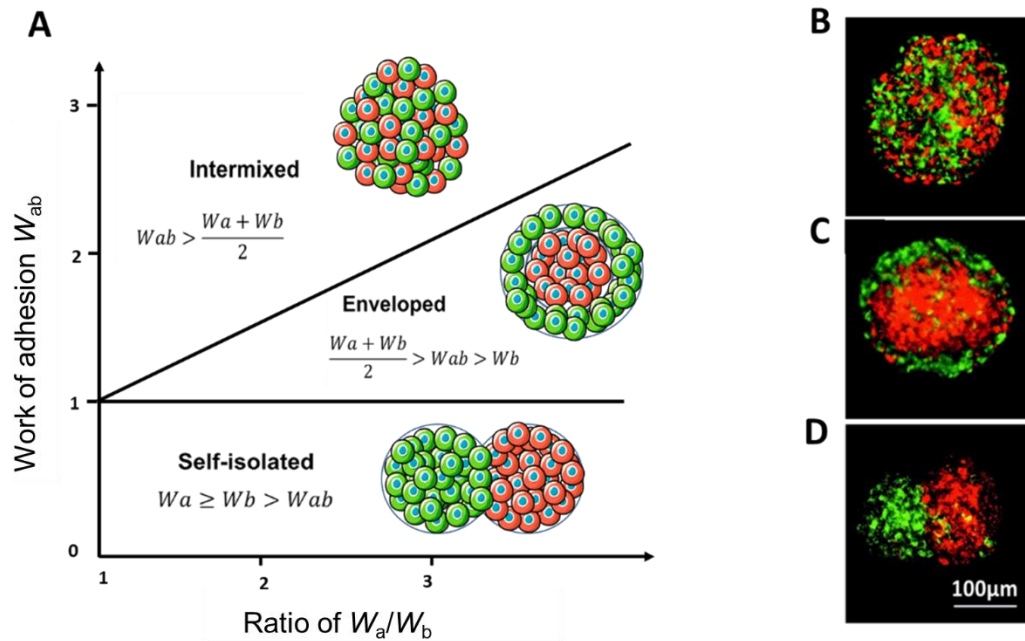


Figure 2: Differential adhesion hypothesis (DAH). A) Different cell assemblies form at equilibrium depending on the work of adhesion between cells of type A (W_a), cells of type B (W_b , defined as 1) and cells of type A and type B (W_{ab}). For instance, in a mixture of cell type A and B, if W_a/W_b is 3, then at $W_{ab}=2.2$ the cell types are intermixed, at $W_{ab}=1.5$ the type A will be enveloped by type B and at $W_{ab}=0.5$ the two cell types will self-isolate. This figure adapted from Steinberg *et al.* 1963⁴¹. B) Spheroids formed from L-cells that express different cadherins. Red and green cells express equal levels of N-cadherin and stay intermixed. C) Red cells express 50% more N-cadherin than green cells and red cells become enveloped by green cells. D) Red cells express R-cadherin, green cells express B-cadherin, which only interact weakly, and the two cell types self-isolate domains. These figures are adapted from Duguay *et al.* 2003.⁴³

The expression level of adhesion molecules is another key factor in cell-sorting. Studies demonstrated that a differences of 25% in the expression level of the same cadherin subtype are enough for two cell populations to sort out from each other.⁴⁴ Moreover, Foty *et al.* showed that the surface tension is directly proportional to the number of adhesion molecules expressed on the cell as demonstrated with cells were transfected with

various amount of specific adhesion molecules.⁴² These experimental results suggest that tissue surface tension are directly governed by adhesion molecules expression level and significantly strengthened the concept of DAH.⁴⁵ This behavior is also homologous to liquid-liquid phase separation, discussed above.³²

Likewise during development, cells expressing different adhesion molecules sort out into discrete tissues, as shown with dissociated cells.⁴⁶ Moreover, Foty *et al.* demonstrated the *in vivo* cell-sorting based on the differential expression of adhesion molecules during oogenesis in *Drosophila* oocytes.⁴⁷

1.2.3 Differential interfacial tension hypothesis (DITH)

The differential interfacial tension hypothesis (DITH), proposed by Brodland states that the contractility of the cortical actomyosin cytoskeleton is a necessary aspect to consider in cell sorting.⁴⁵ This hypothesis points out that cadherin mediated cell-cell adhesions link to the cytoskeleton and cell mechanics contributed to the cell sorting, shape, and migration during development.^{45,48–50} When in suspension, cells tend to adopt a round shape in a way that is similar to a drop of liquid. In liquids, the cohesive forces between molecules are in all directions within the droplet canceling out each other, but point inwards at the surface. These forces give rise to the surface tension and tends to minimize the surface area. Similarly, the tension of the cortical actin layer pulls the cell into a spherical shape.⁵¹ It should be noted that the sustained contraction of the cortical cytoskeleton mainly accounts for the increase of the tension at cell surface.^{51,52}

A number of towards understanding the biophysics of cell sorting during development and how the mechanical forces drive these processes have been reported but there a still a number of open questions in the area. Cadherins as the main cell-cell adhesion molecules link to the actomyosin network through their intracellular domain and consequently, contribute to the interfacial and cortical tension.^{49,53,54} In order to understand the biophysical mechanism of cell sorting, Moore *et al.* knocked out the wild

type N- and E-cadherins in embryoid bodies made from murine stem cells.⁴⁸ When E-cadherin deficient cells were mixed with wild type cells, these cells sorted following the DAH. Conversely, once these cells differentiated they always sorted to the surface and formed an enveloping layer (endoderm) independently of their adhesive strength. Thus, these cells no longer arranged as predicted by the DAH. The reason for this observation was shown to be the apical polarity of these cells after differentiation, which was the determining factor in sorting and positioning.⁴⁸ Moreover, Borghi *et al.* investigated the pulling forces of cells using a cadherin-FRET sensor⁵⁵ and Ng *et al.* studied the forces between cells at individual cell-cell junctions at the multicellular scale.⁵⁶ Both studies found that cadherins function as adhesion-dependent mechanosensors which react to intracellular changes in signaling cascades and extracellular mechanical stress mostly caused by the intracellular binding partner of cadherin, p120 catenin.⁵⁵⁻⁵⁷

1.2.4 Differential surface contraction hypothesis (DSCH)

Harris introduced an alternative explanation for cell-sorting known as the differential surface contraction hypothesis (DSCH).⁵⁸ Harris compared the difference between liquid droplets and cell aggregates, and concluded that the same outcomes as predicted by the DAH can be achieved assuming a differential contraction among cells. While the predicted sorting behavior is the same, the result is not necessarily only a consequence of a differential adhesion between cells but can also be a result of cell deformation. Harris also pointed out that in general, the adhesion plays a critical role in both cases.⁵⁸ The following assumption is the basis of DSC. First, cells present a consistent contraction of the cell cortex when they encounter the external medium. Second, contact between cells causes a 'relaxed' interface and consequently, the contraction is relieved. It should be noted, there is a hierarchy to relaxing the surface contractions between cells and the surface contraction is more reduced when cells are in contact with their same type. Therefore, a given cell type can encounter to a gradient less or more contraction. Thus,

when a cell changes its interface from medium or a cell of a different type to the cell of the same type, it will sort out. Indeed, in Harris' assumption, the endogenous differences in contraction dependent on the cell environment and different cells involved have differential contractile properties.⁵⁸

The first indication that the medium can make cell aggregates round by inducing contraction, comes from a study using explanted neural plates.^{59,60} When cells were put into culture and microfilaments in a bundle were induced to form at the basal side, the whole explant round up. This mechanism was further supported by Lecuit, who considered Echnoid (Ed), a nectin orthologue, which is an adherend junction protein in *Drosophila*, to drive cell sorting in *Drosophila* epithelia.⁶¹ He concludes that Ed plays an important role in cell-sorting, as it induced a contractile actomyosin ring at adhered junctions at cell-cell contacts and leading to apical constriction. This the applied tension along the interface is proposed to be the driving force in the successful cell sorting. In general, he suggested that actomyosin based cortex tension is an important feature of cells that control the arrangement of tissue by modulating their adhesive interactions.^{62,63}

1.2.5 Sorting based on differences in velocity

Jones *et al.* proposed the difference in cell velocities as the source of cell sorting behaviour.⁶⁴ This mechanism is based on two principles. The first one is selective adhesion; cell aggregation occurs based on tissue-specific properties through recognition based on cell-cell adhesions. Second, different cell types arrange and behave based on their relative motilities. Thus, cells with higher mobility will segregate internally. There are no experiments directly supporting the locomotory mechanism of cell sorting. However, it is known that cell adhesions and locomotion are interdependent and closely coordinated features.⁶⁴ In the mechanism, temporary heterotypic interactions support locomotory activity by presenting the needed adhesion for continued cell movement and the exchange of contacts. On the other hand, homotypic contacts

terminate or reduce the movement of cells relative to each other and overall result in cell sorting.⁶⁴

1.2.6 Leading questions in cell sorting

Since the early '70s, the question of whether cell-cell adhesion alone can guide cell sorting behavior *in vitro* and *in vivo* has been under investigation.^{33,34,65,66} All the above summarized hypotheses directly or indirectly involve cell-cell adhesions and are modified versions of the DAH. Therefore, in general, it is certain that the role of adhesion is not negligible but the question is what aspects of adhesions are required. Is cell sorting a direct consequence of cell-cell adhesions or linked to related features such as mechanosensing, cortical tension, contraction or cell signaling?

Couple of years after the DAH formulation, Steinberg stated: "*The specific sorting of cells may result from different mechanisms than from those involved in the initial formation of aggregates*".⁴² Over the years, a number of studies have shown that cell sorting is indeed facilitated by the differential adhesion-governed hierarchy of tissue surface energies⁴² but certainly other cell properties also impact the patterning of a tissue *in vivo*.^{33,67,68}

Until now, studies of cell sorting have used naturally occurring cell adhesion molecules, especially cadherins. The study of only native cell-cell adhesions has limited the possibilities of systematically changing important characteristics of cell-cell adhesions, such as their coupling to intracellular signaling, connection to the actin cytoskeleton etc. In particular, the importance of the cell-cell interaction dynamics in the formation of multicellular structures and cell sorting has not been considered. In fact, native cadherin family based cell-cell adhesions have fast exchange rates and form thermodynamically controlled multicellular structures as predicted by the DAH.⁶⁹ Therefore, the question of what kind of tissue structures can be generated by employing the principles of controlling cell-cell interactions and dynamic interactions to achieve self-organization, remains unanswered.

1.3 Cadherins as cell-cell adhesion molecules and their role in cell-sorting

Cadherins are a class of key adhesive molecules in cell-sorting as well as tissue organization^{46,70} and their expression is regulated during tissue development.^{71,72}

Cadherins are a large family of calcium-dependent cell-cell adhesion molecules with over 350 members.^{73,74} Cadherins are transmembrane molecules and the superfamily of cadherins comprises of different categories named type I and type II cadherins, desmocollins, desmogleins, protocadherins. Type I cadherins interact with molecules of the same kind expressed on neighboring cells. Type I cadherins were named based on the tissues, where they were identified for the first time, e.g. epithelial as E-cadherin and neural as N-cadherin. However, the expression of these cadherins is not always restricted to tissue type they are named after (e.g. N-cadherin is also present on muscle and fibroblasts cells).⁷¹

The structure of type I cadherins consists of an extracellular region, a single pass transmembrane segment, and a cytoplasmic region (Figure 3). The extracellular region includes five extracellular domains linked through calcium ion (Ca^{2+}) binding motifs between them, which are important to maintain their rigid structure.⁷⁵ The cytoplasmic domain interacts with the actin cytoskeleton through adaptor proteins such as β -catenin. Furthermore, the cytoplasmic domain of cadherins connects to intracellular signaling and interacts with proteins partners to activate different pathways.⁷⁶ The connection to the cytoskeleton is necessary for the normal function of cadherins, since the actin cytoskeleton is responsible for force transmission across the cell membrane. Furthermore, the coupling of cadherins to the cytoskeleton is needed for cadherin clustering, maintaining the stable cell contacts as well as cell sorting.^{77,78}

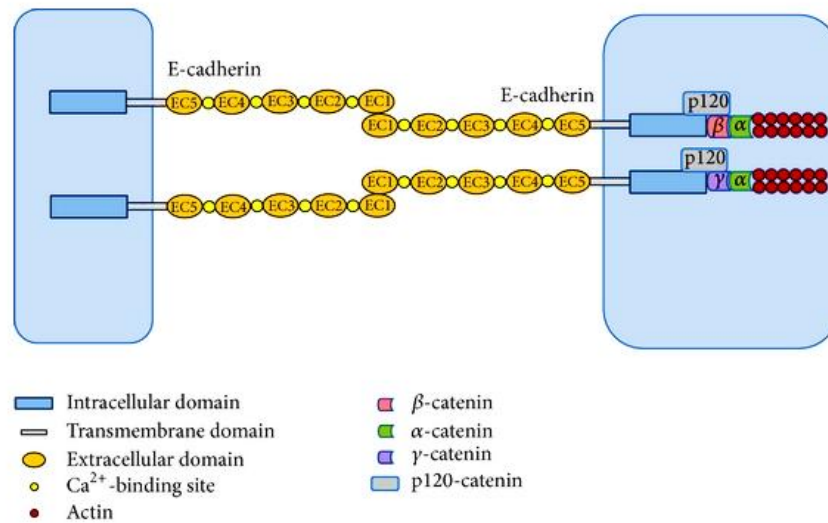


Figure 3: Schematic representation structure of classical cadherin and binding partners. The extracellular region consists of five domains named EC1 to EC5, from outside to the inner side, respectively. Cadherin homophilic interaction occurs at its distal EC1 domain. The figure is adapted from Xin Liu and Kent-Man Chu 2014.⁷⁹

To study the mechanism of cadherin-mediated cell sorting, different assays such as cell aggregation has been used to replicate cell sorting *in vivo*.^{32,80} Notably, Duguay *et al.* quantified the expression of different cadherins such as E-, R-, B-cadherin and their binding specificity to investigate tissue segregation.⁴³ In various combinations of L cells expressing, E-, P-, N-, R-, or B-cadherin, mixed to distinguish whether the final combinations are due to differences in cadherin affinities or expression levels, cells expressing either cadherin at a lower level became the enveloping layer, as predicted by the DAH. However, when cadherin expression levels were equalized, cells were remained intermixed. Therefore, they showed cadherin quantity and affinity can lead to a specific cell adhesion and sorting behavior.⁴³ Edmond *et al.* demonstrate a homophilic specificity of adhesion, mediated by a complex of Protocadherin-19 (Pcdh19) and N-cadherin (Ncad). They showed beads coated with Pcdh19-Ncad did not intermix with Ncad- or Pcdh17-Ncad-coated beads. Therefore they could propose a model in which

association of a protocadherin with Ncad acts as a switch, converting between distinct binding specificities.⁸¹

To determine the contribution of cadherin binding and adhesion specificity to the sorting process, Nissen *et al.* examined the adhesion of cells to different purified cadherin proteins like the aggregation of the purified cadherin extracellular domains of either human E-cadherin or *Xenopus* C-cadherin with Chinese hamster ovary cell lines. They found that cadherins are far more promiscuous in their adhesive-binding capacity than had been expected and that the ability to sort out must be determined by mechanisms other than simple adhesive-binding specificity.⁸⁰

1.4 Candidates for controlling cell-cell contact

Cell-cell contacts are of fundamental importance in many biological processes and key to bottom-up tissue engineering.^{46,70} Besides the natural occurring adhesions, cell-cell interactions can be also be control through the surface modification of cells by biological and chemically approaches. Biological approaches use genetically modified cells that express various adhesive molecules on their surface to control cell-cell interactions. On the other hand, the chemical approaches introduce reactive functional groups on the cell surface in order to control cell-cell reactivity and build the multicellular architectures.⁸²

1.4.1 Chemical modifications

Cell-cell interactions can be controlled through the introduction of reactive functional groups on the cell surface. Such cell-cell interactions can be based on covalent and non-covalent bonds.⁸³

Click chemistry has been one of the main ways to induce cell-cell interactions by functionalizing cell surface with different functional groups using lipid fusion or metabolic labeling with non-natural sugars. For this purpose, the complementary oxyamines and

ketone group as well as alkyne and azide groups are introduced to the cell surface.^{84–86} These types of cell-cell interactions are biorthogonal, form under cell compatible mild conditions and were used to achieve a wide variety of structures. On the down side, through these covalent bonds cells are glue together and the interaction cannot be reversed.

Cell surfaces can also be functionalized with non-covalent binding partners like biotin-avidin or biotin-streptavidin.^{87,88} The biotinylation of cell surfaces was used cross-link cells in the presence of avidin into multicellular aggregates.⁸⁷ Later on, Wang *et al.* induced and controlled cell apoptosis by mixing biotinylated Jurkat cells and streptavidin-functionalized natural killer cells.⁸⁸

The cell-cell interactions between diverse cells can be controlled modifying the cell surfaces with specific DNA hybridization. In this case single-stranded DNA (ssDNA) at the cell surface opens the possibility to form more flexible and diverse structures out of different cell types with specific interactions and cellular connectivity.^{25,89,90} Moreover, the modification of cell surfaces with DNA provides the possibility to target specific cells types with certain surface receptors. These methods add more flexibility to the range of cell-cell interactions with different binding partners but are limited in the controlled reversibility of these interactions.^{25,90} Additionally, all the chemical approaches have the general problems of potential interference with other biological processes, and the difficulty to sustain the modifications over a long period of time. In addition, since the chemical modifications are not embedded in cellular machinery, they will dilute as cells divide and are prone to degradation. Last but not least, they cannot reflect the dynamic nature of cell-cell interactions and provide little spatiotemporal precision. Due to these limitations none of the above mentioned chemical modification methods were able to replicate the cell sorting predicted by the DAH.

1.4.2 Light controlled interactions

An important development in the field of controlling cell-cell adhesions has been the introduction of light responsive groups to the cell surface for photoregulation.^{91,92} The regulation with light comes with precise spatiotemporal control of the cell-cell interactions. Moreover, changing illumination parameters such as light intensity and frequency allow for the dynamic modulation of the interactions. For this purpose, cell surfaces were labeled with β -cyclodextrin using metabolic glycan labeling and bio-orthogonal click chemistry. Subsequently, the host-guest interactions between azobenzenes and β -cyclodextrin were employed as light-responsive cell-cell interaction mediators. More precisely, azobenzenes in the trans- conformation bind to β -cyclodextrin but in the cis- conformation, which forms under UV light illumination, cannot bind to β -cyclodextrin. Therefore, azobenzene-PEG-azobenzene linkers served as a homobifunctional guest molecules to induce cell-cell interactions under visible light and could be reversed under UV light.^{91,92} Overall, this approach allowed the reversible control of cell-cell adhesion with high spatiotemporal control. In another study, Luo *et al.* used a photocleavable linker, which linked neighboring cells through the click reaction between oxyamine and ketone groups. The photocleavage group in the linker could be broke with UV illumination irreversibly and allowed to abolish the formed cell-cell interactions.⁹³ On the down side, the UV light used in both of these examples is toxic to the cells. Moreover, the general problems associated with the chemical modification of the cell surface still exist also in these approaches.

1.4.3 Biological modifications

The expression of native adhesion molecules can be controlled externally or internally and consequently used to control the cell-cell interactions.^{82,94} In an early examples, cells transfected to express E-cadherin and P-cadherin upon induction with tetracycline

sorted out into the predicted 2D and 3D patterns as would be predicted based on the of cell-cell interactions.⁹⁴ More recently, Toda *et al.* designed a synthetic genetic circuit named synNotch to build multicellular structure based on the induced expression of cadherins through neighbouring cells.⁸² Different expression levels of cadherins adjust through the synNotch signalling led to cell-sorting and the subsequent formation of a three-layer envelope shell as well as asymmetric multicellular assemblies.⁸²

After all, a way to control cell-cell interactions with the following advantages is still missing: dynamic, reversible, high spatiotemporal resolution, non-invasive, sustainable, and bio-orthogonal. Therefore, this Ph.D. thesis aims to develop photoswitchable cell-cell interactions that fulfil these criteria and to use them in the assembly of bottom-up multicellular structures following the DAH hypothesis. In this thesis, photoswitchable proteins are employed as adhesion molecules to control the interactions between cells by visible light and the used proteins will be detailed below.

1.5 Photoswitchable proteins

Light is one of the most important environmental signals, which regulates developmental and behavioral responses in the plant, fungal, bacterial, and animal cells. From a more easily visible function like daily activity of a person to the more complicated ones, like the regulation of behavior of photosynthetic organisms up to its usage as the universal energy source, light has a direct or indirect impact on our life.^{95–97} Therefore, all these cells dependent on photoreceptors to detect light. Light absorption by photosensory proteins is the first step for the photo-response by any living cells, which is directly related to the chromophore type. Therefore, photoreceptor scan be categorized into families based on their absorption range and chromophores.

1.5.1 Blue light responsive receptors

Two out of three major types photoreceptors with a flavin chromophore are the light oxygen voltage (LOV) domains and cryptochromes.⁹⁸ The LOV domains are a large class of blue light responsive domain from the phototropin protein family that can be found in bacteria, fungi, algae, or plants (including *Arabidopsis thaliana* and *Avena sativa*).⁹⁹ LOV domains have a conserved core of a Period-Arnt-Single-minded (PAS) fold that is flanked by α -helices. These C- or N- terminal α -helices become untwisted upon under blue light illumination, due to a covalent bond formation between a cysteine at the core of the protein and its chromophore, flavin. This α -helix folds back and associates to the LOV core in its resting dark state, and the cysteinyl-flavin bond hydrolyzes.^{100,101} In the field of optogenetics, different LOV domains have been utilized to control important processes such as gene transcription,^{102,103} cell signaling¹⁰⁴ and protein-protein interaction.¹⁰⁵

Vivid (VVD) from *Neurospora crassa* consists of 186 amino acids and homodimerizes under blue light. The embedded cofactor flavin adenine dinucleotide (FAD) absorbs the blue light, which leads to the reaction between FAD interaction cysteine (Cys108). The formation of the covalent bond between cofactor and the cysteine induces a global the conformational change in the protein and consequently, propagates out to an N-terminal helix, which unwinds and exposes the homodimerization interface (Figure 4).¹⁰¹ Zoltowski *et al.* showed that mutations in the PAS core can alter the interaction strength of VVD proteins and dark reversion times.^{106,107} For instance, VVDHigh is a mutated version of VVD with two mutations in the PAS core that lead to a stronger dimerization and a 10-fold slower dark reversion.¹⁰⁷

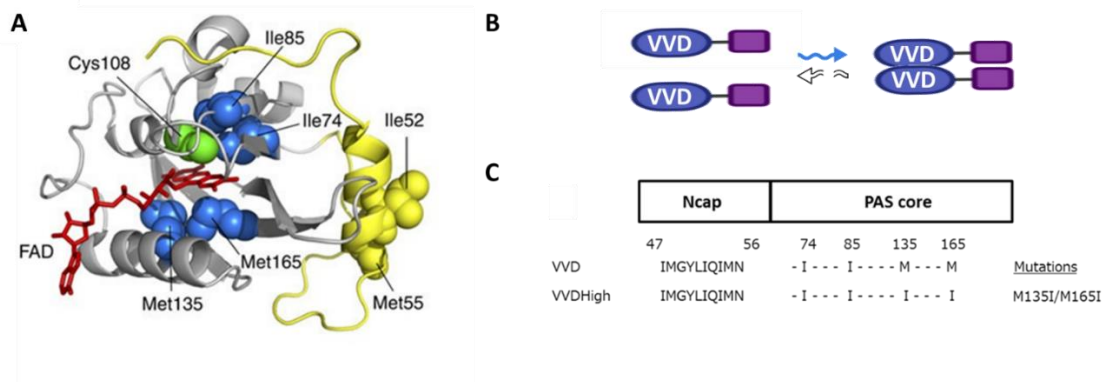


Figure 4: Representation of VVD structure. A) The cartoon structure of VVD with its key amino acid residues. Blue light illumination induces the interaction of the cofactor FAD (red) with Cys108 (green). B) VVD homodimerization interaction. The photocycle-related present in oval purple. The N-terminal α -helix, termed as Ncap (square in purple), is located at the interface of the dimer. C) The amino acid sequence of the Ncap from Isoleucine47 (I) to Asparagine (N) 56 consists of neutral amino acid residues (IMGYLIQIMN). VVDHigh is known as an improved homodimerizing mutated version of VVD. VVDHigh has the same sequence in Ncap. However, in PAS core in two positions instead of Methionine has Isoleucine, M135I, and M165I. Figure is adapted from Kawano *et al.* 2015.¹⁰⁷

The blue light switchable homodimerization of VVD has extensively been used to control the gene expression through the recruitment of transcription activators to promoters or polymerase-based switches in mammalian, bacterial, and fungal cells as well as in mice.^{102,108–110} For example, the split units of T7 RNA polymerase fused to VVD induced the gene expression in *E.coli* with the blue light.¹¹¹ VVD is also used for the spatiotemporal control of Notch activity with blue light pulses to guide the differentiation neural progenitors.¹¹²

Cryptochromes are blue light photoreceptors regulating the growth and development in a plant and the circadian clock in both plants and animals.¹¹³ Cryptochromes were identified first in *Arabidopsis thaliana*. Cryptochromes have two domains; N-terminal photolyase homology region (PHR) and a cryptochromes C-terminal extension (CCE)

domain.¹¹³ The PHR domain is the chromophore binding part that non-covalently interacts with a flavin adenine dinucleotides (FAD).¹¹³ In the dark, FAD is in its oxidized state, and under blue light, the FAD is reduced leading to a conformational change in the cryptochromes.^{101,113}

Cryptochrome 2 (Cry2) and cryptochrome interacting basic helix-loop-helix 1 (CIB1) are a blue light-responsive heterodimerizing protein pair from *Arabidopsis thaliana* that has been co-opted for optogenetic purposes.^{100,101,114} Cry2 is able to bind the CIB1 and itself in response to blue light and these interactions are reversed in the dark. These blue light triggered protein interactions have been used in different biological procedures such as; organelle distribution,¹¹⁵ intracellular signaling events¹¹⁶ and gene expression.¹¹⁷

1.5.2 Red light responsive receptors

The superfamily of phytochrome proteins is sensitive to red and far-red light of the visible spectrum. This family of proteins regulates many developmental processes in plants such as seed germination, seedling de-etiolation, shade avoidance responses, and flowering.⁹⁶ Phytochrome are also found in *cyanobacteria* with different roles in phototaxis,¹¹⁸ nonoxygenic bacteria regulating pigment biosynthesis¹¹⁹ as well in fungi¹²⁰ involved in the repression of sexual development^{121–123} and lately in diatoms.¹²⁴

Cyanobacterial phytochrome 1 (Cph1) is a phytochrome-like protein from *cyanobacteria* *Synechocystis* 6803.¹²² It is a red/far-red light-absorbing protein that can convert between red light-absorbing Pr state under far-red light and far-red light-absorbing Pfr state under red light (Figure 5).¹²³ The chromophore, phycocyanobilin (PCB), covalently attaches to the cGMP phosphodiesterase/adenylyl cyclase/FhlA (GAF) domain through Cys25. It should be noted that the cofactor PCB cannot be naturally produced within mammalian cells and needs to be supplemented to the cells exogenously for optogenetic applications.^{100,101,125}

Chp1 in its Pr form absorbs around 660 nm. At this wavelength about 70% of the Pr form is converted to Pfr form, which homodimerizes with itself.¹²⁶ The absorbance of the Pfr state is maximum at around 705 nm and illumination with this wavelength leads to the back conversion to the Pr state. Therefore, when Chp1 is illuminated with wavelengths in between a photo equilibrium with a mixed population of Pr and Pfr forms.¹²⁶

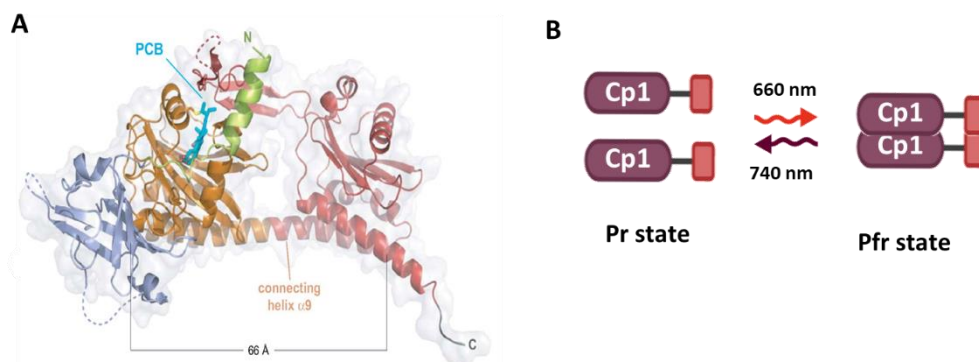


Figure 5: Structure and Schematic representation of the Cph1. A) The cartoon domain structure of Cph1. The PCB Chromophore represents in cyan. This figure is adapted from Winklbaauer et al.2008.¹²⁷ B) Under red light illumination, a mainly monomeric Pr form is converted to a mainly homodimeric Pfr form. This figure is adopted from Reichhart *et al.* 2016.¹²⁸

Cph1 has mostly been used in *E. coli* to control the gene expression and protein interactions.^{129–132} For example, Cph1 has been used to selectively activate bacterial gene expression in biofilms gaining complex chemical images on them with high spatiotemporal resolution. In mammalian cells, Cph1 was used to control signaling pathways and in material science to regulate the self-assembly of colloidal particles.¹²⁸ Reichhart *et al.* used the Cph1 dimerization to trigger mitogen-activated proteins kinase/extracellular signal-related kinase (MAPK/ERK) pathway through receptor tyrosine kinase (RTK) activation.¹²⁸

In order to understand the complexity of cell-cell interactions and their dynamics, I established different photoswitchable cell-cell interactions in the first part of this thesis.

These were used to trigger the self-assembly of multicellular structures under blue and red-light illumination between the same or different cell types. Remarkably, the cell-cell interactions were reversible in the dark and far-red light with different dynamics. Controlling the cell-cell interaction with light comes with the unique advantage of high spatiotemporal resolution and turning on the cell-cell adhesions remotely using low intensity biocompatible light without interfering with other cellular processes.

In the second part of this thesis, I combined different orthogonal cell-cell interactions allowing me to self-assemble mixtures of different cell types into separate self-sorted assemblies.

In the third part of this thesis, the unique features of the photoswitchable cell-cell adhesions enabled me to investigate how the thermodynamics and kinetics of the interactions between the cellular building blocks impact the multicellular assemblies and their sorting out under kinetic and thermodynamic control. Most importantly, regulation with light allowed tuning cell-cell interaction dynamics using pulses of light and regulate multicellular structures formed under kinetic and thermodynamic control.

Chapter 2: Materials and Methods

2.1 Materials

2.1.1 General laboratory equipment

Name	Company
Blue light panel	Abrillo
Electroporator Micro Pulser	Bio-Rad
Centrifuge Avanti J-26x XP	Beckman Coulter
Centrifuge 200	Carl Roth
Centrifuge Micro Star 17	VWR
Cell counting machine	Bio-Rad
Gel electrophoresis	Bio-Rad
Incubator Shaker series Innova 44	New Brunswick
Incubator cell culture C200	Labotect
Milli-Q Synthesis water purification system	Merck
Nano Drop 8-sample Spectrophometer	Peqlab Biotechnology
Pipettboy accu-jet pro	Brand
Plate Reader Tecan Spark	Tecan Group Ltd.
Transmission filter	Alt Intech
Safety Cabinet	Bioair
Scale EMB 1000-2	Kern
Vacunsafe comfort	IBS Integra biosciences
Vortex Genie touch mixer	Scientific Industries
Waterbath	Memmert

2.1.2 Microscopes

Name	Company
CKX41 light microscope	Olympus
DMi8 fluorescence microscope	Leica
SP8 confocal microscope	Leica

2.1.3 Software

Name	Version
ImageJ (Fiji)	V1.51w
Mendeley	1.19.14
Microsoft Office	2016
Origin Pro	2017
MATLAB	2019
SpheroidSizer	2018

2.1.4 Bacteria and cell lines

Name	Version
MDA-MB-231	ATCC
MCF7	ATCC
<i>DH5a</i>	Thermo Fisher Scientific

2.1.5 Antibodies

Name	Company	Ref number
Anti-myc antibody rabbit monoclonal	Thermo Fisher Scientific	700648
Alexa fluor 488 goat anti rabbit	Thermo Fisher Scientific	A27034
Alexa fluor 555 goat anti rabbit	Thermo Fisher Scientific	A27039
Rabbit IgG Isotype Control, FITC, eBioscience™	Thermo Fisher Scientific	11-4614-80

2.1.6 Chemicals

Name	Company	Ref number
Ampicillin sodium salt	Carl Roth	HP62.2
Agar Agar	Carl Roth	5210.2
Bovine Serum Albumin (BSA)	Sigma Aldrich	A2153
Complete Protease Inhibitor cocktail tablets	Hoffmann La Roche	11697498001
Ethylenediaminetetraacetic acid (EDTA)	Sigma Aldrich	E5134
Flavin Adenine Dinucleotide (FAD)	Sigma Aldrich	F8384
Flavin Mononucleotide (FMN)	Sigma Aldrich	F2253
Dimethyl sulfoxide (DMSO)	Sigma Aldrich	D2650
G418 geneticin Solution	Hoffmann La Roche	04727894001
Glycerol	Sigma Aldrich	G5516-500ML
Hepes 1 M	Thermo Fisher Scientific	15630056
Luria-Bertani media	Carl Roth	X968.3
Opti-MEM media	Thermo Fisher Scientific	31985-062
Paraformaldehyd (PFA)	Chem Cruz	SC-281692

PCR purification Kit	Qiagen	28104
Phosphat buffered saline (PBS)	Sigma Aldrich	D8537
Penicillin Streptomycin (PS)	Jena BioScience	ML-105XL
Triton X	Sigma Aldrich	X100
Tryphan blue solution	Sigma Aldrich	T8154

2.1.7 Biochemicals

Name	Company	Ref number
Accutase	Thermo Fisher Scientific	A111051
Cell Tracker green plasma membrane stain	Thermo Fisher Scientific	C2925
Cell Tracker deep red plasma membrane stain	Thermo Fisher Scientific	C34565
Dublecco's modified eagle medium (DMEM)	Thermo Fisher Scientific	10565018
DMEM F12 no phenolred	Thermo Fisher Scientific	21041025
DNA Ladder 1 kb	BioZol	DNA1000
dNTPS mix	Qiagen	201900
Dpn1 restriction enzyme	New England Biolabs	R0176S
Fetal Bovine Serum (FBS)	Sigma Aldrich	F2442
Fluoshield mountain media	Abcam	Ab104139
Gibson Assembly Master Mix	New England Biolabs	E2611S
Hoechst 33342	Invitrogen	H3570
Lipofectamin 3000 Reagent	Thermo Fisher Scientific	L3000001
Phusion HF DNA Polymerase	New England Biolabs	M0530S
Phusion HF Buffer	New England Biolabs	
QIAprep Spin Miniprep Kit	Qiagen	27106

QIAquick PCR Purification Kit	Qiagen	28104
	Bang Laboratories inc	488 A
Quantum Alexa Fluor 488 MESF		
Site directed mutagenesis Kit	Agilent	200523

2.1.8 Primer sequences

Primer name	Primer sequence 5' to 3'
GFP pDisplay Fwd	gacaaagtgt gtaattatga cccgggatcc gcggctgcag
GFP pDisplay Rev	ctgcagccgc ggatcccggg tcataattac acactttgtc
pDisplay GFP Fwd	gggccagcc ggccagatct gtgagcaagg gcgaggagct g
pDisplay GFP Rev	cagctcctcg cccttctca cagatctggc cggtggggcc c
mCherry pDisplay Fwd	gcatggacga gctgtacaag cccgggaatc cgcggtgca g
mCherry pDisplay Rev	ctgcagccgc ggattcccgg gctgtacag ctcgtccatg c
pDisplay mCherry Fwd	ggcccagccg gccagatctg tgagcaagg cgaggagg
pDisplay mCherry Rev	cctcctcgcc cttgctcaca gatctggccg gctggggccc
VVD mCherry Rev	cccttctca cagatctgct accgccttcg gtctc
VVD mCherry Fwd	gcgagaccg aaggcggtag cagatctgtg agcaag
PDisplay VVD Rev	gagcatatag tgtgtgcatg gccggctggg ccccagcata atc
PDisplay VVD Fwd	gattatgctg gggcccagc cggccatgca cacactatag ctc
CpH1 GFP Fwd	acctgattct gctcaagct gagagatctg tgagcaagg
CpH1 GFP Rev	ccttctcac agatctctca gcttgacgca gaatcag
pDisplay CpH1 Rev	cttgaaagta cagattctag gccggctggg ccccagc
pDisplay CpH1 Fwd	gctggggccc agccggccga gaatctgtac ttccaag

2.1.9 Plasmid

Name	Company	Ref number
pDisplay vector	Invitrogen	V66020

2.2 Methods

2.2.1 Cloning

To amplify the DNA and the adding of specific overhanging regions a polymerase chain reaction (PCR) was performed. For the PCR mix 0.5 μ L of the template DNA was mixed with 1 μ L dNTPS (10 mM solution), 1 μ L forward primer (10 pmol), 1 μ L reverse primer (10 pmol), 0.5 μ L of Phusion HF polymerase and the Phusion HF buffer, topped to 25 μ L with miliQ water. The PCR reaction conditions were set to 98 °C for 1 min, 98 °C for 30 sec, 30 sec of the annealing temperature according to primer length and GC content at 62-66 °C, 72 °C for 10 min according to the length of the construct (1 min for 1000 bp). and stored at 4 °C. Steps 2 to 4 were repeated for 35 cycles. After the PCR, the sample was purified to remove primers, nucleotides and enzymes from the DNA with QIAquick PCR purification kit. To 100 μ L of PCR product 500 μ L of Buffer PB was added and the solutions were mixed. The sample was inserted into a QIAquick column tube with a 2 mL collection tube and centrifuged for 60 sec at 13,000 rpm, room temperature. The flow though was discarded and 750 μ L of PE buffer added. The sample was spun down for 60 sec at 13,000 rpm, room temperature. The flow though was discarded again, and the sample centrifuged a second time to remove the residual wash buffer. The QIAquick column was transferred to a new 1.5 mL Eppendorf collection tube and 50 μ L miliQ water was added to elute the PCR product by another round of centrifugation for 1 min at 13,000 rpm, room temperature. The concentration of the PCR product was measured by Nanodrop.

The VVD and the Cph1 gene were synthesized in the pET-21b(+) plasmid between the NdeI - XhoI and NdeI-Sall cutting sites, respectively, by Genscript. The VVDHigh was derived from VVD by point mutations using Agilent kit (Site-Directed Mutagenesis kit, Catalog #200523). In a first step, mCherry and GFP were cloned into the pDisplay mammalian expression vector (Invitrogen V66020) between the Ig κ -chain leader sequence and the platelet derived growth factor receptor (PDGFR) domain using Gibson cloning with the primers listed in Table S1 to yield mCherry-pDisplay and GFP-pDisplay, respectively. In a second step, the photoswitchable proteins VVD- and VVDHigh were cloned into mCherry-pDisplay and Cph1 into GFP-pDisplay between the Ig κ -chain leader sequence and the fluorescent proteins. The pDisplay plasmid (Invitrogen) fuses the photoswitchable protein and the fluorescent protein at the N-terminal to the murine Ig κ -chain leader sequence, which directs the protein to the secretory pathway and at the C-terminal to the platelet-derived growth factor receptor (PDGFR) transmembrane domain, which anchors the proteins on the extracellular part of the plasma membrane. Moreover, the pDisplay plasmid contains a myc-epitope on the extracellular part to detect the expression of surface proteins. The final plasmids were verified by sequencing (StarSEQ).

2.2.2 Preparation of stable cell lines

All cells were cultured in DMEM (Dulbecco's Modified Eagle Medium)/F12 (1:1) (Gibco) supplemented with 10% FBS (fetal bovine serum, Gibco) and 1% penicillin/streptomycin at 37 °C and 5% CO₂. MDA-MB-231 cells were transfected using lipofectamin 3000 (ThermoFisher, L300001) following the manufacturer's protocol for 6 well plate. After 24 hours, the cell culture medium was supplemented with 1800 μ g/ml G418 (geneticin, Roche) and cells were maintained with G418 for all further experiments. After culturing

the cells for two weeks with G418 selection, the transfected cells were sorted at the core facility of the Institute of Molecular Biology (IMB) in Mainz using BD FACS Aria III Cell sorter into 96-well plate with one cell per well. After expanding monoclonal cultures, their fluorescence was measured again by flow cytometry (Attune NXT Acoustic Focusing Cytometer, Invitrogen). The clones with the highest fluorescent signal among all sorted cells were selected for future experiments.

MDA-MB-231 cells were plated in a 6-well plate in total of 5×10^5 cells/well, cultured overnight and placed into fresh Opti-MEM the next day. For each well, 125 μ L Opti-MEM and 3.75-7.5 μ L Lipofectamine 3000 reagent were mixed in one tube and 250 μ L Opti-MEM medium and 5 μ g of plasmid with 10 μ L P3000 reagent in a second tube. The two solutions were mixed together and incubated for 10 to 15 min at room temperature to form the DNA-lipid complex, before adding the solution on to the cells drop-by-drop. The next day, the culture medium was replaced with the regular culture medium containing 1800 μ g/ml G418 for selection of transfected cells. When the cells in the 6-well plate reached confluence, the cells were detached using accutase and transfected cells were selectively and individually sorted into 96-well plate wells containing 200 μ L of DMEM (containing 10% FBS, 1% PS, 2 mM EDTA (Ethylenediaminetetraacetic acid), and 25 mM HEPES (2-[4-(2-hydroxyethyl)piperazin-1-yl]ethanesulfonic acid)) using BD FACS Aria III 352 Cell sorter (Flow Cytometry Core Facility at the Institute of Molecular Biology (IMB), Mainz, Germany). To generate stable monoclonal cell lines, each clone was cultured separately with G418 selection starting from the second day and expanded into 6-well plates. GFP or mCherry protein expression in different clones was quantified based on the fluorescent protein tag using fluorescence microscopy and flow cytometry (Attune NxT acoustic Focusing Cytometer). Stable cell lines for each of the photoswitchable proteins with high protein expression were identified and used in further experiments.

2.2.3 Flow Cytometry analysis for the detection of surface protein expression

Cells were washed with phosphate buffer saline (PBS). Afterwards the cells were detached with accutase (Gibco, Catalog # A1110501) and subsequently washed twice with ice-cold PBS. Subsequently, 1×10^6 cells were resuspended in 100 μ l of 10 μ g/ml of the primary antibody rabbit anti-c-myc (Invitrogen, catalog #700648) in PBS and incubated at 4 °C while gently mixing for 45 min. Then, the cells were washed three times by adding 900 μ l of cold PBS to the cells and thereafter harvested by centrifugation (400 \times g, 4 °C for 5 min). VVD-MDA and VVDHigh-MDA cells were resuspended in 100 μ l of 10 μ g/ml Alexa 488 goat anti-rabbit IgG (Invitrogen, catalog # A27034) and Cph1-MDA cells were resuspended in 100 μ l of 10 μ g/ml of Alexa 594 goat anti-rabbit IgG (Invitrogen, catalog # A-11037) and incubated at 4 °C while gently mixing for 30 min. The cells were washed three times with 900 μ l cold PBS and finally resuspended in 500 μ l cold PBS. The cells were analyzed using flow cytometry (Invitrogen, Attune NxT Flow Cytometer) and each analysis contained at least 10000 gated events. Rabbit-IgG (Invitrogen, catalog # 11-4614-80) was used as a primary antibody isotype control to assess the background signal.

2.2.4 Quantification of protein expression on the cell surfaces

Cells were cultured overnight, 5×10^5 cells per t25-flask with 5 ml of medium. The next day, all cells (VVD-, VVDHigh-, Cph1- MDA and MDA-MB-231) were washed with PBS, detached with accutase and then washed with ice-cold PBS twice. A million of cells from each cell type were incubated with 10 μ g/ml rabbit anti-c-myc (Invitrogen, catalog #700648) in 100 μ l PBS at 4 °C for 45 min while gently mixing. Then, the cells were washed three times with 900 μ l of cold PBS and harvested after each step by centrifugation (400 \times g, 4 °C for 5 min). The cells were resuspended in 100 μ l of 10 μ g/ml Alexa 488 goat anti-rabbit IgG (Invitrogen, catalog # A27034) and incubated at 4 °C for 45 min while gently mixing. The cells were washed three times with 900 μ l cold PBS and finally resuspended in 200 μ l cold PBS. The cells were analyzed using flow cytometry

(Invitrogen, Attune NxT Flow Cytometer). The Quantum Alexa Fluor 488 MESF kit (Bang Laboratories, Inc, 488A) was used for quantification following the manufacture's protocol. The median of fluorescence peak from each cell types were measured and converted into MESF (Molecules of Equivalent Soluble Fluorochrome) based on the calibration curve generated using the QuickCal v.2.4 software from Bang Laboratories. The MESF of same cell type (negative control) that was not incubated with antibodies and MESF for MDA-MB-231 cells incubated with antibodies was subtracted for final calculation of specific MESF of each cells type.

2.2.5 Immunostaining

VVD-MDA, VVDHigh-MDA and Cph1-MDA cells were seeded on μ -Slide 4 Well Glass Bottom (ibidi, catalog #80427) at 2×10^5 cell/well and cultured overnight. The cells were washed three times with PBS and blocked with 1% BSA (bovine serum albumin) in HBSS (Hank's Balanced Salt Solution, Gibco, Catalog #14025050) for 20 min. Afterwards, the cells were stained with the primary antibody rabbit anti-c-myc (Invitrogen, catalog #700648) diluted in HBSS 1:500 and incubated for overnight at 4 °C. Cells were washed three times with cold HBSS, fixed with 2% PFA (paraformaldehyde) in HBSS at room temperature for 10 min and subsequently blocked with 1% BSA for 10 min. The cells were stained with a fluorescently-labelled secondary goat anti-rabbit antibody (Alexa488 labelled for VVD-MDA and VVDHigh-MDA and Alexa594 labelled for Cph1-MDA cells), diluted 1:1000 in HBSS then incubated overnight at 4 °C. The cells were washed four times with HBSS and the nuclei were stained with Hoechst 33342 (Invitrogen, catalog #H3570), diluted to 1:1000, and incubated for 10 min at room temperature. Confocal images were acquired with a 153.6 μ m pinhole in the Hoechst 33342, Alexa488 and Alexa594 channels on a laser scanning confocal microscope (Leica SP8) equipped with 405 nm, 488 nm and 552 nm laser lines and a 20x/0.95 air objective to detect the nuclei, the transfected protein using the c-myc epitope and the protein expression in the fluorescent protein channel (mCherry-tag for VVD and VVDHigh and GFP-tag for Cph1).

2.2.6 Quantifying protein expression on the cell surface

Cells were plated 5×10^5 cells per t25-flask containing 5 mL of media and cultured overnight. The next day, the cells were washed with PBS and detached with 0.5 mL accutase for 5 min at room temperature. Cells were collected in a 1.5 mL Eppendorf tube with 1 mL DMEM media, pelleted at $500 \times g$ for 5 min and resuspended in 500 μ L PBS. The cells were counted, and 2.5×10^5 cells were incubated in 250 μ L PBS containing 2 μ L recombinant monoclonal rabbit anti-Myc primary antibody in the fridge on an orbital shaker at ca. 50 rpm for 45 min. The cells were washed once by adding 1 mL PBS and centrifuge at $500 \times g$ for 5 min at 4 °C. The cell pellets were resuspended in 100 μ L of PBS containing 2 μ L of secondary Alexa fluor 488 goat-anti-rabbit antibody and incubated in the fridge on an orbital shaker at ca. 50 rpm for 60 min. Afterwards the cells were washed once with 1 mL PBS, resuspended in 200 μ L PBS and measured with Axtune Flow Cytometry by using the BL1 laser. For quantification the Quantum Alexa Fluor 488 MESF kit was used following the manufactures protocol. The quantification was done using the QuickCal v. 2.4 software from Bangs Laboratories. For this, the median of the fluorescence peak from each cell type was determined and converted into MESF (Molecules of Equivalent Soluble Fluorochrome) based on the calibration curve. To calculate the specific MESF of each cell type, the MESF for the same cell type (negative control) which was not incubated with antibodies and the MESF for MDA-MB-231 cells incubated with antibodies was subtracted.

2.2.7 Light sources

Two type of light source used in this thesis for the cell clustering experiment the LED grow light panels (Albrillo) were, with one and two neutral-density filter for blue and red light, respectively. The neutral-density filter was used to minimize the scattered light of the light panel. Each neutral-density filter reduced 50% of the light intensity. The light intensities were measured as red (620 nm, 1440 μ W/cm²), far-red light (734 nm, 1120 μ W/cm²), blue light (463 nm, 544 μ W/cm²). For the spheroid experiments, the LED light

module V10 with TS-110 Controller (CLF Plant Climatics GmbH) was used in this experiment (blue light, 463 nm, 20.4 $\mu\text{W}/\text{cm}^2$, red light, 620nm, 23.2 $\mu\text{W}/\text{cm}^2$ and far-red light 734 nm, 25.2 $\mu\text{W}/\text{cm}^2$) as 1% light intensity for all. Consequently, the light intensity of 0.1 and 10% adjusted with controller to find the proper intensity for illumination and afterward for alternative light illumination. The alternative light set up for different on time and off time from 5 to 20 min ranges.

2.2.8 Light-responsive cell-cell interactions in 2D

All cells were washed with PBS and detached with accutase for 10 min at room temperature. Thereafter, for 2D culture experiments cells were seeded at a cell density of approximately 8600 cells/ cm^2 on 24 mm x 24 mm cover glass slides. The LED light module V10 with TS-110 Controller (CLF Plant Climatics GmbH) was used in this experiment and dark samples were wrapped in aluminum foil. VVD- and VVDHigh-MDA cells were cultured in the presence of 0.5 μM FAD (flavin adenine dinucleotide) and cultured either in the dark or under blue light for 4 h at 37 °C and 5% CO₂. Cph1-MDA cells were cultured in the presence of 5 μM of PCB (phycocyanobilin) and cultured either under far-red light or under red light for 4 h at 37 °C and 5% CO₂. Moreover, in clustering experiments MDA-MB-231 and MCF7 cells were used as a negative and positive controls, respectively and were handled as the transfected cells. All cells were fixed with 2 % PFA in PBS for 15 min at room temperature, permeabilized with 0.1% Triton-X-100 in PBS for 5 min and the actin cytoskeleton was stained with Phalloidin-iFlour 488 reagent (Abcam, ab176753) for VVD- and VVDHigh-MDA cells, and Phalloidin-iFlour 594 reagent (Abcam, ab176757) for Cph1-MDA cells according to manufacture protocol. Subsequently, the cells were mounted with mowiol containing 1 $\mu\text{g}/\text{ml}$ DAPI (4',6-Diamidine-2'-phenylindole dihydrochloride) for nuclear staining. Fluorescence images were acquired in the TRITC, FITC and DAPI channels in a tile scan of an area of 1 cm^2 on an inverted fluorescence microscope (Leica DMI8) through a 5x air objective. For the cell clustering analysis 2D cultures the number of cells was quantified based on the DAPI

staining and the number of cells growing in clusters was quantified based on the actin staining using CellProfiler 2.2.046 and MATLAB. In the actin channel, objects with an area $> 300 \mu\text{m}^2$ were classified as cells, objects with an area of $300\text{-}3000 \mu\text{m}^2$ as single cells and objects with an area $> 10000 \mu\text{m}^2$ as clusters of cells¹³³.

2.2.9 Light dependent aggregation in suspension cultures

All cell types were detached using accutase, resuspended at 5×10^4 cell/ml in DMEM/F-12 without phenol red + L-glutamine containing 25 mM of HEPES (4-(2-hydroxyethyl)-1-piperazineethanesulfonic acid), and 1 ml aliquots were added into 1.5 ml LoBind microfuge tubes (Eppendorf). In addition, the medium was supplemented with $0.5 \mu\text{M}$ FAD for VVD- and VVDHigh-MDA cells and $5 \mu\text{M}$ of PCB for Cph1-MDA cells. Afterwards, cells were illuminated with red (620 nm, $1440 \mu\text{W}/\text{cm}^2$), far-red light (734 nm, $1120 \mu\text{W}/\text{cm}^2$), blue light (463 nm, $544 \mu\text{W}/\text{cm}^2$) and in the dark (wrapped in aluminum foil) for 30 min on the 3D orbital shaker at 30 rpm at room temperature. LED grow light panels (Albrillo) were used in this experiment, with one and two neutral-density filter for blue and red light, respectively. The neutral-density filter used to minimize the scattered light of light panel. Each neutral-density filter reducing 50% of the light intensity.

The whole 1ml suspension of cells was fixed with 500 μl of 4% PFA in PBS after the incubation under light or in the dark and transferred to a 12-well plate. Bright field images were acquired for a total area of 2.5 cm^2 (8×8 tile scan images, imaged area 2.5 cm^2) using an inverted fluorescence microscope (Leica DMI8) with a 5x air objective. Images were analyzed with Fiji 1.52d. The bright field of 8×8 tile scan images were individually background corrected for uneven illumination and for dirt/dust on the lenses by using a pseudo flat field correction with a blurring stack of five and merged into a single image. The area of individual cell clusters was determined using a particle analysis tool and clusters were defined as objects $>5000 \mu\text{m}^2$, which corresponds to a projection area of at least 20 cells (area for a single cell is equal to $200\text{-}250 \mu\text{m}^2$). For automated image analysis a macro script was written, which can be found in the supplementary material.

The area of individual cell clusters and the mean cluster area were calculated using OriginPro2019. Each experiment was performed in biological triplicates with two technical replicates ($n=3 \times 2$). The data is presented as the mean cluster area \pm SE for clusters detected in all experiments. The Mann-Whitney test was performed to analyze the statistical difference. $p > 0.1$ ns, $p < 0.01$ presented as** and $p < 0.001$ presented as***.

2.2.10 Dynamics and reversibility of blue and red light-triggered cell-cell interactions

The assembly and disassembly kinetics as well as the repeated on/off switching of cell-cell interactions were evaluated in suspension cultures as described above with variations in the illumination protocols. For the assembly kinetics, the cells were placed under illumination (blue light for VVD-MDA and VVDHigh-MDA, red light for Cph1-MDA) for up to 4 h before fixing the cells. To access the reversion kinetics, cells were first activated for 30 min under illumination and subsequently placed in the dark for VVD-MDA and VVDHigh-MDA, and far-red light for Cph1-MDA cells. For the repeated on/off switching VVD-MDA and VVDHigh-MDA cells were alternated between 30 min blue light and 30 min in the dark, and Cph1-MDA cells were alternated between 30 min red light and 30 min far-red light. After each point in time two samples were fixed with PFA and analyzed as described above.

2.2.11 Reversibility in suspension cultures

The stable cell lines CRY2-MDA and CIBN-MDA are mixed in 1:1 ratio (5×10^5 cells of each) in 1 ml of medium containing with 0.5 μ M FAD and 25 mM of HEPES (4-(2-hydroxyethyl)-1-piperazineethanesulfonic acid) in a 1.5 ml tubes. Cells are alternatingly illuminated with blue light (460 nm, AC85-264V/50-60 Hz) for 30 min and in the dark over 3 cycles on the 3D rocker at 20 rpm at room temperature. At each time point two samples are fixed by adding 500 μ l of 4% PFA. The total volume of each samples (1.5 ml) are

transferred to 12 well plate. Bright field images are acquired for an area of 1.44 cm² with an upright fluorescence microscope (Leica DMI8) with a 5x air objective and using tile scan. The bright field images are analyzed with ImageJ (Fiji 1.52d). The bright field tile scans (6x6 images) are background corrected for uneven illumination and dirt/dust on lenses by using a pseudo flat correction. The number of aggregates and their area was determined using the analyze particles tool. Aggregates are defined as objects > 5000 μm², which corresponds to a projection area of at least 15 cells (area for single cells = ca. 300 μm²). All reversibility experiments are done in biological triplicates with technical duplicates in each experiment (n=6). The number of aggregates and the area covered by aggregates are presented with a mean±SEM calculated using OriginPro9.1.

2.2.12 Layer by layer tissue formation

CRY2-MDA are collected in a tube and stained with CellMask Orange (Thermofischer) for their plasma membrane at 37 °C in water bath for 30 min following the manufacturer's protocol. Cells are washed twice with growth medium and seeded at a density of 10⁵ cells/cm² on μ-Slide 8 well (Ibidi) chamber and grown overnight to form a confluent layer. Similarly, CIBN-MDA cells are stained with CellMask Green (Thermofischer) for their plasma membrane and seeded at a density of 10⁶ cells/cm² on top of MDA-CRY2 cells. Cells are incubated under blue light illumination (471 nm, 80 μW/cm² - LED light module V10 with TS-110 Controller, CLF Plant Climatics GmbH) or in the dark in the presence of 0.5 μM FAD at 37 °C at 5% CO₂ for 4h. Cells are fixed with 2% PFA. Stacks of fluorescence images are acquired in the TRITC (for CellMask Orange) and FITC (for CellMask Green) channels on a Leica SP5 laser scanning confocal microscope 4 equipped with Ar laser (488 nm, 16%), HeNe laser (561 nm, 16%) and with 25x/0.95 air objective. The z-stack size and number of stacks were 0.04 μm and 1103 respectively.

2.2.13 Self-sorting in mixed cell populations

VVD-MDA and Cph1-MDA in suspension were stained with CellMask Deep Red Plasma Membrane (Invitrogen, C10046) and CellTracker Green CMFDA Dye (Invitrogen, C2925), respectively, using a 1:1000 dilution of each dye and incubating them at 37 °C for 30 min, while mixing the cells every 10 min. The cells were covered with aluminum foil to protect them from light. The cells were then centrifuged at 400×g for 5 min, the medium was discarded and cell pellets were resuspended in DMEM/F12 medium supplemented with 25 mM HEPES, 0.5 μM FAD and 5 μM PCB. The stained VVD-MDA and Cph1-MDA were mixed in a 1:1 ratio in total 1×10^5 cell/ml density in a total volume of 1 ml in 1.5 ml Lobind tubes and the cell mixtures were illuminated with blue light, red light, blue and red light, or kept in the dark for 30 min on the 3D orbital shaker at 15 rpm at room temperature. The cells were fixed with 500 μl of 4% PFA and fluorescent images were acquired on a confocal microscope. The same experiment was repeated with unstained cells, and after fixation bright field images were acquired for aggregation analysis. To exclude the effect of staining on the cell clustering, the cell clustering experiments were performed with stained and unstained VVD-MDA and Cph1-MDA cells under blue and red light, respectively.

2.2.14 Colocalization analysis

The confocal images of the self-sorting were analyzed by using *imagJ* and the plugin *EzColocalization*¹³⁴. The images in the red and green fluorescent channels were loaded into the *EzColocalization* and the colocalization of the two fluorescent signals was analyzed using the TOS (Threshold Overlap Score, linearly rescaled) and PCC (Pearson's Correlation Coefficient) with 10% FT (Top Percentage of Pixels Threshold). Both for TOS and PCC values of -1 represent complete anticlocalization, values of 0 represent no colocalization and values of 1 represent complete colocalization^{134,135}.

2.2.15 Cell viability

VVD-MDA and Cph1-MDA cells were prepared as for light-dependent aggregation studies at 5×10^4 cells in total volume of 1 ml media in 1.5 ml Lobind tubes and incubated under illumination or in the dark for 30 min. Subsequently, 100 μ l of medium containing cells was transferred to a 96-well plate. The viability of the cells was measured using the CellTiter-Glo2.0 Assay (Promega) according to manufacturer's instructions.

2.2.16 Light toxicity for spheroids

For all experiments, cell viability is crucial. Therefore, from the beginning the intensity of lights and then after the selected intensity the light toxicity measured for continues 3 days. Each measurement performed using CellTiter-Glo® 3D Cell Viability Assay (G9682, Promega). A defined number of transfected cells were used same as mentioned above and based on the manufacture company. The defined amount of cells transferred to the opaque-walled 96-well plate (655083, Greiner Bio-One) after with different light intensity and in different day's illumination. To equilibrate the plates and its contents, incubate the plate for 30 min at room temperature. Afterward, the equal amount of CellTiter-Glo® 3D Reagen to the volume of the cells and their medium added and mix it vigorously for 5 min on order to induce cell lysis properly then incubate at room temperature for 25 min and the end the luminescence is read.

2.2.17 Methylcellulose (MC) medium preparation

Preparation of methylcellulose divided to three phase; i) dissolve 1.5 g of methylcellulose (M7027-Sigma-Aldrich) in 100ml of the DMEM medium without phenol red DMEM (Dulbecco's Modified Eagle Medium)/F12 (1:1) (Gibco) at room temperature (RT) for 30min with stirrer. ii) afterward, the mixture got semi dissolved 125ml of DMEM added and mixed on stirrer for 90 min at RT. iii) the agitation kept continued for an overnight at 4 °C. The suspension (the appearance should be clear) supplemented with 2% FBS and

1% penicillin/streptomycin and pass through a 0.22 µm filter to sterilize as well remove undissolved solids.

2.2.18 Spheroid culturing and cell staining

Frozen cell vials removed from the liquid N₂ storage and thawed in a 37 °C water bath, the cell vial has to kept above the water surface to avoid the chance of contamination, when cells almost thawed (only a small piece of ice) transferred to the T25 flask with DMEM F-12 supplemented with 10% FBS and 1% penicillin and streptomycin and incubated for an overnight in 37 °C with 5% CO₂ incubator. Afterward, removed the medium and washed seeded cells twice with PBS 1X and let cell grow to get around 80-85% confluence. For co-culture of spheroids, the passage number of each cell type should be kept the same, also for measurement of light pulsing effect all cell types for VVD-, VVDHigh and Cph1-MDA had same passage number. Cells with 80% confluence washed twice with adding 3 ml PBS and afterward detached from the surface by adding 0.5 ml of accutase (A1110501, ThermoFischer (Gibco)). 4.5 ml of normal DMEM medium added to flask and pipette it well to have a proper cell suspension and transfer to the 15 ml tube for counting cells and 0.3 ml of the cell suspension used for next cell passage. 10 µl of cell suspension mixed with 10 µl of trypan blue for counting cells. Cells were counted manually according to standard Neubauer Haemocytometry assay. The U-bottom 96 well (650185, Greiner Bio-One) used for seeding the spheroids. Based on well amounts and 150 µl of MC per each well the total volume of medium we needed have been calculated. For Cph1-MDA 5 µM of PCB and for VVD and VVDHigh-MDA 0.5 µM of FAD are needed. When the total volume of MC and the cofactors calculated the MC medium supplemented with cofactor should be filtered to eliminated and remove unwanted dirt. 150 µl of MC added to internal wells of the 96-well plate and the exterior wells for each edges filled with 200 µl of PBS to minimize evaporation of the medium. To decrease the pipette error of seeding low amount of cells after counting cells transferred to 1.5 ml tube then 500 and 200 cells added per each well and pipette well into the well

to have homogeneous cell suspension. The 96-well plate covered with parafilm to eliminate the medium evaporation. The dark sample always covered with Aluminum foil. Cells in 96-well plates at 200xg for 3 min and afterward, plates transferred in 37°C with 5% CO₂ incubator. Cph1-, VVD and VVDHigh-MDA spheroids illuminated with 1% red and blue light using light modules. The illumination was from the top the plates with the distance of 3 cm.

2.2.19 Staining and co-culture of spheroids

Cells stained with Vybrant™ DiO (V22886, Invitrogen) and DiD (V22887, Invitrogen) Cell Labeling Solution with 1:500 and 1:1000 concentration respectively. Dyes added to flask containing cells an overnight before seeding the spheroids. Afterward, cells normally washed twice with PBC as long as are adhering on surface and then detached with accutase. Cells counted and the MC prepared same as previous. The co-culture experiment done with 1:1 ratio of each cell types to have in total the same amount of 500 and 200 cells as seeded. After plating cells in each well, the plates were spine down at 200xg for 3 min and incubated at 37 °C and 5% CO₂ under correspondence light illumination.

2.2.20 Statistical analysis

All the experiments performed with 2 technical in 3 biological replications. The statistical analyses determined using non-parametric test by independent two samples Mann-Whitney test. All the data are shown as mean±SE. In box plots each box is defined as 25th and 75th percentile of the data, the line in the box represents the median, the dots the mean and whiskers the 10th and 90th percentiles. Mann-Whitney-U test was performed to analyze the statistical difference, and represented by *p*-values *p*>0.05 (not significant), *p* < 0.05 (presented as a star), *p* < 0.01 (presented as double star) and *p* < 0.001 (presented as triple star). OriginPro software version 2019 (OriginLAB, Corporation, Northampton, MA, USA) was used for all analyses.

2.2.21 Image analysis for cell clustering

All the image analysis was performed using Fiji-ImageJ 1.52d.¹³⁶ Bright field images acquired at the end of the cell clustering experiments, were background corrected for noise and differences in grey scale with the plugin “bioVoxel” with a pseudo flat field correction. Single images acquired in the tile scan (25 (5×5) to 64 (8×8) images) were stitched together into a larger image (1 cm² to 2.56 cm²) with the “Montage” plugin for the cell clustering analysis and with the “Stitching”¹³⁷ plugin for fractal dimension analysis. To detect clusters of cells, objects > 5000 μm² (corresponding to a projected area of more than 20 cells) were detected using the “analyze particles” plugin. The following macro script was used for this image analysis:

```
run("Set Scale...", "distance=1024 known=1000 pixel= 1 = global");
run("Images to Stack", "name=Stack title=[] use");
run("Pseudo flat field correction", "blurring=50 stack");
close();
run("Make Montage...", "columns=8 rows=8 scale=1");
run("Sharpen");
run("Smooth");
run("Median...", "radius=8");
run("Gaussian Blur...", "sigma=2");
setAutoThreshold("Default dark");
setAutoThreshold("Default dark");
setOption("BlackBackground", false);
run("Convert to Mask");
setAutoThreshold("Default");
call("ij.plugin.frame.ThresholdAdjuster.setMode", "B&W");
run("Convert to Mask");
setAutoThreshold("Default dark");
run("Fill Holes");
run("Undo");
run("Convert to Mask");
setAutoThreshold("Default");
```

```
run("Convert to Mask");  
run("Fill Holes");  
waitForUser("Do something, then click OK.");  
run("Analyze Particles...", "size=5000-Infinity  
show=[Bare Outlines] display include add");
```

The areas of all recorded cell clusters were analyzed with OriginPro2019 for average area and the total number of the cell clusters in each sample. The statistical significance was calculated from at least two biological repetitions and 3 technical replicates in each repetition using OriginPro2019. Mann-Withney-U test was performed to analyze the statistical difference, and represented by p-values ns>0.05, **<0.05 and ***<0.001.

2.2.22 Microscopy and image analysis of spheroids

The bright field images were taken with inverted fluorescence microscope (Leica DMI8) through a 5x air objective. The confocal images were acquired with a 56.4 μm pinhole in the Alexa488 and Alexa594 channels on a laser scanning confocal microscope (Leica SP8) equipped with 488 nm and 552 nm laser lines and a 20x/0.95 air objective to detect the green and red cells which stained with Vybrant™ DiO (V22886, Invitrogen) and DiD (V22887, Invitrogen) Cell Labeling Solution, respectively. All the images converted to 8-bit using Fiji-ImageJ 1.52d. To prepare the image scale/resolution of the imaging system determined from the imaging software and for spheroid size measurements using the SpheroidSizer which is a MATLAB-based and open source software¹³⁸. After the setting up the proper ratio of scale/resolution of the images the software automatically analyzing the images. The result saved in a excel file that displays on data like; Volume (mm^3).

In our study we measured data set based on the volume of spheroids which calculated based on the two factors, major axis as length and minor axis a width. Stacks of fluorescence images are acquired in the TRITC (Vybrant™ DiD) and FITC (Vybrant™ DiO) channels on a Leica SP8 laser scanning confocal microscope equipped with OPAL 488 (5%), Diode 638 (1%) and with 25x/0.95 air objective.

Chapter 3: Result and Discussion

3.1 Blue light switchable cell-cell interactions provide reversible and spatiotemporal control towards bottom-up tissue engineering

The following section is based on:

The Blue Light Switchable Cell–Cell Interactions Provide Reversible and Spatiotemporal Control Towards Bottom-Up Tissue Engineering

Yüz S. G.*, **Rasoulinejad S.***, Mueller M., Wegner A. E., and Wegner, S. V

Adv. Biosyst., 3, 1800310 (2019), doi: 10.1002/adbi.201800310

Contributions

I performed the immunostaining and imaging, reversibility in suspension cultures and the layer by layer tissue formation experiments including the analysis of the data for these parts. The stabilization of heterodimerization of Cry2 and CIBN protein on cell surface, Light induced clustering analysis and the live cell imaging for dynamic analysis of cell-cell interaction formation and reversion experiments performed by Simge G. Yuez. The mathematical analysis with the Ripley's K-function was performed by Anatol E. Wegner. Seraphine V. Wegner supervised the work.

Controlling cell–cell interactions is central for understanding key cellular processes and bottom-up tissue assembly from single cells. The challenge is to control cell–cell interactions dynamically and reversibly with high spatiotemporal precision noninvasively and sustainably. In this study, cell–cell interactions are controlled with visible light using

an optogenetic approach by expressing the blue light switchable proteins CRY2 or CIBN on the surfaces of cells. CRY2 and CIBN expressing cells form specific heterophilic interactions under blue light providing precise control in space and time. Further, these interactions are reversible in the dark and can be repeatedly and dynamically switched on and off. Unlike previous approaches, these genetically encoded proteins allow for long-term expression of the interaction domains and respond to nontoxic low intensity blue light. In addition, these interactions are suitable to assemble cells into 3D multicellular architectures. Overall, this approach captures the dynamic and reversible nature of cell–cell interactions and controls them noninvasively and sustainably both in space and time. This provides a new way of studying cell–cell interactions and assembling cellular building blocks into tissues with unmatched flexibility.

It is the vision of bottom-up tissue engineering to assemble cellular building blocks into multicellular functional tissues. This requires precisely controlling the interactions between the cells in space and time to obtain multicellular architectures that match the complexity of natural tissues.⁸² In fact cell–cell interactions play a crucial role not only in maintaining tissue integrity, but also in how cells organize with respect to each other, work together, and regulate cell behaviour through associated intracellular signalling (motility, collective migration, differentiation, etc.).⁷¹ In general cell–cell interactions and the associated signalling are very dynamic while being spatially and temporally tightly regulated during important events such as embryogenesis, wound healing, and cancer progression.¹³⁹ It is this tight regulation of cell–cell interactions and signals that is in part responsible for the proper development of tissues and organs at the right time in the right place,⁴³ and their dysregulation is involved in cancer cells leaving the primary tumour and metastasizing in other organs.¹⁴⁰ Clearly, the ability to regulate cell–cell interactions dynamically and with high spatiotemporal control is a key to assembling cellular building blocks into predictable tissue structures in the context of bottom-up tissue engineering, as well as to understanding and manipulating biological processes where cell–cell

interactions play a pivotal role. The fabrication of precisely controlled biomimetic materials has provided us with a detailed picture of cell–matrix interactions allowing us to design scaffolding materials for regenerative medicine.¹⁴¹ However, our ability to control cell–cell interactions with high spatial and temporal precision lags behind this development. The main difficulty is that, in contrast to synthetic materials, it is far from straightforward to modify the surface of the cell directly and sustainably in a way that will provide control in space and time. In recent years, chemical modification of cell surfaces with bioorthogonal functional groups has become an attractive way to control cell–cell interactions. Bioorthogonal functional groups (e.g., azides-alkynes,⁸⁶ oxyamines-ketones⁸⁴), or strong noncovalent interaction partners¹⁴² (e.g., complementary DNA strands,²⁵ biotin-avidin⁸⁷), have been introduced to the cell surface through liposome fusion or modified sugars¹⁴³ to induce specific interactions between cells with complementary reactive groups. However, unlike natural cell–cell interactions, these interactions are neither reversible nor dynamic. While DNA based cell assemblies can be reversed using degrading enzymes, increased temperatures, and displacing stands, these methods are either invasive or irreversible.²⁵ Only the surface modification of cells with lipid-chemically self-assembled nanorings allows to reversibly induce cell–cell interactions.¹⁴²

Another limitation is that chemical modifications to the cell surface can interfere unpredictably with other biological processes. Notably, such unnatural modifications only physically bring cells into proximity but do not directly communicate the signals associated to natural cell–cell interactions and only indirectly lead to cellular responses.^{25,84,86,144} Additionally, chemical modifications are difficult to sustain over longer periods since they are not embedded in any cellular machinery, and will diminish as cells divide and degrade them. Most importantly, these chemical modifications do not provide high spatial or temporal control over the cell–cell interactions.

Recently, light responsive chemical groups have been introduced to the cell surface to gain better spatiotemporal control over cell–cell interactions. For example, cell–cell interactions that were mediated by a linker with a nitrobenzene group can be locally disrupted when illuminated with UV light.⁸⁵ Similarly, the photoswitchable binding between azobenzene and cyclodextrin has been integrated on the cell surface to provide the first reversible switching of cell–cell interactions with light and have been used to study cell–cell communication.⁹² On the down side, however, all of these interactions respond to UV light, which is toxic for cells and the general problems associated with the chemical modification of cell surfaces still hold true. Genetically encoded cell–cell interactions are an alternative to chemical modifications on the cell surface.⁹⁴ These are sustained over time and are biocompatible, but it is problematic—if not impossible—to alter these cell–cell interactions locally and rapidly. Overall, a platform is still missing in order to control cell–cell interactions dynamically, reversibly, and with high spatial and temporal resolution in a noninvasive, sustainable, and bio-orthogonal way. Clearly, the design and development of photoswitchable cell cell interactions that fulfill these requirements would enable us to study cell–cell interactions and to buildup complex multicellular architectures. Herein, we developed blue light switchable cell–cell interactions, which can overcome all the above-listed limitations. We express the protein CRY2 (cryptochrome 2) and its interaction partner, CIBN (N-terminal of Cry-interacting basic helix-loop-helix protein 1) on the surfaces of cells, as photoswitchable building blocks to mediate cell–cell interactions. CRY2 and CIBN bind to each other upon blue light (480 nm) illumination and reversibly dissociate in the dark within minutes.¹⁴⁵ Using the blue light-dependent heterodimerization of CRY2 and CIBN provide us with the desired high spatial and temporal control and offer us an interactions that is both dynamic and reversible.¹⁴⁶ The CRY2/CIBN interaction has already been used to control a variety of intracellular functions (e.g., gene transcription¹¹⁷, protein–protein interactions¹⁴⁷, cell signalling,¹⁴⁸ organelle distribution,¹¹⁵ mechanotransduction¹⁴⁹) and cell adhesion to substrates,¹⁵⁰ which also shows the high bioorthogonality of the CRY2/CIBN interaction.

This interaction is induced by using low intensities of visible blue light, making this optogenetic approach noninvasive. The fact that these proteins are genetically encoded provides us with sustainable expression of these proteins on the cell surface over time. Like other examples to control cell–cell interactions, we use the CRY2/CIBN protein pair to control the interactions but not the signalling associated to cell–cell interactions. To attain blue-light dependent cell–cell interactions, we expressed CRY2 and CIBN on the surfaces of MDA-MB-231 cells, which lack E-cadherin expression and do not form any native cell–cell contacts.¹⁵¹ We hypothesized that upon blue light illumination those cells expressing the complementary interaction partners CRY2 and CIBN would interact and form cell clusters (Figure 6A). To express these proteins on the cell surface, we inserted CRY2-mCherry and CIBN-GFP (green fluorescent protein) into a pDisplay plasmid with an N-terminal Ig κ -chain leader sequence to direct the protein to the secretory pathway and a C-terminal transmembrane domain of the PDGFR (platelet derived growth factor receptor) for anchoring in the cell membrane. Subsequently, we transfected MDA-MB-231 cells with one of these plasmids and generated the stable cell lines, CRY2-MDA and CIBN-MDA, which constantly express the respective protein on the cell surface.

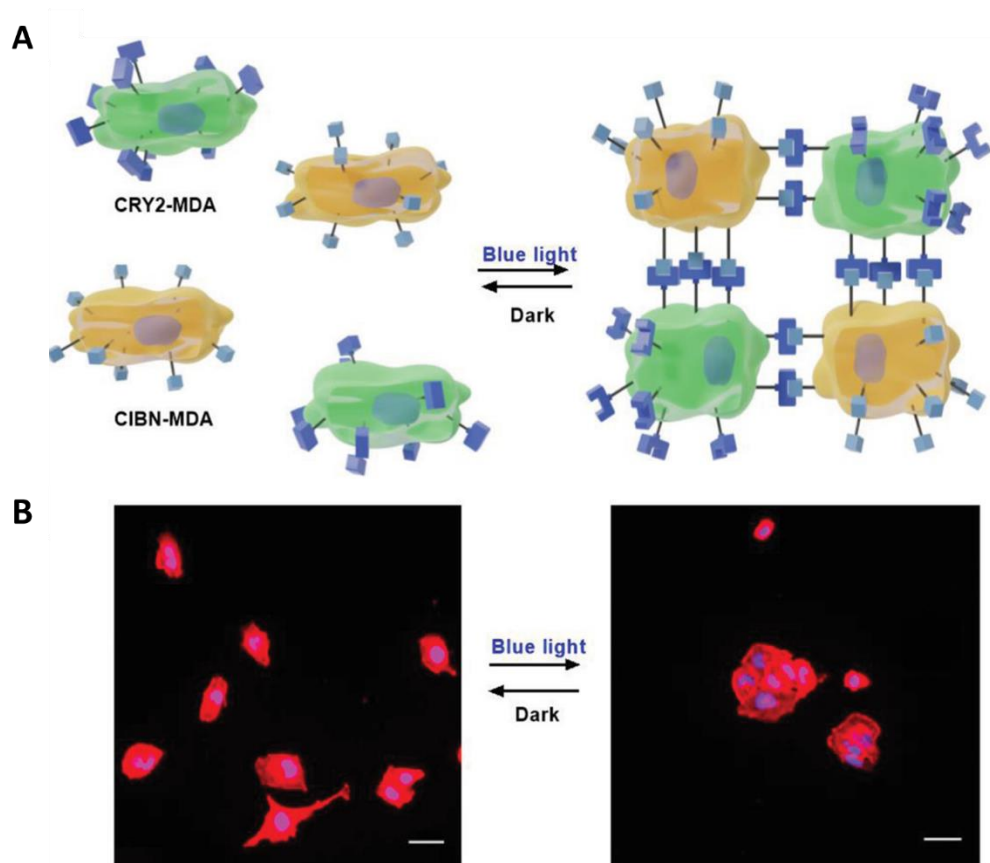


Figure 6: Blue-light switchable cell–cell interactions. A) Cells that express CRY2 (green) and CIBN (yellow) form cell–cell interactions under blue light and dissociate from each other in the dark. B) CRY2-MDA and CIBN-MDA cells are mixed in equal proportions and cultured in the dark or under blue light illumination. Cells cultured in the dark remain as single cells, but cells cultured under blue light form cell clusters due to CRY2-CIBN heterodimerization. Red: actin stain, Blue: nuclear stain. Scale bars are 50 μm.

Immunostainings of unpermeabilized cells for c-myc epitope, also included in the extracellular part of the displayed proteins, and fluorescence images of the fused fluorescent proteins show that the proteins are expressed and displayed on the cell surface (Figures 7).

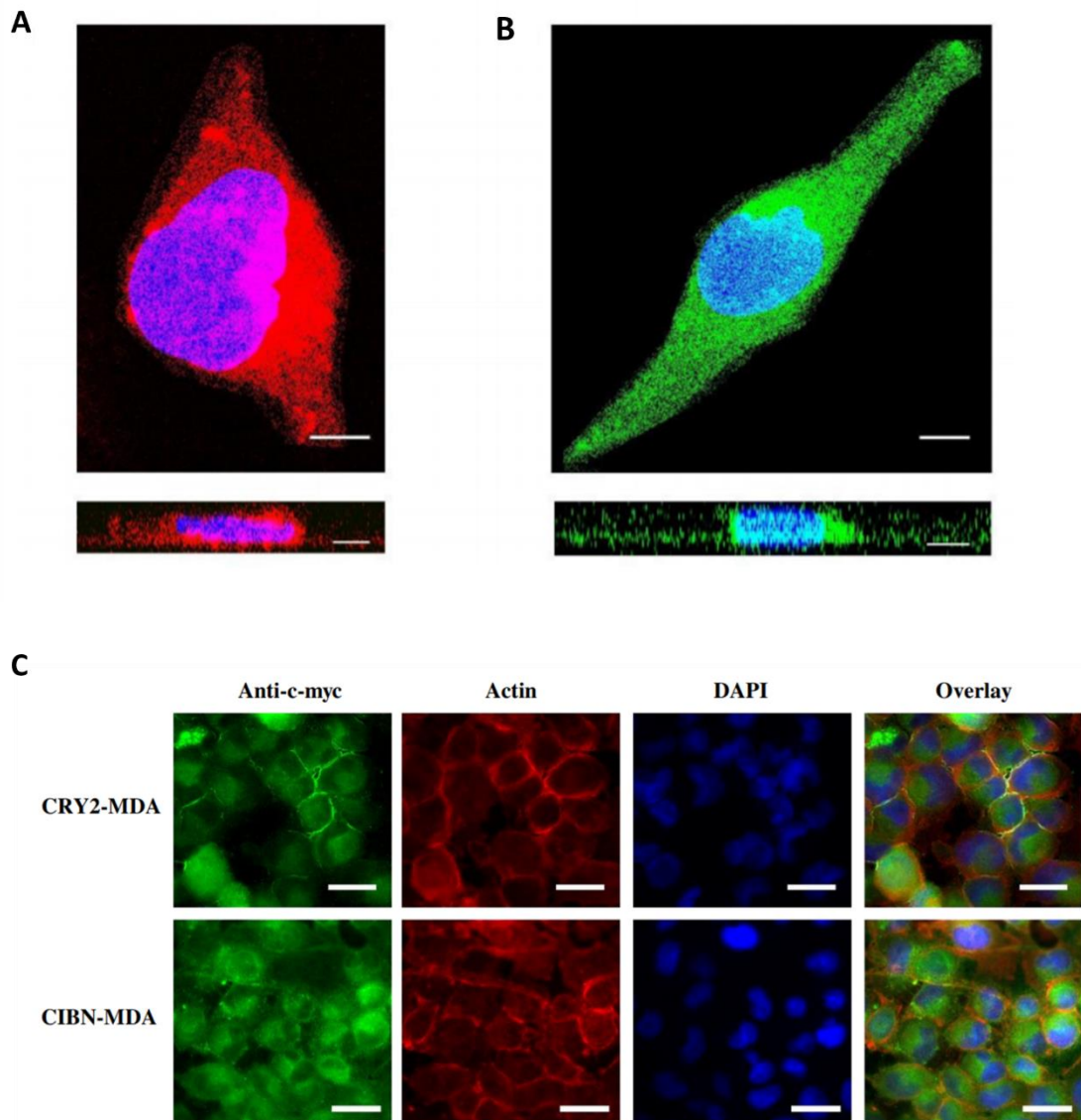


Figure 7: Fluorescent images of the stable cell lines. A) CRY2-mCherry expressing cell (CRY2-MDA). B) CIBN-GFP expressing cell (CIBN-MDA). View from z-axis (top) and from x-axis (bottom). The discontinuous signal on view from x-axis is due to the proteins on the plasma membrane. Red: mCherry, Green: GFP, Blue: Nuclear stain (DAPI). Scale bars are 5 μ m. C) Immunostaining for c-myc epitope to show the expression of CRY2 and CIBN on the cell surface. In the pDisplay plasmid, CRY2-mCherry and CIBN-GFP are fused to a c-myc epitope, which is used to detect protein expression on the cell surface (impermeable). Cells are neither fixed nor permeabilized before incubation with the primary c-myc antibody to stain only the proteins on the cell surface. Blue: Nuclear stain (DAPI), Red: Actin stain (phalloidin-TRITC), Green: c-myc epitope (goat anti-Mouse Alexa Fluor 488). Scale bars are 20 μ m.

Yet, attempts to quantify the protein expression levels in these cells with western blot, flow cytometry, and mass spectroscopy failed, presumably due to low protein expression. Nonetheless, we explored if the displayed CRY2 and CIBN proteins can mediate blue light dependent cell–cell interactions. Cells grow as single cells in the absence of cell–cell interactions (e.g., MDA-MB-231 cells) but grow in clusters of cells if cell–cell interactions are strong like cells of epithelial types (e.g., MCF7 cells). In order to check if the CRY2 and CIBN expressing cells form cell–cell interactions under blue light, we mixed CRY2-MDA and CIBN-MDA cells in equal proportions and cocultured them on a glass substrate either in the dark or under blue light for 4 h. To better visualize the cell boundaries and their positions, we stained the actin cytoskeleton with phalloidin tetramethyl rhodamine and the nuclei with 4',6-diamidino2-phenylindole (DAPI). In the dark, the mixed CRY2-MDA and CIBN-MDA cells grow as single cells similar to the parent MDAMB-231 cells and have little interaction with neighbouring cells as can be observed in fluorescent images (Figure 6B; Figure 8). On the other hand, under blue light illumination the mixed cells grow in clusters and showed cell–cell contacts between neighbouring cells. This finding already shows that the blue light-dependent interaction between CRY2 and CIBN is suitable to prompt cell–cell interactions. To demonstrate that there is significantly more cell–cell interactions under blue light than in the dark we used two different methods; an analysis of cells that are in direct contact, i.e., growth in clusters and a statistical analysis of the cell positions' in space. As mentioned above a direct consequence of strong cell–cell interactions are that the cells start to grow in clusters.

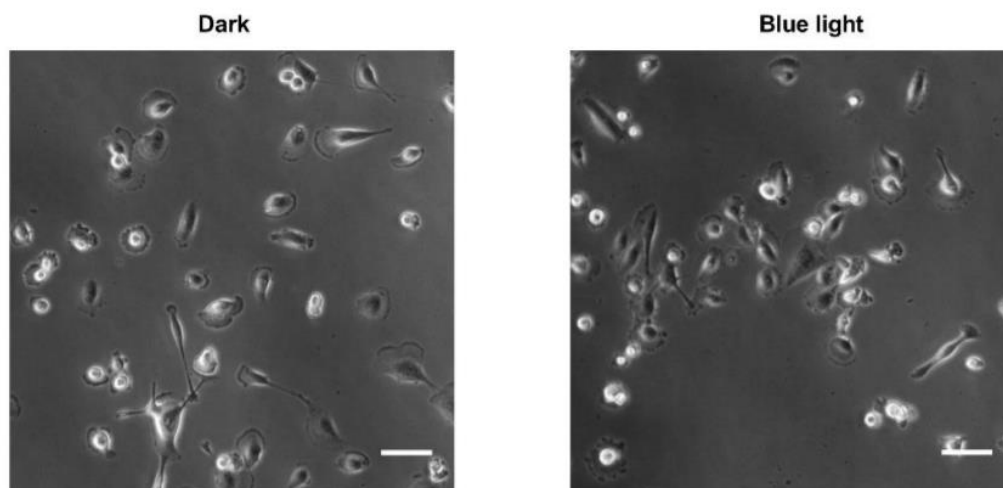


Figure 8: Bright field images of co-cultured CRY2-MDA and CIBN-MDA cells. In the dark cells stay as single cells (left) but under blue light the cells grow in clusters (right). Scale bars are 80 μm .

To investigate blue light dependent cell–cell interactions, we quantified the number of cells that grow in clusters and as single cells in the dark and under blue light. For this purpose, we mixed CRY2- MDA and CIBN-MDA cells and cultured them in the dark or under blue light for 4 h during which they could form cell–cell interactions and also adhere to a glass surface. First, we varied the overall cell density of cultured cells so that we could reliably observe light dependent cell–cell interactions. We determined the optimal density to be 5000 cells cm^{-2} ($\approx 5\%$ confluency) since at higher cell densities the light dependent cell–cell interactions are not distinguishable from general crowding in the cell culture and at lower cell densities the cells are too sparse to efficiently find each other (Figure 9A, C).

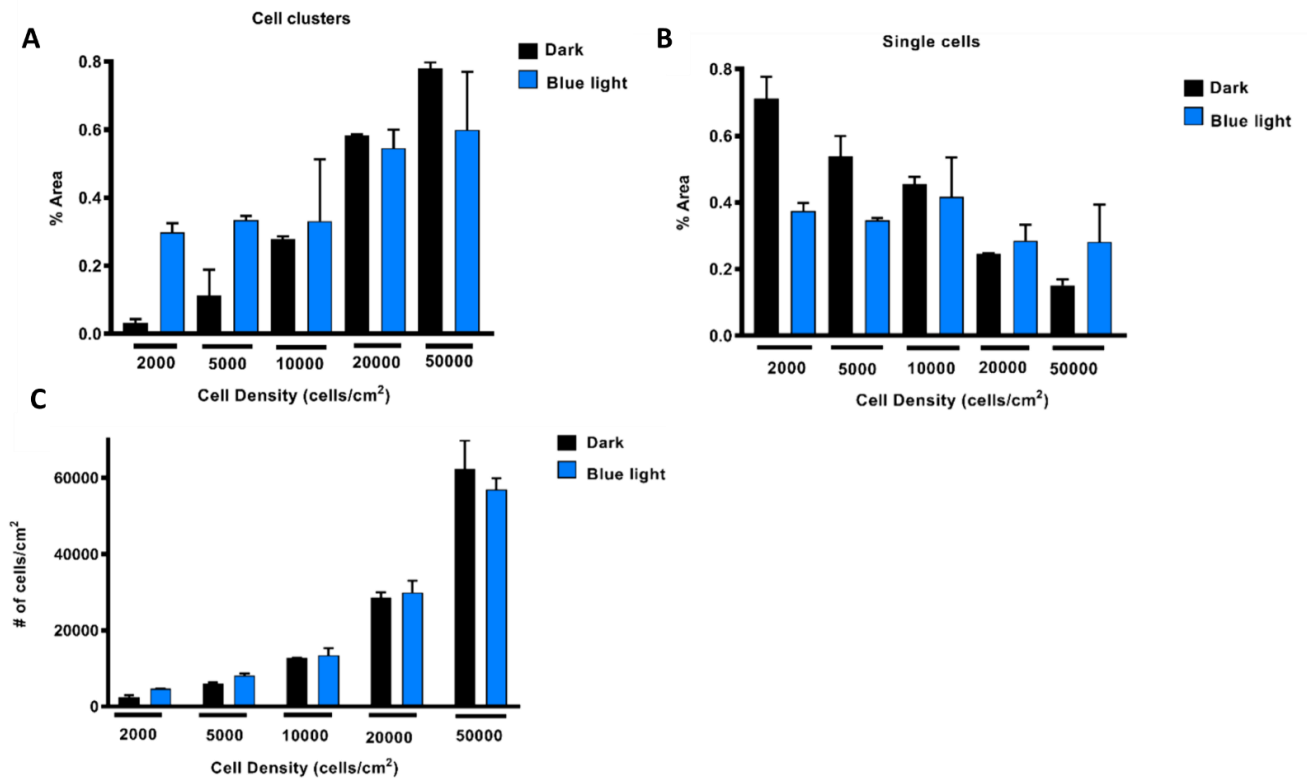


Figure 9: Cell number optimization for blue light dependent cell-cell interactions. CRY2-MDA and CIBN-MDA cells are seeded in equal proportions at different cell densities. A) % Area occupied by cell clusters. B) % Area occupied by single cells. C) Total cell density is determined from DAPI stain. The error bars show standard error of the mean (n=2).

To visualize cells in close proximity, which presumably form cell–cell interactions, we stained the actin cytoskeleton, acquired fluorescence images for a total area of 1 cm² (≈ 5000 cells cm⁻², technical duplicates with two replicates each) and analysed the spreading area for all objects in these images. The actin staining allowed us to distinguish single cells (spreading area, i.e., objects with an area of 300–3000 μm^2) from cell clusters that contain more than three cells (clusters of connected cells; objects with an area > 10000 μm^2) since cells growing in a cluster have an at least three times larger combined spreading area than a single cell. (Objects with an area of 3000–10000 μm^2 are not assigned in the clustering analysis as they contain 1–3 cells and it is difficult to

classify them reliably as single cells or clusters) In a 1:1 mixed coculture of CRY2-MDA and CIBN-MDA cells, we detected about 180 cell clusters cm^{-2} under blue light while there were only about 20 clusters cm^{-2} in the dark (Figure 10A). Conversely, in the same cultures the number of single cells was also significantly less under blue light compared to those in the dark. Likewise, the percent of area occupied by cell clusters compared to the area of all cells, which is proportional to the percentage of cells involved in cell clusters, is six fold higher under blue light than in the dark (Figure 10B). In fact, under blue light about 30% of cells grow in clusters of cells that contain more than three cells and only 30% are growing as single cells, while in the dark about 70% are growing as single cells.

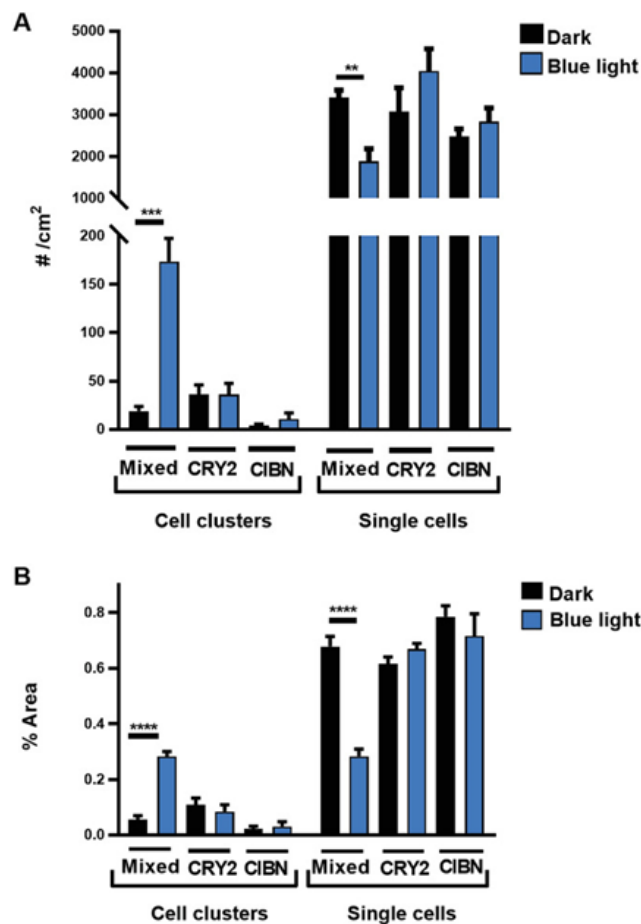


Figure 10: Quantification of cell–cell interactions between CRY2-MDA and CIBN-MDA cells in the dark and under blue light. A) The number of cell clusters > three cells and single cells in the dark and under blue light. B) Percentage of Area of cells that grow in cell clusters and as single cells. The cells kept in the dark mainly stay as single cells, whereas cells grown under blue light show a higher number of cell clusters. CRY2-MDA

and CIBN-MDA cells form heterophilic and not homophilic interactions as cells in monocultures grow as single cells. The error bars are the standard error of technical duplicates with two replicates ($n = 4$). Unpaired t-test is used for statistical significance (p value <0.01 (**), <0.001 (***), <0.0001 (****)).

All of these parameters demonstrate clearly that CRY2 and CIBN expressing cells interact more with each other under blue light than in the dark. To make sure that the increase in cell clustering under blue light is not due to differences in cell seeding or light toxicity, we measured the total number of cells in each culture based on the nuclear DAPI stain. We found that there were no significant differences in the total number of cells between cultures (Figure 11A). Next, we verified that blue light illumination did not lead to toxicity. In the parent cell line (MDA-MB-231), we did not observe any phototoxicity even at $8000 \mu\text{W cm}^{-2}$ after 4 h, which is 100-fold higher light intensity than we used in cell clustering experiments (Figure 11B). This also demonstrates that the light intensities used here are far below the toxic dose, making this approach noninvasive for cells.

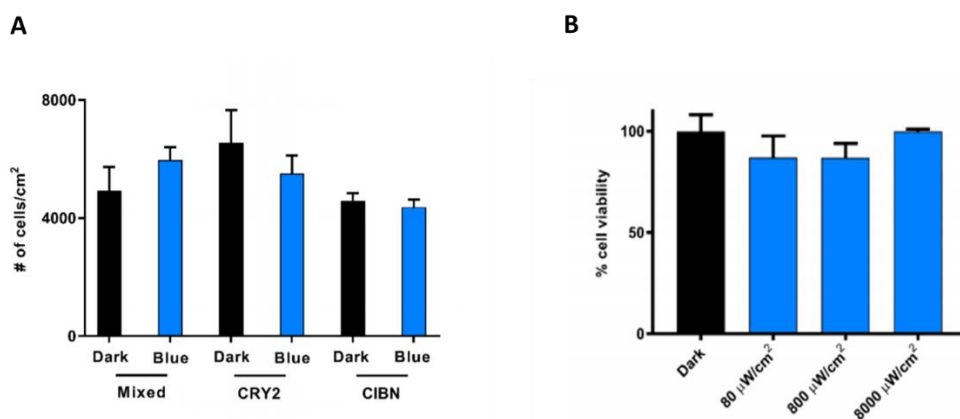


Figure 11: A) Total number of cells for blue light dependent cell clustering. The number of cells in the coand mono-cultures of CRY2-MDA and CIBN-MDA cells are measured to prevent any errors due to cell number. We did not observe any significant difference between the number of cells, which may affect the size or amount of the clusters. The error bars show standard error of the mean ($n=4$). B) Cell viability under blue light illumination. Wild type MDA-MB-231 cells are incubated under three different intensities of blue light and in dark for 4 hours. Subsequently, cell viability is measured by MTT assay. The absorbance values are normalized to the dark value to determine % cell viability. Even at the highest tested blue light intensity, we

did not observe any light toxicity. 80 $\mu\text{W}/\text{cm}^2$ blue light illumination is used in all cell experiments. The error bars show standard error of the mean ($n=2$).

The Ripley's K-function¹⁵² is a standard statistical measure to determine if points in space are clustered ($K(r) > K_0(r)$), randomly distributed ($K(r) = K_0(r)$) or dispersed ($K(r) < K_0(r)$) compared to a random distribution of points (K_0) at length scale r . In this study, we took the center of mass for each cell nucleus detected by DAPI staining as a point and analyzed if these points cluster more under blue light illumination compared to the dark. We use the variance stabilized transformation of Ripley's K-function known as the L-function. Indeed, the L-function analysis shows that there is significantly more clustering under blue light than in the dark, since $L_{\text{blue}} > L_{\text{dark}}$ at distances of 10–80 μm , which is reasonable considering the average size of a cell is $\approx 30 \mu\text{m}$ (Figure 12A). We also considered the pair correlation function (pcf)¹⁵² to complement our analysis. Likewise, the pcf based comparison of the point distributions shows a higher density of cells at distances close to the average cell size under blue light than in the dark, which is another indicator of the blue light dependent cell–cell interactions (Figure 12B). Yet, Ripley's K-function and the pcf are sensitive to variations in cell counts/density from one sample to the next, which was not the case for the clustering analysis described above. Therefore, we only compare samples with small differences in cell number using the Ripley's K and the pcf. From here on we use the clustering analysis as it is more robust against variations in cell density. Cell–cell interactions are known to be specific in nature and a cell can specifically adhere either to the same type of cell or to that of a different type. We expected to find only heterophilic interactions between CRY2-MDA and CIBN-MDA cells, but not homophilic ones. In order to demonstrate that the blue light dependent cell–cell interactions are the result of specific binding of CRY2 and CIBN under blue light, we quantified cell clustering in monocultures of CRY2-MDA and CIBN-MDA cells using the same procedure as described above. In these monocultures, cells cluster neither in the dark nor under blue light and have similar clustering parameters as those observed for

mixed cultures in the dark (Figure 10A,B). CRY2 has been reported to homodimerize under blue light to some extent.¹¹⁵ However, this interaction does not seem to be strong enough to induce significant cell–cell interactions between CRY2-MDA cells under blue light. Overall, these results show that the cell–cell interactions are only due to the specific heterodimerization of CRY2 and CIBN under blue light. Accordingly, only cells of different types that display these complementary interaction partners will interact with each other under blue light, but not cells of the same type.

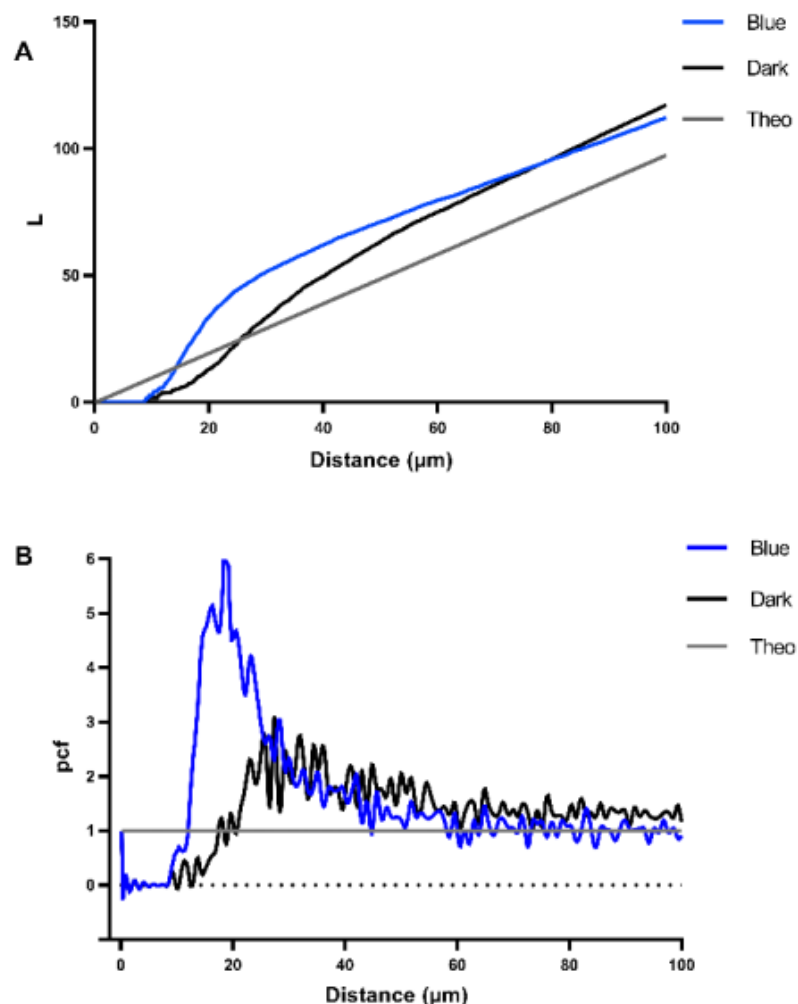


Figure 12: The Ripley's K-function. A) Ripley's K analysis and B) pair correlation function (pcf) analysis for mixed co-cultures of CRY2-MDA and CIBN-MDA cells. The cell nuclei were stained with DAPI and the center of mass for each nucleus was used as a point in the statistical analysis.

A key advantage of the CRY2-CIBN based cell–cell interactions is their reversibility in the dark and the repeated switchability, which reflects the reversible and dynamic nature of native cell–cell interactions. To show that the blue light dependent cell–cell interactions are reversed in the dark, we analyzed the aggregation of the cells in suspension in a light dependent fashion. For this purpose, we co-cultured a 1:1 mixture of CRY2-MDA and CIBN-MDA cells in suspension under constant low agitation (20 rpm) first for 30 min under blue light and then for 30 min in the dark over multiple light/dark cycles. Bright field images taken at each time point allowed visualizing the formation or dissociation of cell aggregates at each stage over three light/dark cycles. We observe that the cells aggregate significantly after each blue light illumination step and that the aggregates dissociate fully after each incubation step in the dark (Figure 13A–F). To quantify the cell aggregation, we defined the objects with an area $> 5000 \mu\text{m}^2$ as aggregates (at least 15 cells in each aggregate) and computed the percentage of area occupied by clusters and their numbers in the imaged area (Figure 13G). This analysis shows that both the area covered by large cell aggregates and their overall number is higher under blue light compared to the dark. Hence, we conclude that these blue light dependent cell–cell interactions are both reversible in the dark and can be switched on and off repeatedly.

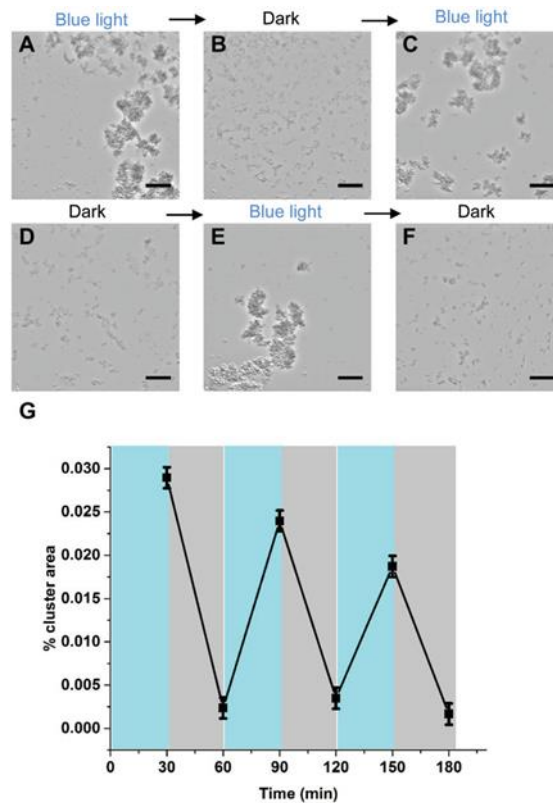


Figure 13: Reversible control of cell–cell interactions. A–F) Bright field images of 1:1 suspension coculture of CRY2-MDA and CIBN-MDA in blue light (30 min) and in the dark (30 min) over repeated cycles. The scale bars are 40 μm . G) The change in the percentage cluster area over time in light/dark cycles. Cells formed big clusters under blue light illumination whereas in the dark they dissociated and found to be rather as single cells. The error bars show standard error of the mean ($n = 6$).

The dynamics of the blue light dependent cell–cell interactions are another key property that requires investigation at the level of single cell–cell interactions. In order to determine duration needed for the cells to interact under blue light and dissociate in the dark, we observed single cell–cell interactions live and recorded time-lapse movies. For this purpose, we seeded CRY2-MDA cells on adhesive 700 μm^2 circular patterns, so that isolated CRY2-MDA cells grew on an otherwise nonadhesive background. Subsequently, we added CIBN-MDA cells in suspension to these surfaces and examined their interaction with the CRY2-MDA cells first under blue light and then in the dark (Figure 14A). We further analyzed the distance between the CIBN-MDA and CRY2-MDA

cells over time for the light/dark cycle for multiple cells (Figure 14B). When the CIBN-MDA cells are added under blue light illumination the cells quickly bound to the CRY2-MDA cell on the pattern within few minutes resulting in reduced mobility and no measurable distance between the two cells. Further, the two cells remained bound over the 30 min of the blue light illumination. Then, the light was switched off for 20 min and the CIBN-MDA cell separated from the CRY2-MDA cell, gaining mobility. We observed that the CIBN-MDA cell dissociated from the CRY2-MDA cell within a few minutes once the light was turned off. The proteins CRY2 and CIBN interact with each other under blue light after just a few seconds and dissociate from each other in the dark in about 10 min¹⁴⁵. Hence, for the formation of the CRY2/CIBN mediated cell–cell interactions the rate limiting step seems to be the cells finding each other as once the two cells were in close proximity the cells were not dissociating from each other. On the other hand, the cells dissociated from each other in the dark in a few minutes; a time range typical for the CRY2/CIBN interaction yet somewhat quicker than the time required for full reversion. Potential reasons for this could be that the switching dynamics are quicker in the extracellular environment than inside the cell or that a minimum number of CRY2/CIBN interaction are required to maintain the cell–cell interactions and when the number of reversed interactions exceeds this limit the cells do not interact anymore.

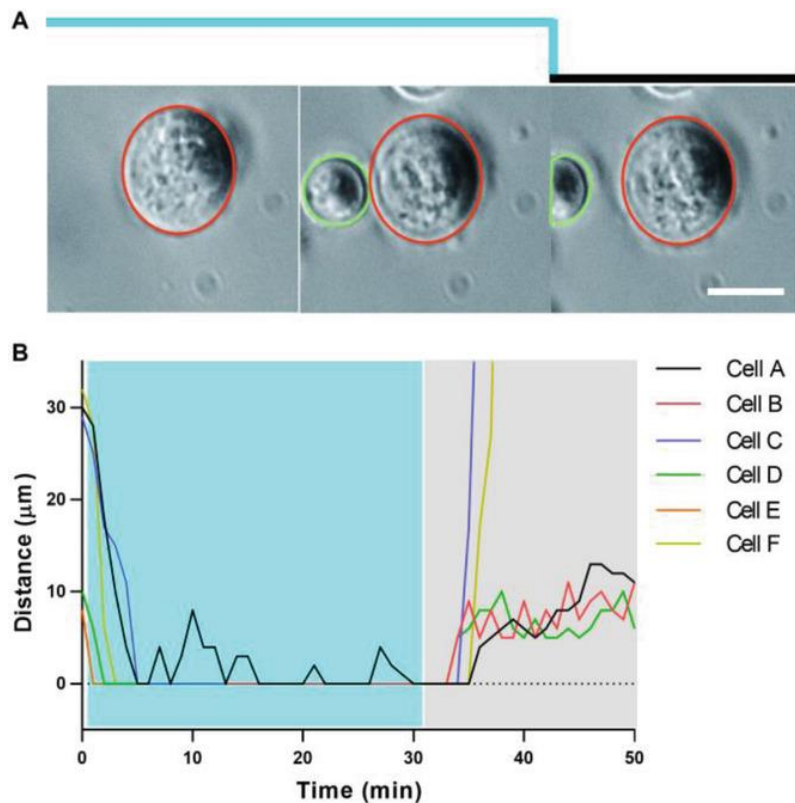


Figure 14: Dynamics of light dependent cell–cell interactions. A) Phase contrast images from a time-lapse movie showing the binding of a CIBN-MDA cell to a CRY2-MDA cell under blue light and its dissociation in the dark. The CRY2-MDA cell (red circle) adhered in a circular adhesive pattern with a nonadhesive surrounding. CIBN-MDA (green circle) was added and their interaction was monitored under blue light and in the dark. Scale bar is 25 μm . B) Distance between the CRY2-MDA cells and the CIBN-MDA over time. The distance between the two cells decreases under blue light due to the CRY2/CIBN heterodimerization and increases in the dark due the CRY2/CIBN dissociation.

These blue light switchable cell–cell interactions are suitable to control how cells arrange in tissue culture and produce layered cell structures. Towards this aim, CRY2-MDA and CIBN-MDA cells were used as cellular building blocks to generate a 3D architecture by seeding them layer-by-layer (Figure 15A). First, we seeded CRY2-MDA cells (prestained with a red fluorescent dye) on a glass substrate and grew them to confluency. Then, CIBN-MDA cells (prestained with a green fluorescent dye) were seeded on top of the CRY2-MDA cells and were illuminated with blue light for 4h. The confocal images of the coculture showed two layers of cells with red stain CRY2- MDA cells on the bottom and

the green stain CIBN-MDA cells on top (Figure 15B–D). Such layered cell structures only formed under blue light illumination and did not form when the CIBNMDA cells were seeded on top of CRY2-MDA cells in the dark (Figure 16). Overall, this demonstrates that the blue light dependent cell-cell interactions can be used to form 3D cellular structures from the bottom-up in a controlled manner.

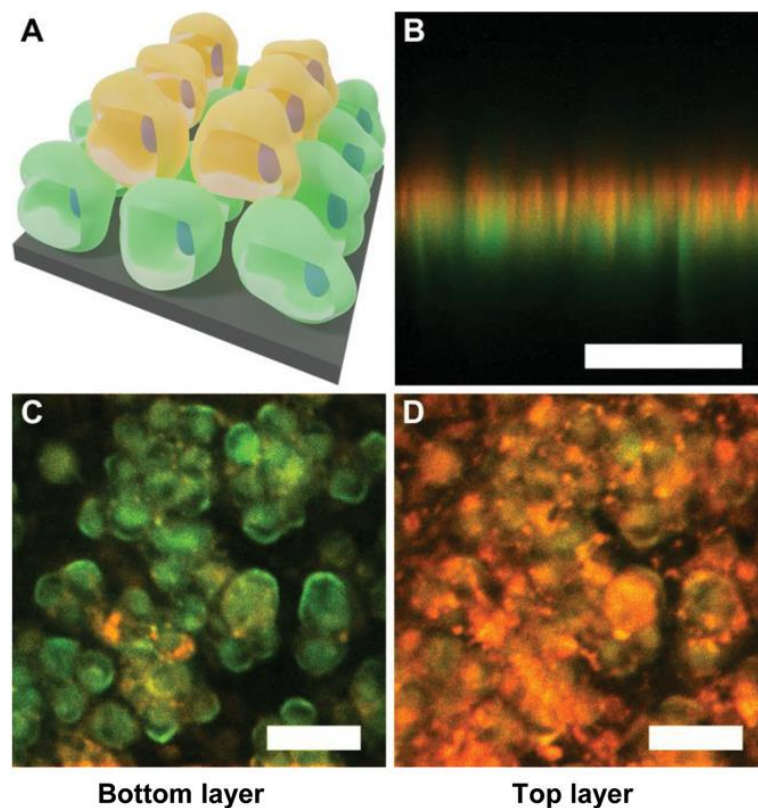


Figure 15: Layer by layer 3D architecture. A) Schematic representation of the layered cell structure under blue light. CRY2-MDA cells (green) were grown to confluency, before CIBN-MDA cells (red) are added on top under blue light illumination. CIBN-MDA cells stack on top of the CRY2-MDA cells under blue light illumination resulting in two layers of cells. Confocal images of the B) side view, C) bottom layer, and D) top layer. The scale bars are 50 μm .

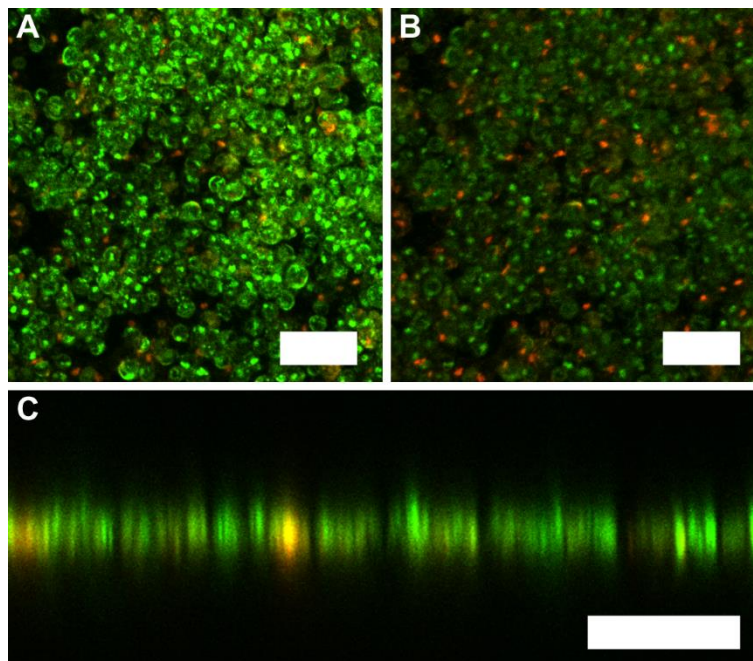


Figure 16: Formation of a 3D architecture layer by layer in the dark. CRY2-MDA cells (green) were grown to confluency, before CIBN-MDA cells (red) are added on top in the dark. Confocal images from the A) bottom B) top C) side. The scale bars are 50 μ m. In the dark, the CIBN-MDA cells fail to form a second layer of cells on top of the CRY2-MDA cells because the photoswitchable cell-cell interactions are not activated.

Summery

In summary, we have developed blue light switchable cell–cell interactions by using the blue light-dependent heterodimerization of CRY2 and CIBN. We were able to induce interactions between CRY2-MDA and CIBN-MDA cells that express the respective proteins on their surfaces upon blue light illumination and then simply turn them off by switching off the blue light. These photoswitchable cell–cell interactions have the potential to capture key features of native cell–cell interactions in terms of spatiotemporal control, sustainability, dynamics, and reversibility but not cellular signalling associated to cell–cell interaction. Notably, the control with light makes it possible to induce these interactions with unmatched precision in space and time. These interactions are dynamic and reversible, which enables modifying cell–cell interactions over time as observed during biological processes. Additionally, these protein-based photoswitches are well-

suited to sustainably control the cell–cell interactions over a long period of time because they are genetically encodable and new proteins are expressed in the cells as they degrade and the cell divides. The high specificity of the CRY2-CIBN heterodimerization allows us to specifically induce heterophilic interactions but not homophilic ones. Finally, the low intensity blue light that triggers these cell–cell interactions is noninvasive for the cells. These blue light switchable cell–cell interactions can be used to build multicellular architectures, used in scaffold-free bottom-up tissue engineering and also to study biological processes where cell–cell interactions play a pivotal role.

Controlling the cell-cell interaction with light comes with the unique advantage of high spatiotemporal resolution and turning on the cell-cell adhesions remotely using low intensity biocompatible light without interfering with other cellular processes. Therefore, the incoming section we developed the homodimerization cell-cell interaction with specific light illumination to combined different orthogonal cell-cell interactions to self-assemble mixtures of different cell types into separate self-sorted assemblies.

3.2 Orthogonal Blue and Red Light Controlled Cell-Cell Adhesions enable Sorting-out in Multicellular Structures

The following section is based on:

Orthogonal Blue and Red Light Controlled Cell-Cell Adhesions enable Sorting-out in Multicellular Structures

Rasoulinejad S., Mueller M., Nzigou, M. B., Wegner, S. V. (2020)

ACS Synth. Biol., 9, 2076–2086 (2020), doi:10.1021/acssynbio.0c00150

Contributions

I performed all experiments including the analysis of the data. B. N. helped with the quantification of protein expression and MCF7 cells clustering. M.M helped for sorting cell. Seraphine V. Wegner supervised the work.

During embryo development an initially symmetric multicellular structure undergoes spatiotemporally controlled morphogenic changes to self-organize into complex tissue architectures. At early stages, cells not only have the intrinsic capacity to self-assemble into multicellular structures, but different types of cells also self-sort into distinct patterns, which is the prerequisite for the proper formation of subsequent embryo architectures.^{2,32} Even in vitro dissociated cells self-assemble into multicellular structures due to cell-cell adhesion and mixtures of cells derived from different tissues possess the remarkable ability to self-sort themselves into precise structures that resemble the tissues of origin⁴¹. In these multicellular structures cells are able to organize by distinguishing “self” from “non-self” based on differences in homophilic and heterophilic cell-cell adhesions.^{43,153} In addition to the cellular arrangement, interactions between cells also fundamentally

govern cell biology by communicating both biochemical and biophysical signals.^{154,155} This is the reason why the misregulation of cell-cell adhesions is associated with diseases such as cancer, inflammation and autoimmune diseases.^{92,156} Furthermore, recent advances in organoid formation from different progenitor cell types⁸³ and the self-assembly of embryo mimetic structures from embryonic and extraembryonic stem cells^{5,6} all demonstrate the enormous potential of multicellular architectures in regenerative medicine and synthetic biology.^{21,157} Fundamentally, controlling when and where cell-cell adhesions of different type form is a major driving force in controlling the organization in multicellular structures and consequently their function.⁸² Therefore, the approaches to control different types of cell-cell interactions independently with high spatiotemporal control are powerful in the assembly and self-sorting of cells into desired multicellular architectures from the bottom-up and understanding principles that govern multicellular architectures.¹

Key prerequisites to achieve the desired self-assembly and self-sorting in multicellular structures include the independent control over different cell-cell adhesions within a mixture of different cell types. Up to now, both genetic^{82,158} and chemical^{84,85} approaches that alter the cell surface have been developed to regulate cell-cell adhesions for bottom-up tissue engineering and to further understanding of the role of cell-cell adhesions in cell biology. It is possible to regulate the adhesiveness between different cell types by adjusting the expression of different native cell-cell adhesion receptors, such as cadherins,^{43,46,59,82,153} and cells expressing different types of cadherins, aggregate separately when shaken in suspension, i.e. sort out/self-sort.^{43,159} However, it is not possible to locally alter cell interactions or reverse them at a desired point in time using this approach and even less so for multiple cell types. On the other hand, the chemical reactive groups, formerly also used for self-assembly and self-sorting in colloidal systems, have been introduced onto the cell surfaces such as clickable groups,^{84–86,127,160} single stranded DNA^{90,158,161,162} and supramolecular interaction partners.⁹² All these

synthetic cell-cell interaction provide some spatiotemporal regulation,⁸³ but suffer from dilution in the long term as the cells divide, poor reversibility and do not allow us to control of multiple cell types in the same mixture. Consequently, these limitations neither enable self-sorting in multicellular mixtures, nor specifically manipulating different cell types in multicellular mixtures.

This study shows how we can regulate the adhesion of two different types of cells independently using blue or red light. For this purpose, we developed blue and red light switchable cell-cell interactions using photoswitchable proteins as artificial adhesion molecules enabling the assembly of desired multicellular structures by simply turning on the right color of light. We show how these cell-cell interactions can be used to independently and reversibly trigger both the self-assembly of each cell type and the self-sorting in a multicellular mixture. This study was inspired by a concept established with mixtures of two types of colloidal polystyrene particles, which could self-sort into distinct groups (also known as narcissistic or asocial self-sorting in the colloidal self-assembly community) using different colors of light.¹⁶³ In this study, we extend the concept of asocial self-sorting established for nonliving colloidal particles to cells for the assembly of multicellular tissue-like structures in the context of bottom-up tissue engineering. In this respect, this study is a demonstration of how well-established concepts of self-assembly and self-sorting for colloidal particles can be extended to multicellular systems and the parallels between self-sorting in colloidal mixtures and sorting-out in multicellular mixtures.

Design of photoswitchable homophilic cell-cell adhesions. In the first step, we focused on engineering two different cell types that be triggered with blue or red light independently to form homophilic cell-cell interactions. Our aim was to control each cell type using different colours of light as an external trigger to later address them separately in multicellular mixtures that self-sort. For this purpose, we expressed different photoswitchable proteins that homodimerize after exposure to light illumination as new

adhesion receptors on the surfaces of cells. As photoswitchable cell adhesion receptors, we chose two different proteins that respond to different wavelengths: the blue light (450 nm) responsive protein LOV domain VVD from *Neurospora crassa*¹⁶⁴ and the red light (660 nm) responsive protein Cph1 phytochrome-like protein from *Cyanobacterium Synechocystis*.¹²⁸ Both of these proteins homodimerize upon light illumination and reversibly dissociate from each other in the dark as well as under far-red light (720 nm) for Cph1. Using these two molecularly orthogonal and independently addressable homophilic cell-cell interactions, we aimed to control the self-assembly and the self-sorting of each cell type individually (Figure 17A and B).

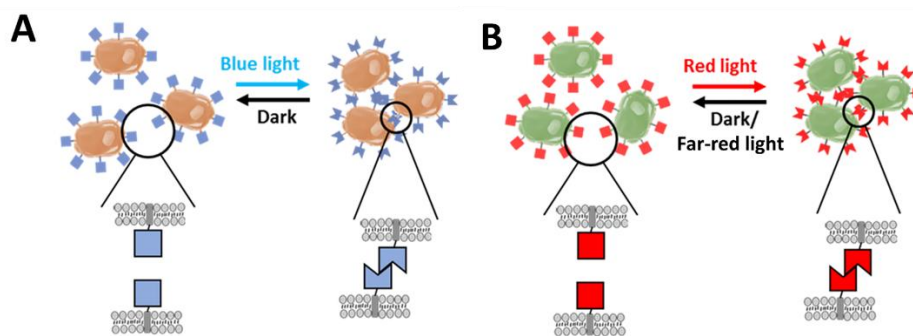


Figure 17: Blue and red light controlled cell-cell adhesions. A) Cells expressing VVD or VVDHigh on their surfaces do not interact in the dark. Upon blue light illumination, the photoswitchable proteins on neighbouring cells homodimerize and result in cell-cell adhesions. B) Cells expressing Cph1 on their surface do not interact with each other in the dark. Under red light, Cph1 proteins on neighbouring cells homodimerize and lead to cell-cell adhesions.

We assumed that cells expressing VVD on their surfaces would only interact with each other under blue light, but not under red light, and cells expressing Cph1 on their surfaces would only interact under red light, but not under blue light. Furthermore, we expected that under co-illumination with blue and red light each cell type would sort itself out to form distinct clusters, analogous to the self-sorting behaviour observed when two cell types expressing two different types of cadherins are mixed. The photoswitchable

proteins used in this study form head-to-tail homodimers (i.e. the N-terminal of one protein binds to the C-terminal of the other protein) as shown by crystallography^{127,164} and can mediate homophilic cell-cell interactions between neighbouring cells that express the protein. Unlike other examples of artificial cell-cell adhesions, which form heterophilic cell-cell adhesion (interaction between cells of different types),^{19,92,133,162} here presented cell-cell adhesions are homophilic. In this respect, the photoswitchable cell-cell interactions mirror the homophilic interaction mode of cadherin mediated cell-cell adhesions, but are different in terms of cell signalling as they do not have an intracellular tail to link to the cell cytoskeleton like cadherins. In addition, general advantages of photoregulation are the high spatiotemporal control, tuneable dynamics and high orthogonality without interference from other cellular processes, as previously demonstrated in numerous optogenetic studies.^{19,165}

To generate photoswitchable cell-cell interactions, we first expressed the proteins VVD or Cph1 on the surfaces of cells. In our strategy, the photoswitchable proteins were cloned into the pDisplay plasmid with an N-terminal murine Ig κ -chain leader sequence, which directs the protein to the secretory pathway, and a C-terminal platelet derived growth factor receptor (PDGFR) transmembrane domain, which anchors the protein to the plasma membrane, displaying it on the extracellular side. Additionally, VVD variants and Cph1 were fused at their C-termini to the fluorescent tags mCherry and GFP (green fluorescent protein), respectively (Figure 18).

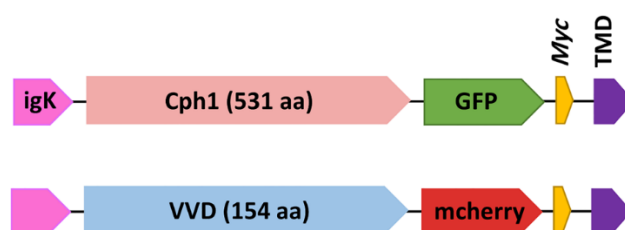


Figure 18: Schematic representation of Cph1 and VVD constructs in pDisplay. The constructs include a N-terminal igK-chain leader sequence, which directs the protein to the secretory pathway, the photoswitchable

protein, a fluorescent protein tag, a Myc epitope and the TMD (transmembrane domain), which has been derived from platelet growth factor receptor (PDGFR). The Myc epitope was used for immunostaining and detection in flow cytometry. Fluorescent proteins as GFP (green fluorescent protein) and mCherry were used as spacers from the membrane and for direct monitoring of protein expression.

Two variants of the VVD protein were used, VVD and VVD High, a mutant of VVD, which is a stronger homodimerizer and reverses slower in the dark¹⁰⁶ These constructs were transfected into the breast cancer cell line MDA-MB-231, which was chosen because it

does not express Type I cadherins and therefore does not form strong native cell-cell adhesions.¹⁵¹ Stable monoclonal cell lines, expressing the photoswitchable proteins on their surfaces (VVD-MDA, VVDHigh-MDA and Cph1-MDA) were isolated by fluorescence-activated cell sorting (FACS) and single clones with a high fluorescent signal were selected for future experiments (Figure 19 A-C).

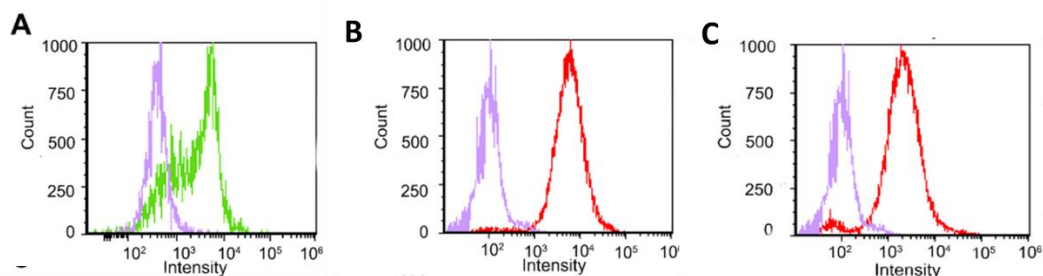


Figure 19: Sorting of photoswitchable protein expression on MDA-MB-231 cells. A-C) Flow cytometry analysis of cell lines expressing photoswitchable proteins on their cell surface. Direct detection of the fluorescent fusion proteins. A) GFP channel of Cph1-MDA (green) and MDA-MB-231(purple) cells, 89 % of Cph1-MDA cells displayed a higher signal than MDA-MB-231 cells. mCherry channel of (B) VVD-MDA (red). C) VVDHigh-MDA (red) and MDA-MB-231 (purple) cells. VVD-MDA and VVDHigh-MDA cells displayed 99 % and 90 % a higher signal than MDA-MB-231 cells, respectively.

The expression of the photoswitchable protein on the cell surface was confirmed by antibody staining of live cells without permeabilization using flow cytometry and fluorescent microscopy (Figure 20 A-D). Moreover, quantitative flow cytometry showed that 1×10^4 photoswitchable proteins per cell were expressed on the cell surface and the different photoswitchable proteins were expressed at similar levels (Table 1).

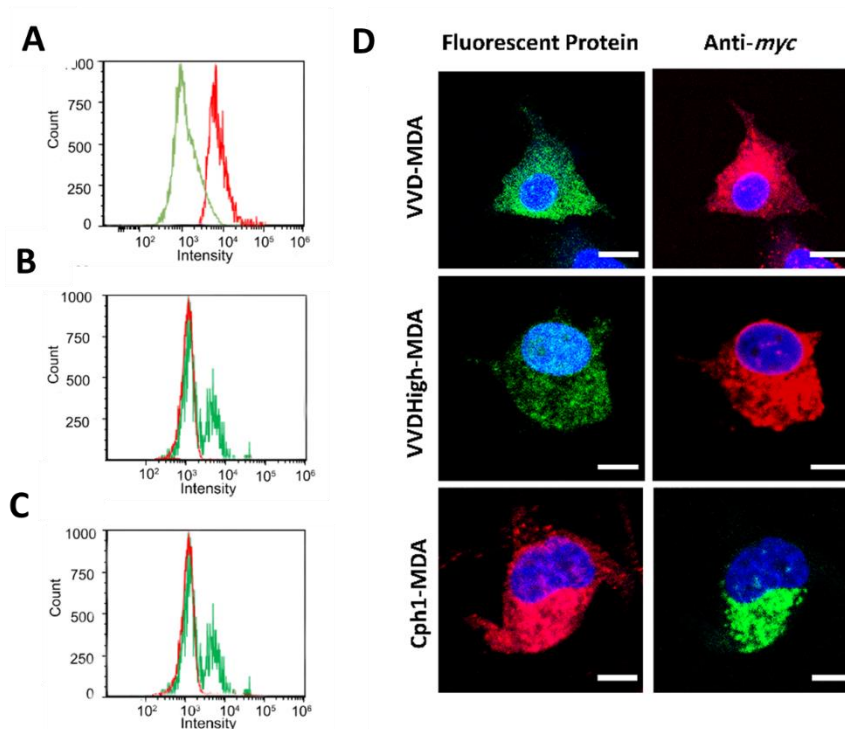


Figure 20: Protein expression on the cell surfaces. Indirect detection of surface displayed proteins through myc-antibody staining of live cells for (A) Cph1-MDA, (B) VVD-MDA and (C) VVDHigh-MDA cells stained with myc-antibody (green) and isotype antibody (red). An Alexa594 labelled secondary antibody was used for Cph1-MDA cells and an Alexa488 secondary antibody was used for VVD-MDA and VVDHigh-MDA cell to avoid interference with the fused fluorescent protein. D) Confocal images of cells expressing different photoswitchable proteins at their surface. The overall expression of transfected proteins was detected using the fused fluorescent proteins, GFP (green) for Cph1-MDA cells and mCherry (red) for VVD-MDA and VVDHigh-MDA cells. The surface displayed proteins were detected using a myc-antibody in unpermeabilized cells. An Alexa594 labelled secondary antibody (red) was used for Cph1-MDA cells and an Alexa488 secondary antibody (green) was used for VVD-MDA and VVDHigh-MDA cell to avoid interference with the fused fluorescent protein. The cell nuclei were stained with Hoechst 33341 (blue). Scale bars are 10 μ m.

Table 1: Quantification of protein expression on cell surface using quantitative flow cytometry.

Cell lines	Molecules of Equivalent Soluble Fluorochrome) MESF \pm SE
VVD	10058 \pm 30
VVD ^{High}	10583 \pm 474
CPH1	10117 \pm 335

Blue and red light-responsive cell-cell interactions. In a first step, we investigated whether cells expressing the photoswitchable proteins VVD, VVD^{High} and Cph1 were able to form cell-cell interactions upon photoactivation under blue and red light, respectively. For this purpose, the cells were seeded in 2D culture on glass substrates at sub-confluent densities (8600 cells/cm²) and were incubated for 4 hours in the dark (or far-red for Cph1-MDA) or under activating illumination (blue light for VVD- and VVD^{High}-MDA, red light for Cph1-MDA). During this time, cell-cell interactions could form as the cells settled down and adhered to the glass surface. Subsequently, the cell nuclei and the actin cytoskeleton were stained to visualize the cell-cell interactions using the fluorescence microscopy. In the dark, VVD- and VVD^{High}-MDA cells were evenly distributed over the substrate with few contacts between cells and their morphology resembled the non-transfected MDA-MB-231 cells. In contrast, under blue light these cells grew in clusters and resembled cells, which form strong cell-cell adhesions (Figure 21A and C). Similarly, Cph1-MDA distributed as a single cells under far-red light, but formed large groups under red light illumination (Figure 21B). In a control experiment with the parent MDA-MB-231 cell line, no light dependent cell clustering was observed (Figure 21A and B).

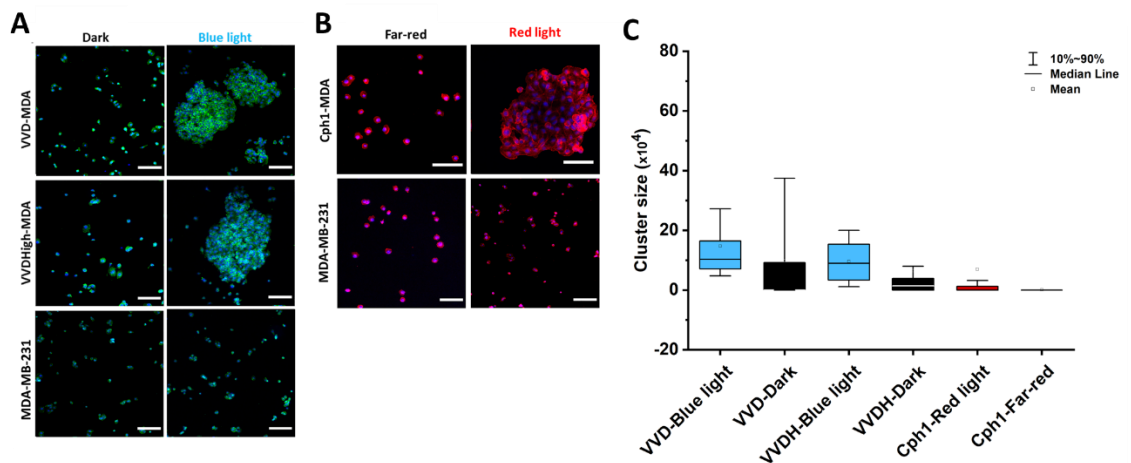


Figure 21: Blue and red light controlled cell–cell adhesions. A) VVD-MDA and VVDHigh-MDA cells grew as single cells in the dark and in large clusters under blue light 4 h after seeding in 2D culture at 8600 cells/cm². Green: actin phalloidin stain, blue: nuclear DAPI stain. B) Cph1-MDA cells grew as single cells under far-red and in large clusters under red light 4 h after seeding in 2D culture at 8600 cells/cm². Red: actin phalloidin stain, blue: nuclear DAPI stain. All scale bars are 200 μ m. The non-modified MDA-MB-231 cells used as negative control do not cluster independent of illumination. C) Cluster size distribution upon light triggered cell aggregation. The cluster area distribution were shown as a box plot, where each box is defined as the first and third quartile of the data, the line in the box represents the median, the dots are mean and whiskers the 10th and 90th percentiles.

Quantification of the light triggered clustering of VVD and Cph1 expressing cell lines in 2D further supported these observations (Figure 22A and B).

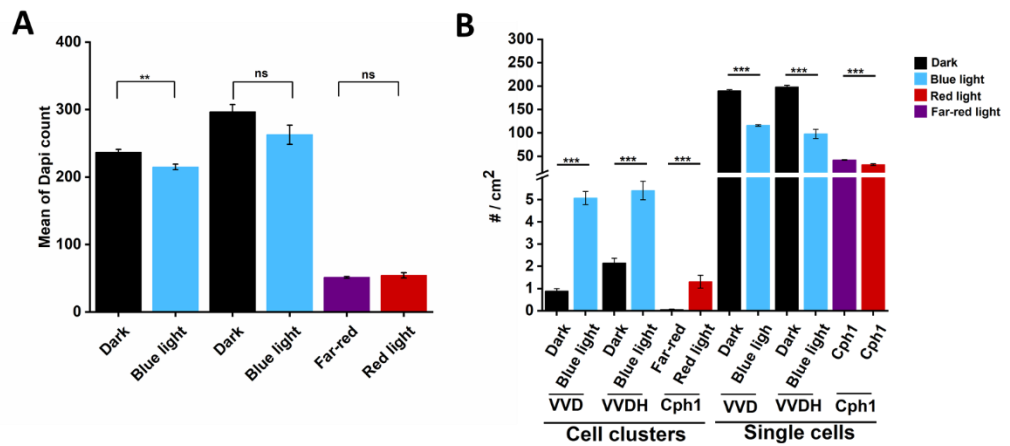


Figure 22: Quantification light triggered cell-cell interactions in 2D cell cultures. A) The number of cells counted in each experiment. The same number of cells was for each cell type to exclude changes in clustering resulting from different cell densities. B) The number of cell clusters > 3 cells and single cells in the dark and under blue light for VVD- and VVDHigh-MDA and under far-red light and red light for Cph1-MDA. In each of the cultures more cells grow in clusters and less cells as single cells when the cell-cell interactions were activated with light. The error bars are the standard error of mean of 3 biological replications, $p < 0.01$ presented as ** and p -value < 0.001 represented as ***.

The results showed that VVD and Cph1 are suitable as adhesion receptors to form homophilic cell-cell interactions. Unlike approaches that rely on the chemical modification of cell surfaces to control cell-cell interactions, the genetically encoded optogenetic adhesion molecules guarantee stable expression on the cell surface as the cells were expanded and did not require constant cell surface modification.

Independent photoactivation of VVD and Cph1 mediated cell-cell adhesions. In multicellular architectures, it is highly desirable to control different cell types independently. To demonstrate that the two different cell types that respond to blue and red light can be triggered without interference, we quantified the aggregation of cells expressing different photoswitchable proteins under different illumination conditions in suspension cultures. In suspension, cells expressing different photoswitchable proteins

on their surfaces (5×10^4 cells/ml) were incubated on a 3D orbital shaker at 30 rpm for 30 minutes in the dark, or either under far-red, blue or red light illumination (Figure 23).

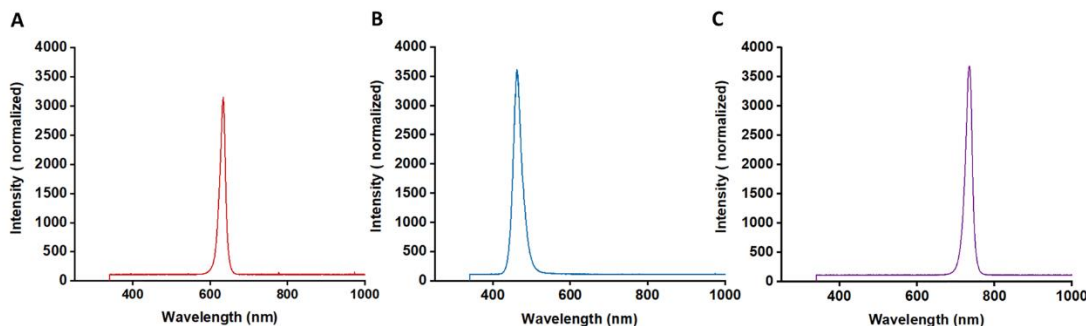


Figure 23: Spectra of used light sources. A) Blue light, (B) red light and (C) far-red light.

Appropriate shaking was important to increase the likelihood of cells coming into proximity, allowing the formation of cell-cell interactions and preventing sedimentation; however, too high shear forces can also disrupt the clusters.⁴³ Microscopy images of the suspension cultures showed that the blue light responsive VVD- and VVDHigh-MDA cells remained mostly as single cells in the dark as well as under far-red and red light illumination, but formed large aggregates under blue light (Figure 24A and B, tile scan image of the entire sample over 2.5 cm^2). On the other hand, red light responsive Cph1-MDA cells remained scattered in the dark as well as under far-red and blue light illumination, but assembled into aggregates under red light (Figure 24A). To support this qualitative observation of orthogonal response to blue and red light for VVD and Cph1 expressing cells, the aggregation was quantified by identifying clusters of cells (objects with an area $> 5000 \text{ } \mu\text{m}^2$, i.e. contain at least 20 cells) in the sample. This analysis showed that VVD- and VVDHigh-MDA as well as Cph1-MDA cells formed similarly large clusters with an average projected area of ca. $23000 \text{ } \mu\text{m}^2$ upon photoactivation (Figure 24C, D cluster size distribution). Yet, for all three cell lines the aggregation in the dark or under illumination that does not activate the photoswitchable proteins was comparable to the background levels observed for the parent MDA-MB-231 cell (Figure 24C, B and

C). Moreover, we also demonstrated that for VVD- and VVDHigh-MDA cells co-illumination with far-red light, which deactivates Cph1-MDA cells, does not interfere with the blue light triggered clustering. Overall, this analysis showed that VVD/VVDHigh-MDA and Cph1-MDA cells formed cell-cell interactions only upon blue and red light illumination, respectively, and therefore can be triggered independently from each other without interference.

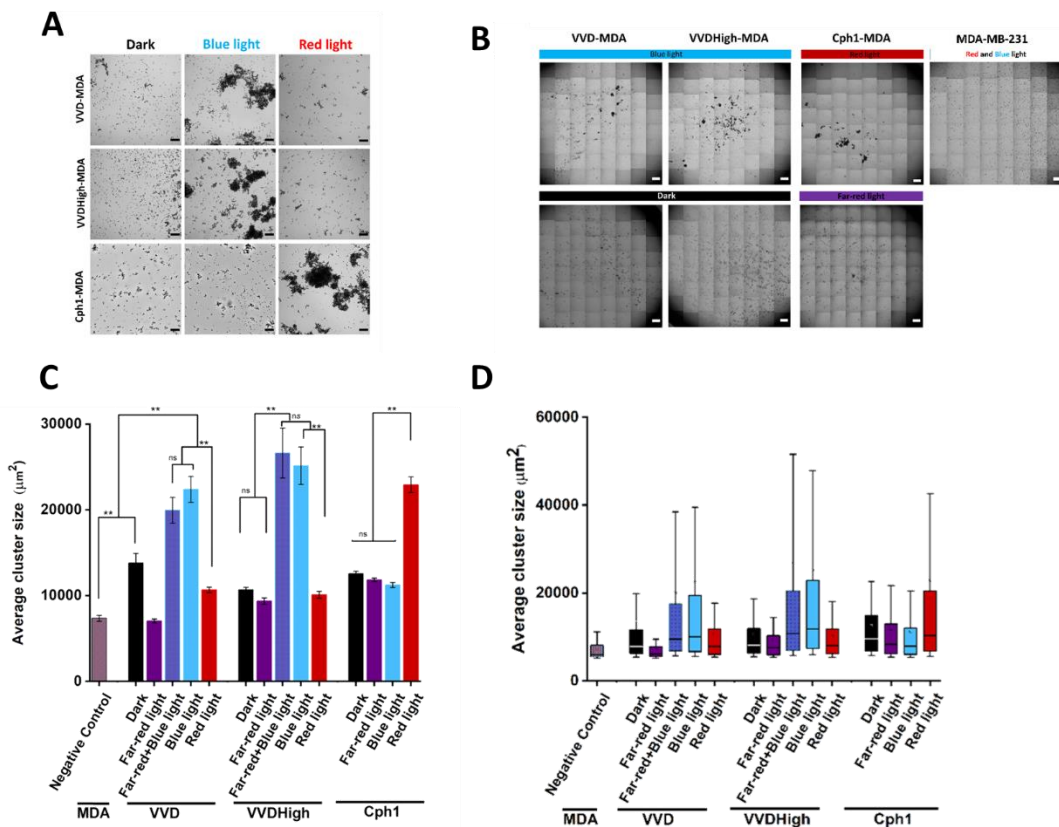


Figure 24: Independent control over cell-cell interactions with blue and red light. A) Bright field images of cells expressing different photoswitchable proteins at their surface (5×10^4 cells/ml) incubated for 30 minutes on a 3D orbital shaker at 30 rpm in suspension under different illumination conditions. VVD-MDA and VVDHigh-MDA cells aggregated only under blue light and Cph1-MDA cells only under red light but not in the dark or illumination with the other color of light. Scale bars are 200 μm . B) Exemplary tile scan bright field microscopy images of suspension cultures when cell-cell interactions were activated (upper row: VVD- and VVDHigh-MDA under blue light, Cph1-MDA under red light) and inactive (lower row: VVD- and VVDHigh-MDA in the dark, Cph1-MDA under far-red light). Cells expressing different photoswitchable proteins at their surface (5×10^4 cells/ml) were incubated for 30 minutes on 3D orbital shaker at 30 rpm in suspension under

different illumination conditions. For each data point in the aggregation analysis, such tile scan images composed of 64 fields of view were stitched together and analyzed using the MATLAB macro. All objects $>5000 \mu\text{m}^2$ (contain at least 20 cells) were identified as clusters. Each experiment was performed in biological triplicates with two technical replicates each. The scale bars are $1000\mu\text{m}$. C) Quantification of the cell aggregation in suspension cultures. For each sample an area of 2.5 cm^2 (64 fields of view) was imaged using a tile scan and stitched together. All objects $>5000 \mu\text{m}^2$ (contain at least 20 cells) were identified as clusters. The quantification showed that cells aggregation was light specific and illumination with other wavelengths of light did not lead to significant clustering beyond the dark control. Background clustering of MDA-MB-231 cells (negative control) show the background clustering compare with the light responsive cells kept in dark that is significant. Each experiment was performed in biological triplicates with two technical replicates each. Error bars are the standard error of the mean cluster area, $p < 0.01$ presented as **. D) Cluster size distribution upon light triggered cell aggregation. The cluster area distribution were shown as a box plot, where each box is defined as the first and third quartile of the data, the line in the box represents the median, the dots are mean and whiskers the 10th and 90th percentiles.

It should also be noted that the blue and red light used had no toxic effect on the cells as confirmed by a cell viability assay in suspension cells for 30 min (Figure 25).

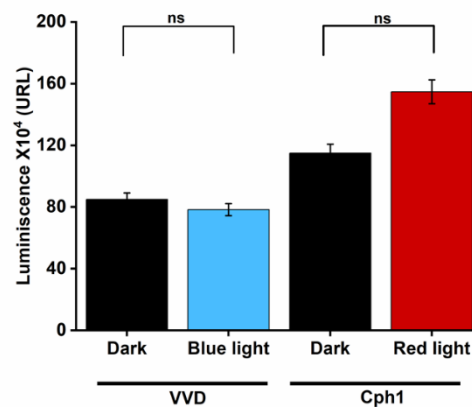


Figure 25: Light toxicity in cell aggregation experiments. VVD-MDA and Cph1-MDA cells were incubated for 30 min under blue and red light, respectively. The cell viability of illuminated cells was compared to cells kept in the dark using the CellTiter-Glo 2.0 Assay. No light toxicity was detected for either cells line. The error bars are the standard error of the mean from biological duplicates.

Dynamics and reversibility of light responsive cell-cell interactions. The reversibility and dynamics of cell-cell adhesions are important characteristics for their biological function, allowing cells to reorganize during morphogenesis and even allowing cells to break free of multicellular structures.^{166,167} Tools that allow for such dynamic and reversible regulation of cell-cell interactions are therefore extremely valuable when it comes to investigating the importance of spatiotemporal regulation of cell-cell interactions.^{19,92,133} For the here presented cell-cell interactions, we investigated the assembly and disassembly kinetics as well as the repeated switchability of multicellular structures formed from blue and red light responsive cells.

When cell-cell interactions were photoactivated VVD-MDA, VVDHigh-MDA and Cph1-MDA cells required different lengths of time to form aggregates in suspension cultures (Figure 26). Under blue light, VVDHigh-MDA cells formed aggregates of maximal size within the first 30 minutes. The size of these aggregates then decreased to a certain extent over the next few hours, presumably due to compacting of the clusters. In contrast, VVD-MDA cells required 2.5 hours under blue light to assemble into aggregates of a maximum size. Interestingly, while VVDHigh-MDA cells assembled faster than VVD-MDA cells, the VVD-MDA cells assembled into larger aggregates than VVDHigh-MDA cells. Cph1-MDA cells formed much larger multicellular assemblies under red light over the course of 3 hours compared with cells expressing VVD proteins under blue light (ca. 2.5 fold). In fact, Cph1-MDA cells formed even larger clusters than MCF7 cells, which are like MDA-MB-231 are a breast cancer cell line but with high E-cadherin expression. On the other side, cells expressing VVD proteins clustered less than MCF7 cells. Moreover, the cell clustering under light was faster for all photoswitchable proteins and already significant after 30 min, while the E-cadherin based clustering of MCF7 cells was slower and took over one hour. These differences in assembly dynamics and final aggregate size could be explained by factors including the differences in intrinsic

properties of the photoswitchable proteins, such as the thermodynamic and mechanical stability of the dimerization and the protein-protein interaction dynamics.¹⁹

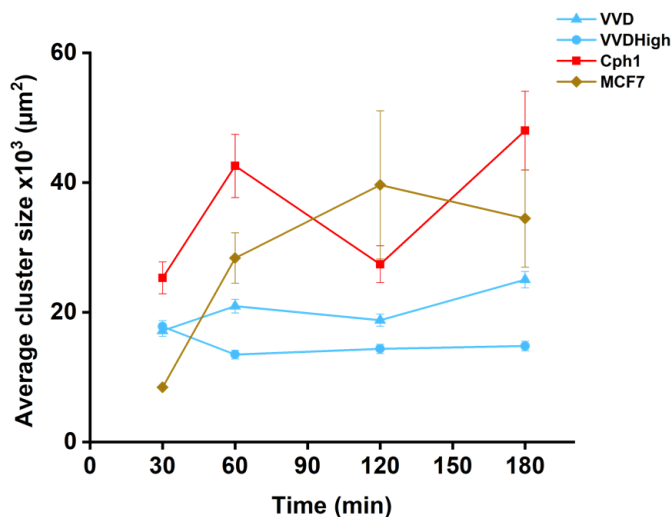


Figure 26: Comparison of photoswitchable protein mediated cell clustering under light and MCF7 cells as Cadherin mediated clustering. Cells Assembly and disassembly kinetics of multicellular aggregates. The VVD-MDA, VVDHigh-MDA and Cph1-MDA cells (5×10^4 cells/ml) were incubated on 3D orbital shaker at 30 rpm in suspension under blue light and red light, respectively and MCF7 for different durations. The average cluster size for VVD-MDA cell was approximately 2 fold larger than for VVDHigh-MDA cells. However, the average cluster size for Cph1-MDA is significantly higher than blue light dependent clustering. The data demonstrate that MCF7 cells as cadherin mediated clustering has a slower aggregation than our photoswitchable proteins which after 30 min still show no clustering. Although, through the time the average cluster size of MCF7 cells increasing and after 2 hours reach to saturated point which has higher average size than our blue light dependent clustering but the Cph1-MDA still has a significantly higher average cluster size.

An important feature of native cell-cell adhesions is their reversibility. Likewise, the cell-cell interactions mediated by the photoswitchable proteins were expected to be reversible due to the reversibility of the homodimerization of VVD in the dark and Cph1 under far-red light (Figure 27). In order to confirm this, the different cell types (VVD-MDA, VVDHigh-MDA and Cph1-MDA) were first aggregated under illumination that activated

cell-cell adhesions for 30 min and subsequently placed in the dark for VVD- and VVDHigh-MDA or under far-red light for Cph1-MDA cells.

The aggregation analysis for all cell types showed that within 10 min of stopping the photoactivation most of the aggregates significantly disassembled and within 30 min the aggregation was comparable to cells that were not photoactivated (kept in the dark for VVD- and VVDHigh-MDA and under far-red light for Cph1-MDA for the entire duration of the experiment). Interestingly, the reversion kinetics for the different cell types were similar despite the different reversion kinetics of the photoswitchable proteins at the molecular level (VVD in dark $t_{1/2}$ = 2 h, VVD-High in dark $t_{1/2}$ = 4.7 h, Chp1 under far-red light $t_{1/2}$ = ca. ms). The differences in reversion time at the molecular level and the cell-cell interactions show that it is not the reversion at the molecular level but other steps such as the separation of two cells from each other, the number of multivalent interactions and the disassembly of the multicellular clusters that are the rate determining steps. It should be noted that we have observed similar differences in the reversion kinetics at the molecular and the cell-cell adhesion level using other heterophilic light responsive protein-protein interactions.

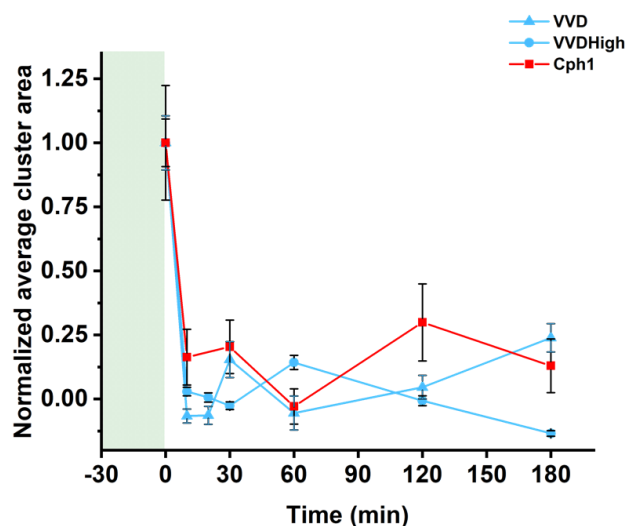


Figure 27: Light reversion kinetics. Reversibility of the light mediated cell-cell interactions in the dark and far-red light after 0 min preillumination with blue (for VVD- and VVDHigh-MDA cell) and red light (For Cph1-MDA cells). The mean cluster area was normalized to control samples kept in dark. Error bars are the

standard error of the mean cluster area. Each experiment was performed in biological duplicates with two technical replicates each.

The reversibility of the blue and red light-triggered cell-cell adhesions allowed us to switch them on and off repeatedly. To check repeated switchability, suspensions of different cell types were alternated over three cycles between 30 min light activation and 30 min reversion. Bright field images acquired after each step showed that VVD- and VVDHigh-MDA cells associated into multicellular clusters every time they were incubated under blue light and dissociated from each other every time they were placed in the dark (Figure 28A and B). Similarly, Cph1-MDA cells associated and dissociated over multiple cycles when they were alternated between red and far-red light (Figure 28C).

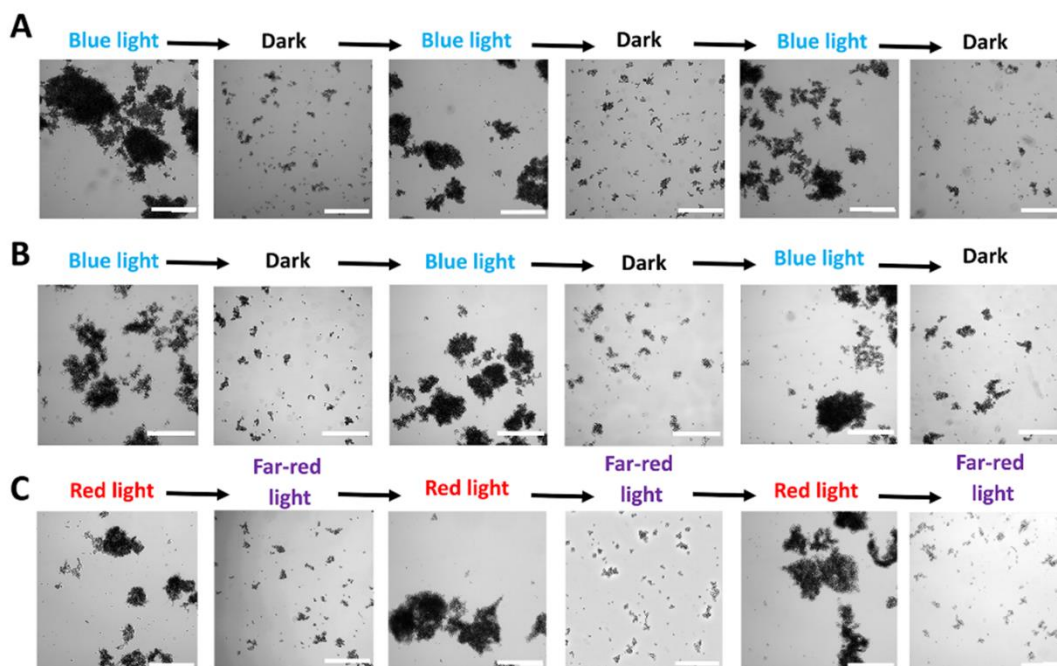


Figure 28: Reversibility of the photoswitchable cell-cell interactions. Bright field images of (A) VVD-MDA, (B) VVDHigh-MDA and (C) Cph1-MDA cells in a suspension (5×10^4 cells/ml) altered between activating (30 min) and deactivating (30 min) conditions over multiple cycles. Scale bars are 300 μm .

The quantitative analysis of the aggregation showed that for all three cell types' reversion was complete each time the interactions were turned off following photoactivation.

Further, in VVD-MDA cells the amount of aggregation decreased in the second and third blue light activation cycle compared to the first light activation, which indicates partial fatigue (Figure 29A). In contrast, VVDHigh-MDA and Cph1-MDA cells aggregated equally well after each illumination cycle and showed no fatigue, i.e. no change in aggregation over multiple cycles (Figure 29B, C). Overall, both the blue and red light switchable cell-cell interactions were reversible and could be switched on and off repeatedly, which captures important properties of cell-cell interactions.

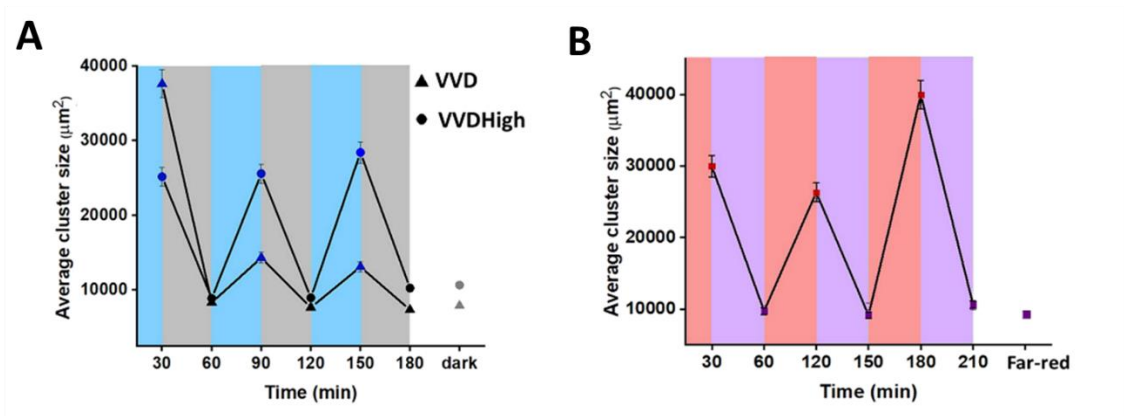


Figure 29: Reversibility of the photoswitchable cell-cell interactions. A) Average cluster size for VVD-MDA (triangles) and VVDHigh-MDA (circles) over multiple blue light (blue points) /dark (black points) cycles. Blue and grey shaded backgrounds indicate 30 min periods where the blue light illumination was turned on and off, respectively. B) Average cluster size for Cph1-MDA cells under altered illumination. Red and violet shaded backgrounds indicate 30 min periods under red (red square) and far-red (violet square) light, respectively. Cells were kept in the dark (VVD- and VVDHigh-MDA) or under far-red light (Cph1-MDA) as negative controls for the entire experiment. Both blue and red light dependent cell-cell interactions switched on and off over multiple cycles. For each sample an area of 2.5 cm² (64 fields of view) was imaged using a tile scan and stitched together. Each experiment was performed in biological triplicates with two technical replicates each. Error bars are the standard error of the mean cluster area.

Light specific self-sorting in multicellular mixtures. Finally, we explored whether we could control self-sorting in a multicellular mixtures and address different cell types within the mixture independently after exposure to blue and red light. For this purpose, we mixed equal numbers of VVD-MDA (labelled with a red fluorescent dye) and Cph1-MDA (labelled with a green fluorescent dye) cells and observed their assembly either under blue or red light or co-illumination with both colours of light after 30 min incubation with . In the dark, the two cell types were well dispersed (Figure 30A) and their self-assembly was inducible for one cell type at a time using two different wavelengths of light. Under blue light, VVD-MDA cells assembled into clusters, which were observable as large red fluorescent aggregates, and Cph1-MDA cells labelled in green remained dispersed (Figure 30B). Conversely, under red light, only Cph1-MDA cells self-assembled into large aggregates, observed as large green fluorescent objects, whereas VVD-MDA cells remained more scattered (Figure 30C). Most remarkably, the simultaneous illumination with blue and red light, resulted in the self-sorting of VVD-MDA and Cph1-MDA cells into distinct green and red fluorescent cell clusters with almost no intermixing of the two cell types within the same cluster (Figure 30D). The sorting out of the two cell types was also confirmed by 3D confocal microscopy cross-sections of the clusters (Figure 30E).

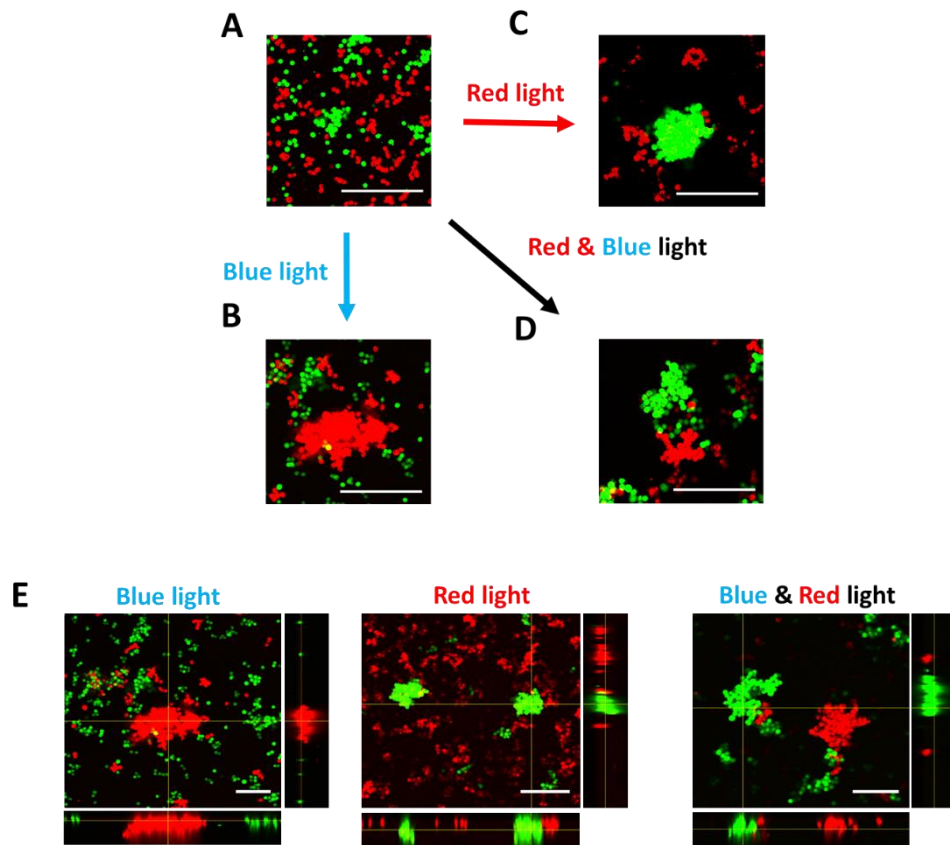


Figure 30: Blue and red light controlled self-assembly and self-sorting. Confocal images of VVD-MDA (red fluorescence channel) and Cph1-MDA (green fluorescence channel) mixed in a 1:1 ratio (A) in the dark, (B) under blue light, (C) under red light and (D) under coillumination with blue and red light. E) Confocal images in self-sorting multicellular mixtures. Confocal images of VVD-MDA (red fluorescence channel) and Cph1-MDA (green fluorescence channel) under blue, red light and coillumination with blue and red light. Scale bars are 200 μm .

For quantification the images were analyzed by using colocalization of the fluorescence signals. The threshold overlap score (TOS) and Pearson's Correlation Coefficient (POS) value described the colocalization from complete colocalization (value 1) over noncolocalisation (value 0) to complete anticlocalization (value -1), (Figure 31). The result shown a minus TOS and POS, meaning complete anticlocalized by light illumination (Figure 31D).

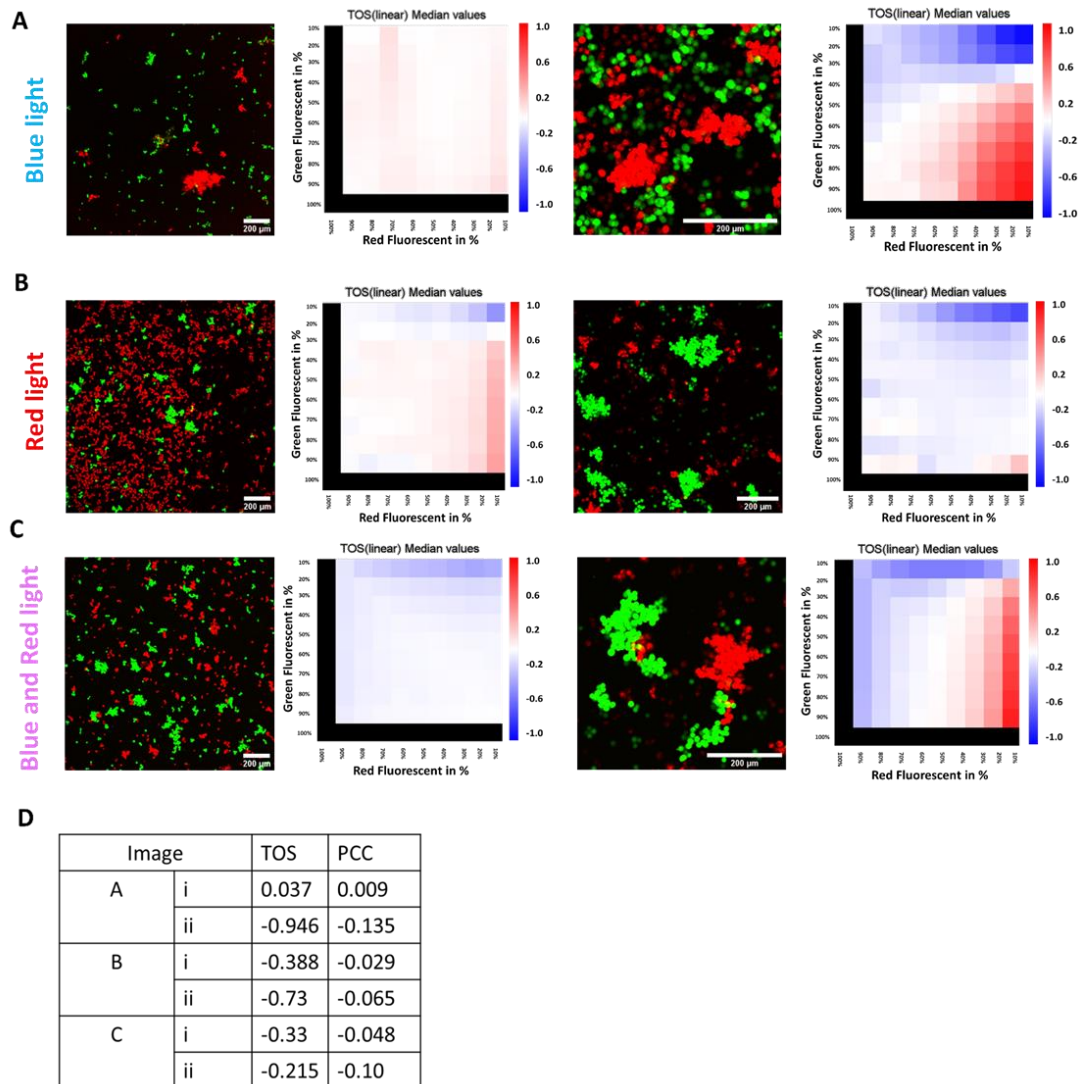


Figure 31: Colocalization analysis of different cell types during self-sorting. Confocal images and metric matrix for TOS (Threshold Overlap Score) for 1:1 mixtures of VVD-MDA (in red) and Cph1-MDA (in green) (A) under blue light, (B) under red light and (C) under both blue and red light. A TOS (and PCC (Pearson's Correlation Coefficient)) of red and green fluorescent pixels of -1 shows complete anticlocalization, of 0 shows no colocalization and 1 shows complete colocalization. Scale bars are 200 μm . (D) Overall TOS and PCC of images in A-C. In each of the samples the red and green pixels have negative TOS and PCC scores showing no colocalization and hence self-isolated clusters of each cell type.

The qualitative observations of light specific cell-sorting was further supported by quantitative aggregation analysis in mixed VVD-MDA and Cph1-MDA cultures based on bright field microscopy images as described above (Figure 32).

In the 1:1 mixed VVD-MDA and Cph1-MDA cultures, the aggregation increased both upon blue or red light illumination when compared to experiments in the dark. Moreover, the amount of aggregation doubled under co-illumination with blue and red light compared to illumination with just one colour of light, as both cell types were photoactivated.

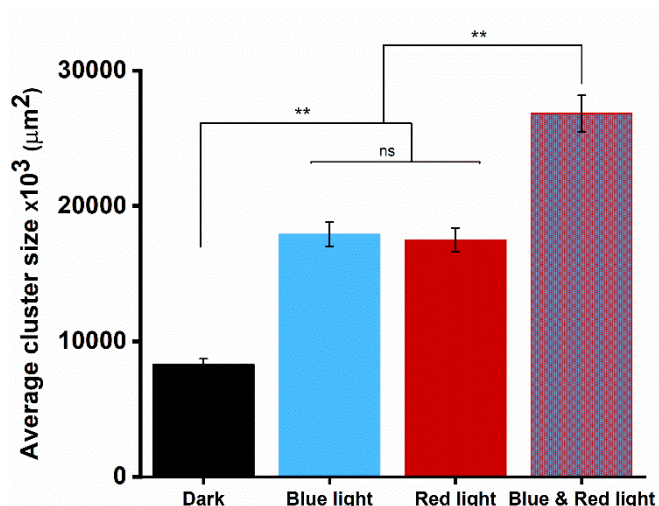


Figure 32: Blue and red light controlled self-assembly and self-sorting. Average cluster size analysis of VVD-MDA and Cph1-MDA cells mixed in a 1:1 ratio under different illumination. For each sample an area of 2.5 cm² (64 fields of view) was imaged using a tile scan and stitched together. Each experiment was performed in biological triplicates with two technical replicates each. Error bars are the standard error of the mean cluster area, p <0.01 presented as **.

It should be noted that the labelling with the fluorescent dyes had no effect on the cell aggregation under light activation (Figure 33).

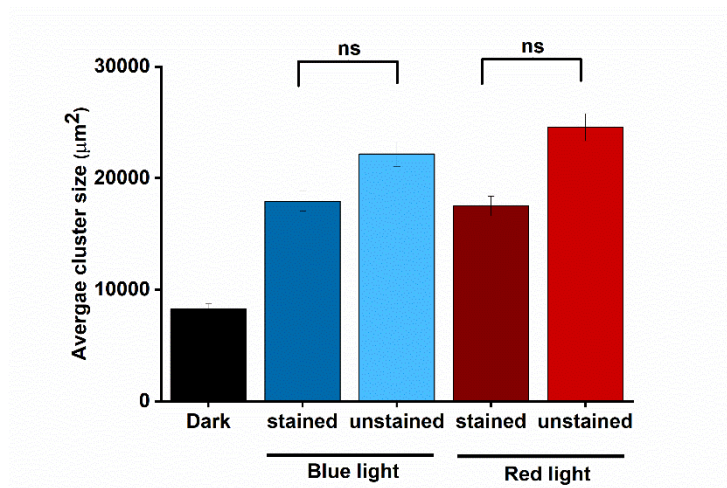


Figure 33: Effect of cell staining on light triggered cell-sorting. The comparison of the average cluster size in mixtures of VVD-MDA and Cph1-MDA cells that were either stained or unstained. The analysis shows no significant effect of staining on the clustering. Error bars are the standard error of the mean cluster area. The experiments were performed in biological triplicates with two technical repetitions each.

Summery

The self-assembly of different cell types into multicellular structures and their organization into spatiotemporally controlled patterns are both challenging and extremely powerful to understand how cells function within tissues and for bottom-up tissue engineering. Here, we not only independently control the self-assembly of two cell types into multicellular architectures with blue and red light, but also achieve their self-sorting into distinct assemblies. This required developing two cell types that form selective and homophilic cell-cell interactions either under blue or red light using photoswitchable proteins as artificial adhesion molecules. The interactions were individually triggerable with different colors of light, reversible in the dark and provide non-invasive and temporal control over the cell-cell adhesions. In multicellular mixtures, upon orthogonal photoactivation each cell type self-assembled independently and cells sorted out into separate assemblies based on specific self-recognition. These self-sorted multicellular architectures provide us with a powerful tool for producing tissue-like structures from multiple cell types and investigate principles that govern them.

Summary

In summary we developed a homodimerization cell-cell system that can independently control the self-assembly of two cell populations into blue and red light dependent into distinct assemblies. Therefore, by using the blue and red light dependent homodimerization of VVD and Cph1, respectively. We were able to induce interactions between VVD-MDA cells and Cph1-MDA cells that express the respective proteins on their surfaces upon blue and red light illumination and then simply not only turn them off by switching off the light, but also could self-assemble them into distinct cellular interactions. These photoswitchable cell–cell interactions have the potential to capture key features of native cell–cell interactions in terms of spatiotemporal control, sustainability, dynamics, and reversibility but not cellular signalling associated to cell–cell interaction. Additionally, these protein-based photoswitches are well-suited to sustainably control the cell–cell interactions over a long period of time because they are genetically encodable and new proteins are expressed in the cells as they degrade and the cell divides. Moreover, the low intensity of blue and red light that triggers these cell–cell interactions are noninvasive for the cells. Notably, the control with light makes it possible to induce these interactions with unmatched precision in space and time. These interactions are dynamic and reversible, which enables modifying cell–cell interactions over time as observed during biological processes. These light dependent switchable cell–cell interactions can be used to build multicellular architectures, used in scaffold-free bottom-up tissue engineering and also to study biological processes where cell–cell interactions play an important role.

3.3 The dynamic differential adhesion hypothesis: The role of cell-cell adhesion dynamics in cell sorting

Following section is based on:

The dynamic differential adhesion hypothesis: the role of the cell-cell adhesion dynamics in cell sorting

Rasoulinejad S., Wegner, S. V. (2020), Submitted

Contribution

I performed all the experiments including the analysis of the data and Seraphine V.

Wegner supervised the work.

Building multicellular structures based on self-assembly count as challenging to understand how cells function within tissues and simultaneously is a bottleneck in bottom-up tissue engineering. Although the importance of the cell-cell adhesion for tissue growth and multicellular pattern formation already noticed but understanding the role of the dynamic interaction of cells remain unanswered. The *de novo* self-assembly of spatially ordered cellular structures from cells as the basic building blocks is the ultimate challenge in tissue engineering.¹ To build multicellular structures, one cannot simply put the cells together in a solution and obtain the right arrangement of cells; the assembly into a tissue like structure requires precise interactions between the cells such that they can properly organize. The correct spatial organization of these building blocks into hierarchical structures is primordial to generate a functional tissue such that cells can work together.^{2,3}

The bottom-up approach to tissue assembly parallels observations during early tissue formation, where no template or scaffold is needed. In particular, cell-cell interactions are a major driving force that determines their organization.⁴ Even more remarkably, dissociated cells from different tissues are able to self-aggregate and self-sort again into multicellular structures replicate the arrangement in their tissues of origin.^{5,6} Going forward it is necessary to understand how cells as the basic building blocks of tissue self-assemble and sort into organized tissue and how far the principles of self-assembly known for nonliving cell sized objects applying to the cells and to what extent the cell biology plays a role. Such insight would allow building up multicellular architectures with more programmable organization and understand the limits of multicellular structures that can be generated based on self-assembly and where further biological signals are required.⁷ This puts forward the importance of controlling different aspects of cell-cell interactions; their strength, their exchange dynamics and their connection to intracellular signaling.

There are several hypothesis to explain how cells self-assemble into multicellular structures and sort out in vitro and during embryogenesis. In 1955, Townes and Holtfreter studied the organization of different cell types that originate from different germ layers of the early vertebrate embryo.³⁸ The observations showed that cell sorting and tissue reorganization depends on the selective affinity and directed migration during embryo development.^{38,39} Later, these and other experiments led to the proposal of the Differential Adhesion Hypothesis (DAH) by Steinberg as a model to predict cell-sorting behavior.⁴⁰ The DAH propose that the differences in the adhesion energies between cells, which come from the identity of the adhesive molecules on cell surface and their expression levels, cause cells to sort out in order to reduce their interfacial free energy.^{41–43} The DAH states that cells can explore various configurations to finally reach the lowest-energy configuration and predicts that the final configuration is where cell-cell adhesions are maximized. This sorting behavior is homologous to the organization observed in

liquid-liquid phase separation.³² The simplicity of the DAH, where cells organize under thermodynamic control, provides a basis for the free-scaffold of assemble in bottom-up tissue engineering.

Other mechanisms of cell sorting have also been proposed. Jones *et al*,⁶⁴ proposed cell sorting based on differences in cell velocity. Here, two factors lead to cell sorting in heterotypic aggregation. The first one is selective adhesion between different cell types; cell aggregation occurs based on tissue-specific properties through recognition procedure. Second, the different cell types arrange according to their relative motilities, such that cells with higher mobility will segregate internally.⁶⁴ The differential interfacial tension hypothesis (DITH), introduced by Brodland, places the contractility of the cortical actomyosin cytoskeleton as a major driving force of cell sorting.⁴⁵ The DITH states that the cytoskeleton components and cell adhesion mechanisms contributed to the cell sorting, shape, and migration during development.^{45,48-50} All the above hypotheses are directly or indirectly based on the cell adhesion with a small difference in definition with DAH. Therefore, in general, it pointed out the role of cell-cell adhesions is not negligible but if the adhesion between the cells is sufficient for sorting out or if it requires connection to the actin cytoskeleton as assumed by the DITH or differences in cell behavior upon intracellular signaling is not clear. It should be noted that after the DAH formulation, the author stated: "*that the specific sorting of cells may result from different mechanisms than from those involved in the initial formation of aggregates*". Studies presented that cell sorting is indeed facilitated by the differential adhesion-governed hierarchy of tissue surface energies⁴² and other cell properties probably impact the patterning of a tissue *in vivo*.^{33,67,68}

Cells adhere to neighbouring cells and form cell-cell contact mainly through cadherins at the cell surface. Through their intracellular domains cadherins connect to the actin cytoskeleton and mechanosensing as well as signalling cascades. Cell-cell adhesions form dynamically and are tightly regulated in space and time during many biological

events including embryogenesis, wound healing and cancer development. Consequently, controlling cells interactions is important for both understanding the biochemical machinery and for application in biomedicine such as bottom-up tissue engineering and cell-based screening devices. Current approach for controlling cell-cell interaction are limited in term of dynamicity, sustainability, high spatiotemporal resolution and reversibility.

While all the above-mentioned cell sorting mechanisms show the importance of cell-cell adhesions, the importance of the cell-cell interaction dynamics for the final multicellular structure has been overlooked. In all the studies until now using the native cadherins the fast exchange rates of cadherins have led to the thermodynamically controlled multicellular structures predicted by the DAH.⁶⁹ Yet, the dynamic nature of the cell-cell adhesions was assumed to be a given. Therefore, the question of what kind of tissue structures can be generated based on the principles of self-assembly and self-sorting using cell-cell interactions with different exchange dynamics remains unanswered. In this study we address two open questions in the field of cell sorting; if the connection to the intracellular signaling and actin cytoskeleton is required for cells to sort out and how cell-cell interaction dynamics impact the formation of multicellular structures and cell sorting. To tackle these questions, we use previously described blue and red light switchable artificial cell-cell interactions, which can selectively be turned on simply turning on the right color of light, and examine the formation of multicellular structures of cells of two different types of cells. The photoswitchable interactions allow for the regulation of cell-cell adhesions without directly connecting to the intracellular signaling and pulsed photoactivation for varying the exchange rate of cell-cell adhesions. . In spheroids we demonstrate that cell sorting is possible with these artificial cell adhesion molecules and the cell sorting follows the patterns predicted by the DAH. In the cell sorting process, the cell-cell adhesions being dynamic is of critical importance; only if cell-cell adhesions are dynamic cell sorting is possible and multicellular structures that maximize cell-cell

adhesions under thermodynamic control form. On the other hand, if they are not kinetically trapped cellular assemblies form. These results support the concept of Steinberg's differential adhesion hypothesis and highlight the importance of cell adhesion dynamics.

The connection between cell-cell adhesion dynamics and spheroid compactness.

The dynamic exchange of protein-protein interactions that mediate the cell-cell interactions is an important characteristic for their biological function and is critical during the reorganization of cells in morphogenesis and assembly of multicellular structures.^{166,167} The importance of the strength of cell-cell adhesions in the compacting of multicellular structures is evident when comparing the two breast cancer cell lines MDA-MB-231 and MCF-7. MDA-MB-231 cells that lack cell-cell adhesion molecules on cell surface form loose aggregates with little direct contacts between the cells (Figure 34). On the other hand, MCF-7 cells, which have a high E-cadherin expression, form round and compact spheroids. In this case, the adhesion molecules on cell surface lead to efficient cell interactions and as a consequence result in more prominent compactness into a sphere (Figure 34). For the tissue or any other multicellular structure to form, the free edges of cells have to meet each other and establish cell-cell interaction. Therefore, classic cadherin as adhesive molecules help to stabilize these physical contacts. Furthermore, cadherin mediated interactions are connected to their partner protein to anchor them to the actin cytoskeleton as the cell scaffold.¹⁶⁸ To this point, photoswitchable proteins as adhesive cell surface molecules were presented on cell surface to mirror these natural physical interactions but not the connection to the actin network.

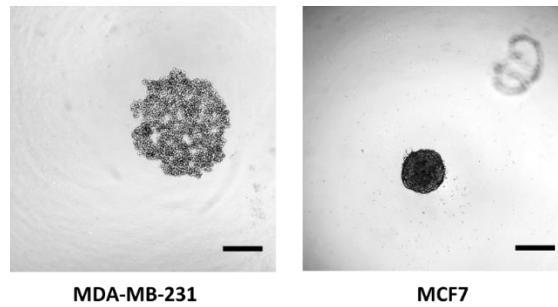


Figure 34: Bright field images of spheroid formation of MDA-MB-231 and MCF7 cells, 3000 cells/well. The MDA-MB-231 spheroid is loose with porous structure in comparison to the MCF7 spheroid, which is circular and compact. Scale bar is 300 μm .

To investigate if the light inducible cell-cell interactions can lead to spheroid compacting, cells with blue or red light switchable cell-cell interactions were investigated under different illumination conditions. For this purpose, 5×10^2 or 2×10^2 VVD-, VVDHigh and Cph1- MDA cells per well were seeded in 3D culture (gently centrifuged (200xg for 3 min) to let them settle down through the methylcellulose) and afterwards either illuminated continuously in activating light (blue light for VVD- and VVDHigh-MDA, red light for Cph1-MDA) or kept in the dark (as well as under far-red light for Cph1-MDA), where the cell-cell adhesion are not active, overnight.

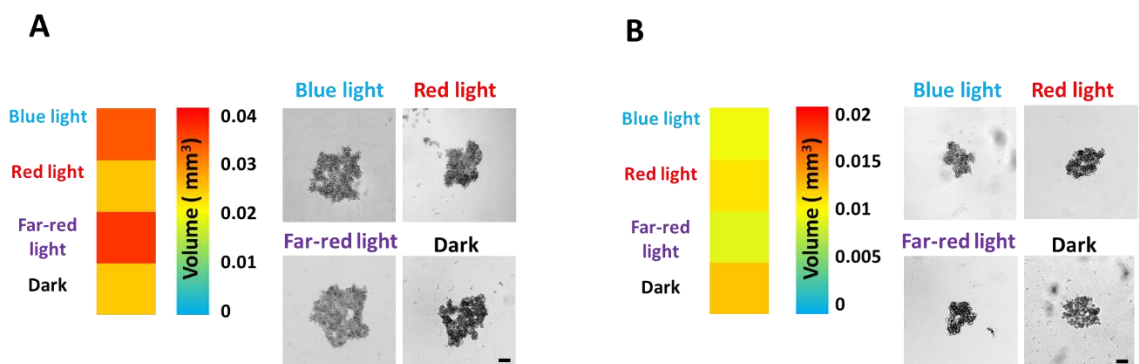


Figure 35: MDA-MB-231 spheroid size under light illumination. A) 500 cells/well of MDA-MB-231 illuminated under different lights. B) 200 cells/well of MDA-MB-231 illuminated under different lights. Scale bars are 100 μm

The bright field microscopy images showed, all three cell types in the dark as well as Cph1-MDA under far-red light showed similar loose cell aggregates as the parent MDA-MB-231 cells (Figure 35, 36). This was expected as in the dark the cells can move freely to interact but they do not adhere to each other strongly. Thus, in this scenario cells have the required dynamic exchange of cellular interaction partners but not the required interaction strength. Consequently, they are not able to form a compact spheroid. More surprisingly, under continuous activating illumination still also only loose cellular aggregates and not compact spheroids form despite the cells interacting with to each other. To support this qualitative observation of spheroid compactness in the dark and in response to blue or red light for VVD, VVD^{High} and Cph1 expressing cells, the spheroid volume was quantified by identifying the minor and major axis of spheroids in each well. The analysis showed indeed that although the cells interaction induces under light illumination, as previously demonstrated in suspension culture, the spheroids did not compact upon illumination. One possible explanation for this observation is the lack of cell-cell adhesion dynamics. Under continuous light illumination the cell-cell adhesions are very strong and permanent that the cells do not have time to exchange neighbours and rearrange, which is required for compacting. In other words, the strong and undynamic cell-cell adhesion freeze the cells in place and prevent spheroid compacting (Figure 36A-C).

To test this hypothesis, the dynamics of the cell-cell adhesions was increased. In particular, the spheroids were illuminated with pulses of light with different on (1, 5, 10 min) and off (1, 5, 10, 20 min) durations. Spheroids of all three cell types altered their compacting depending on the on and off time of the illumination. In all three cases both too short light activation of 1 min and too long light activation of 20 min, resulted in lower compacting compared to intermediate duration light pulses of 5 min, regardless of the off time. For example, VVD-MDA spheroids (5×10^2 cells per well) under 1 min or 20 min blue light illumination with different off times from 1 min to 20 min had an average

spheroid size around 0.03 mm^3 . On the other hand, the same spheroids with 5 min blue light illumination with different off timing has around 0.019 mm^3 and at 5 min on and 20 min off reach to their most compact state, which is around 0.01 mm^3 (Figure 36A). For VVD-MDA spheroids the compacting increased as the off time in the pulsing protocol increased from 1 to 20 min as long as the blue light illumination time was kept at 5 min. On the other hand, for 1 min illumination, where the cell-cell interactions are not completely activated, the spheroid compactness was higher at lower off times, probably due to a higher overall photoactivation.

These findings show that neither too little interaction between the cells, which is the case with short photoactivation, nor too much interactions between the cells, which is the case with long photoactivation, improves the total cell-cell adhesions. It seems that the fine balance between cell-cell adhesions but also the possibility to exchange interaction partners is critical.

The VVDHigh-MDA spheroids (5×10^2 cells per well) at 20 min blue light illumination with different off times the largest spheroids are obtained with short off times and are in the range of 0.03 mm^3 . Although with short off times the spheroids at 1 and 5 min blue light illumination seem similar, more compact spheroids form at 5 min on/20 min off with a size of 0.006 mm^3 . Similarly compact spheroids form under 1 min blue light and 1 min dark illumination has the size of 0.0128 mm^3 . On the other hand at 20 min on/ 20 min off they reach to their minimum compactness which is near to the deactivation which is 0.037 and 0.036 mm^3 . The comparison between VVD-MDA and VVDHigh-MDA under 5 min on /20 min dark, with respectively size of the spheroid from 0.0148 mm^3 to 0.006 mm^3 , shows although both cell type in this time range has the most compactness but VVDHigh-MDA still become more compact than VVD-MDA (Figure 36A and B).

Similar to the VVD- and VVDHigh-MDA spheroids, also for the Cph1-MDA spheroids (5×10^2 cells-well) under 1 and 20 min red light illumination with different off times less compact spheroids formed compared to 5 min red light illumination. from 1 min to 20

min showed they have similar range around 0.02 mm^3 and under 5 min red light illumination has the minimum spheroid volume size around 0.001 mm^3 , which under 5 min on and 20 min off time is about 0.007 mm^3 (Figure 36C).

Interestingly, for all three different cell types the same light pulsing protocol of 5 min on/20 min off, led to the highest compactness. This finding is consistent with previous result, which showed that these three cell types have similar reversion kinetics in the dark.¹⁶⁹

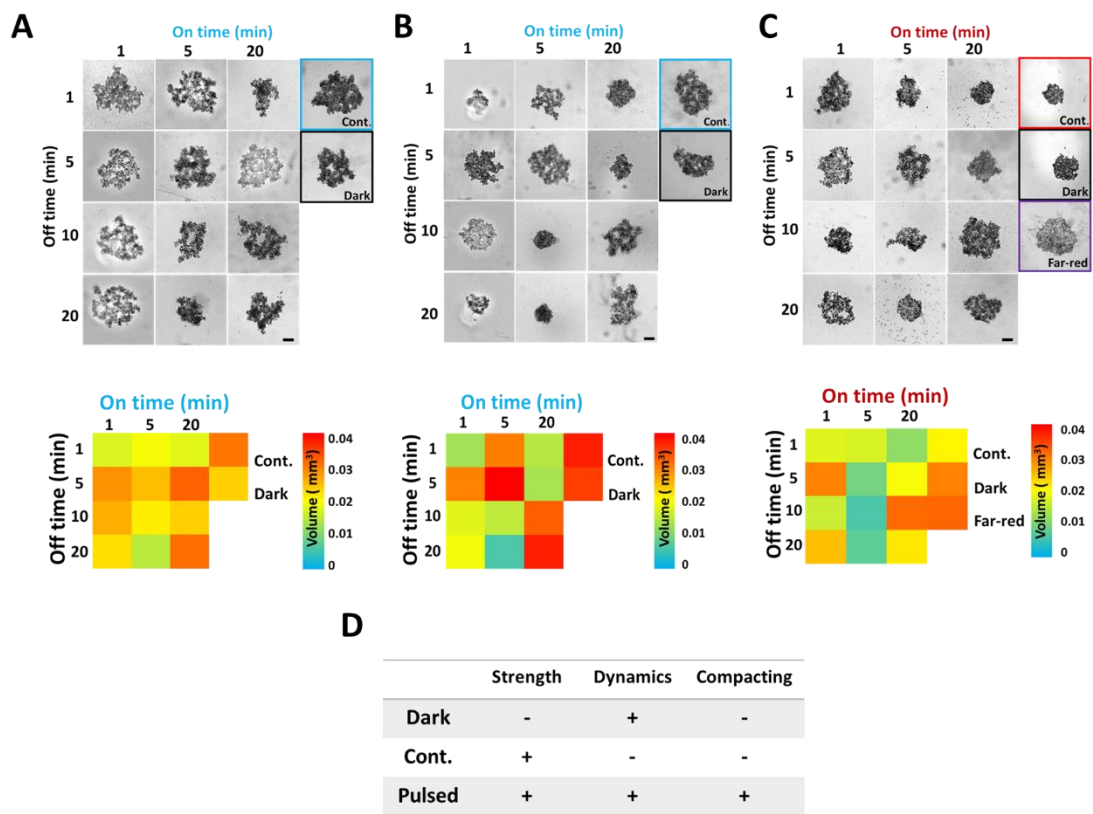


Figure 36: Dynamics of cell-cell adhesions. The result of blue and red light illumination under different condition. (A) VVD (B) VVDHigh cells are illuminated under dark, continues and alternating blue light and (C) Cph1 cells are illuminated under dark, far-red, continues and alternating red light. The bright filed images and the color map both demonstrate difference between activation and deactivation of adhesion molecules when they controlled under kinetic and thermodynamic. Scale bars are $100\mu\text{m}$. Amount of cell for each well is about 500 cells/well. The color map data analyzed using Excel. D) The summery table of the combination of dynamic and active strength of interactions and their influence on cell compacting as final result.

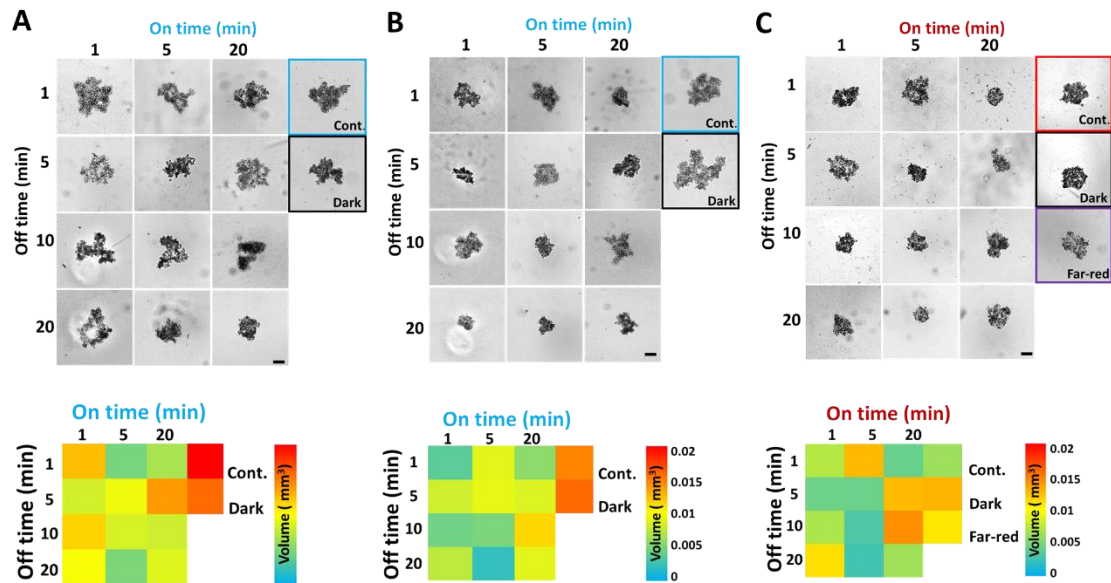


Figure 37: Dynamics of cell-cell adhesions. The result of blue and red light illumination under different condition. A) VVD (B) VVDHigh cells are illuminated under dark, continues and alternating blue light and (C) Cph1 cells are illuminated under dark, far-red, continues and alternating red light. The bright filled images and the color map both demonstrate difference between activation and deactivation of adhesion molecules when they controlled under kinetic and thermodynamic. Interestingly, the optimum dynamic interaction (5 min on and 20 min off time) for different cell types are similar, which is agreement of the previous data showed these three cell types has similar reversion kinetic (cite our paper which is under review). All scale bars are 100 μ m and 200 cells/well are seeded. The color map data analyzed using Excel.

In the compacting of the spheroids the balance between cell-cell adhesion strength and their dynamics is altered through the balance of activation and deactivation with pulsed light. Under continuous illumination and 20 min light activation the cells the cell-cell adhesion strength is high yet the spheroids were large in size and did not compact. On the other hand, 1 min illumination did not activate cell-cell adhesions enough to result in compacting. When intermediate activation with 5 min illumination is used cells deform to come in contact with each other, indeed they build and increase the adhesion area which will lead to increase the surface free energy. The dynamics of the cell-cell interactions allow for the maximization of the free energy, meaning that cells exchange their position and interactions form with higher probability if this exchange is energetically

favorable.^{138,170–172} Based on these observations when the interactions between cells are dynamic, the spheroids get more compact and more circular under this thermodynamic control. However, when the interactions are not dynamic and the spheroid formation is controlled kinetically, the cells do not exchange neighbours and porous and loose spheroids form as observed under continuous illumination. Therefore, the compactness of spheroid is dependent on how cell interactions will be controlled, thermodynamically or kinetically. In fact, when cells that express photoswitchable proteins at their surface are activated with pulses of light, cell-cell adhesions form during the on time and dissociate during the off time. This dynamic exchange of cell-cell adhesions, controlled by the illumination protocol, allows the cells to reposition themselves such that they can maximize the adhesions to their neighbours.

According to classical Derjaguin-Landau-Verwey-Overbeek (DLVO) theory, the probability of two particles (here cells) to adhere to each other is called “Sticking coefficient – (α) “. Whenever the sticking coefficient is equal to 1, particles stick together the first time they meet or in other words the chance of adhering together is 100%. As a result dendritic shaped assemblies form. In contrast, if the sticking coefficient be less than 1, it allows the particles to reposition and leads to the formation of denser and more compact structures. Finally, when the sticking coefficient is zero the particles do not stick together and no assembly takes place.¹⁷³

The protein-protein interaction to mediate the adhesions are dynamic as they are based on non-covalent bonds at the protein surfaces. Thus, the formed cell-cell adhesions undergo assembly and disassembly at steady state. At different illumination and deactivation, the equilibrium is shifted and changes the dynamics of the cell-cell adhesions. In terms of the sticking coefficient it means that at high photoactivation it is closer to 1 and as the dynamics increase it decreases to result in more compact structures. At too low photoactivation or in the dark the sticking coefficient is close to zero and as a result again the spheroids do not compact.

Each on and off illumination cycle can be seen as a two step event. At first upon photoactivation, the cells increase the adhesion energy to their neighbours for the duration of the light pulse. In the second stage, during the off time, the cells partially let go and can move to find a potential better binding partner. The higher the interaction strength the less likely the cell is to let go of its neighbour. If the off time is shorter or longer than they need, this process will not be efficient. Thus, the proper balance between the activation and deactivation of cell-cell interactions leads to the proper compacting. In the two extremes, in the dark and under continuous illumination the first and the second stage, respectively, do not take place and thus compacting is not observed.

It should be noted that the blue and red light used in these experiments had no toxic effect on the cells as confirmed by a cell viability assay in spheroid culture. For this purpose, the cell viability was measured for the continuous illumination at different light intensities over 3 days. 0.1, 1 and 10 percent intensity of blue, red and far/red light measured (Figure 38 A and B). After overnight light illumination red light, far-red and blue light did not show any significant light toxicity at any of the tested intensities compared to the dark control. However, in all experiments 1% intensity of light was used during the illumination protocols (Figure 35-37). Moreover, the light toxicity at 1% light intensity was measured over 3 days. The result showed for all three colours of light after 3 days continuous illumination had no significant difference with the first day (Figure 39).

A

Intensity percentage	0.1	1	10
Blue light	2.04 ($\mu\text{w}/\text{cm}^2$)	20.4 ($\mu\text{w}/\text{cm}^2$)	204 ($\mu\text{w}/\text{cm}^2$)
Red light	2.32 ($\mu\text{w}/\text{cm}^2$)	23.2 ($\mu\text{w}/\text{cm}^2$)	232 ($\mu\text{w}/\text{cm}^2$)
Far-red light	2.52 ($\mu\text{w}/\text{cm}^2$)	25.2 ($\mu\text{w}/\text{cm}^2$)	252 ($\mu\text{w}/\text{cm}^2$)

B

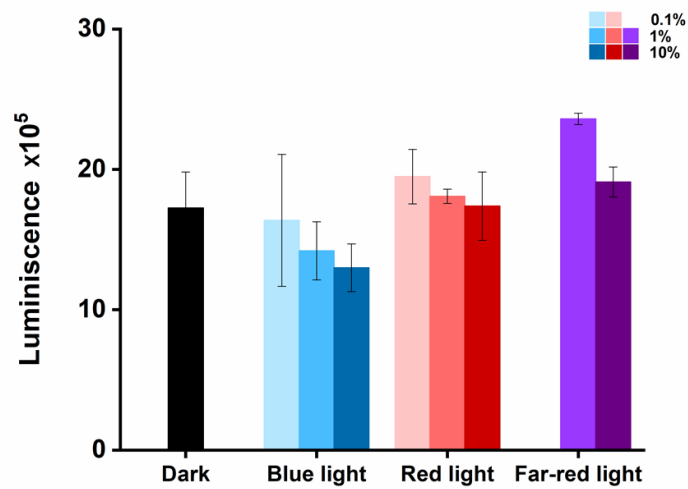


Figure 38: The toxicity of different light intensity and wavelengths. The toxicity of different light intensity and wavelengths. The result of cell viability under different light intensity illuminations. The 1% intensity selected for further illumination. The statistical analyses showed any significant difference for these three light intensity. Mann-Withney-U test was performed to analyze the statistical difference, p-values $p > 0.05$ (not significant).

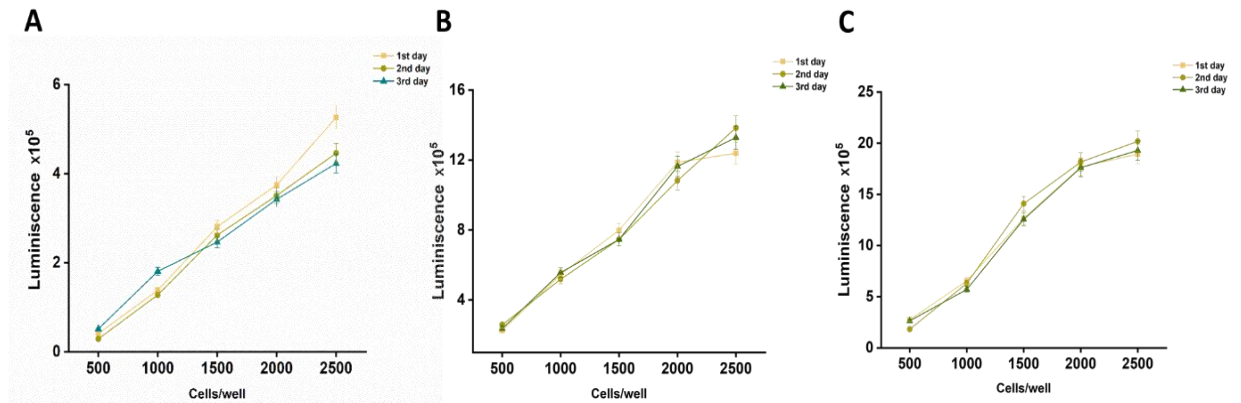


Figure 39: The measurement of light effect and toxicity of cells for different light in 3 continues illumination. Cells illuminated under corresponded (A) blue, (B) red and (C) far-red light in 3 days as 1% continues illumination. Afterward, the viability of each set measured by CellTiter-Glo® 3D Reagen. The statistical analysis of 3 days does not show any significant difference.

The importance of cell-cell adhesion dynamics in cell sorting following the DAH hypothesis. In a binary mixture of cells the arrangement of the cell types depends on the relative adhesion energies of the cell types. Consequently, controlling the cell-cell interactions and their dynamics is a crucial factor that determines the final outcome. In this part of the work we explored whether the sorting behavior of cells could be influenced using the blue and red light switchable cell-cell adhesions in mixtures with two cell types. For this purpose, we mixed equal numbers of VVD-, VVDHigh- (labeled with red fluorescent dye) or Cph1-MDA (labeled with green fluorescent dye) with MDA-MB-231 cells (labeled with green or red fluorescent dye, respectively) and observed their sorting within a spheroid either under continues or pulsed (5 min on/ 20 min off) activating illumination or in the dark. In the dark and under continues light illumination, the two cell types were totally intermixed in the spheroids (Figure 40A). However, most remarkably under pulsed light, the VVD-, VVDHigh- and Cph1-MDA were either enveloped by the MDA-MB-231 cells or formed self-isolated clusters from the MDA-MB-231 cells (Figure 40A, B and Figure 41).

These qualitative observation of light dependent self-sorting were further supported by quantitative analysis in a large sample size and different types of sorted structure i.e intermixed, enveloped and self-isolated, were considered (Figure 40B). In the all cases, separation of the transfected cells (cell type a) from the MDA-MB-231 cells (cell type b) was observed in the spheroids upon blue or red light pulsing illumination when compared to the dark and continuous illumination.

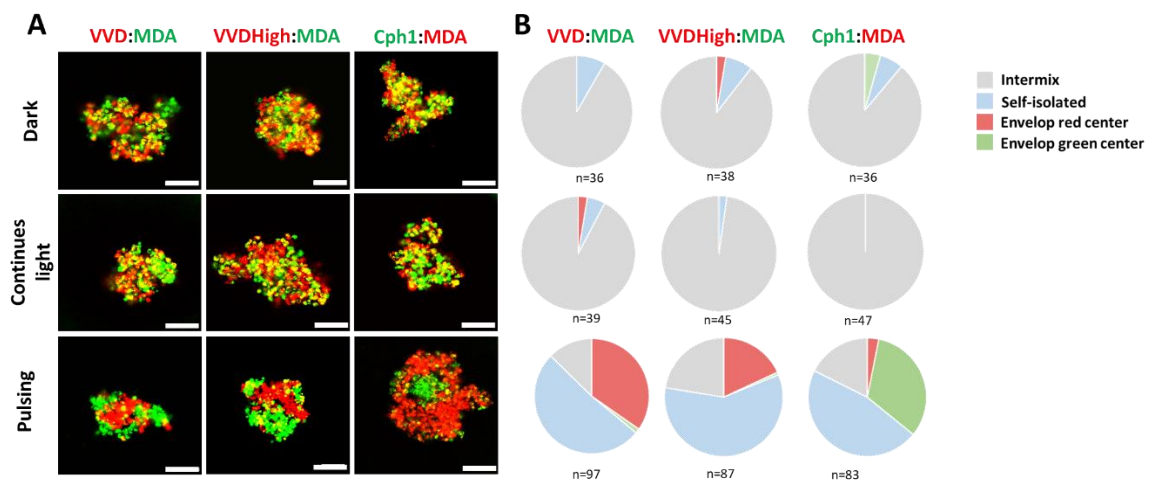


Figure 40: Cell sorting of an initially intermixed heterotypic cell suspension. A) Cells can either isolate or stay intermixed. According to the DAH, from dark to blue light or red light illumination the cells which have the photoswitchable protein in their surface, with higher adhesion and MDA-MB-231 with lower adhesion compared to transfected cells should have ended up to the predictive structures. However, continues illumination demonstrate a similar structure as dark structures. The predictive DAH structures only can accessible when cells alternatively illuminated which means it most happen when proteins on cells surface not only has to active but also be in their dynamic range. All the pulsing or alternatively illumination pointed to 5 min on 20 min off time. All scale bars are 100 μ m. B) The distribution of structures generated in multiples independent wells under dark and continues and alternative light illumination. Under dark, the 90% of the spheroid showed intermix formation of co culture of transfected cell with MDA-MB-231. Under continues, blue and red light, about 90 to 100% of spheroids showed the intermixed formation. Comparing, continue illumination to dark, distributions, shows in dark as long as we have the dynamic, it can be explained why in dark with ambient light some cell sorting happen. Under alternative (pulsing) blue and red light illumination, about 90% of the spheroid isolated from each other and formed the homologous interactions.

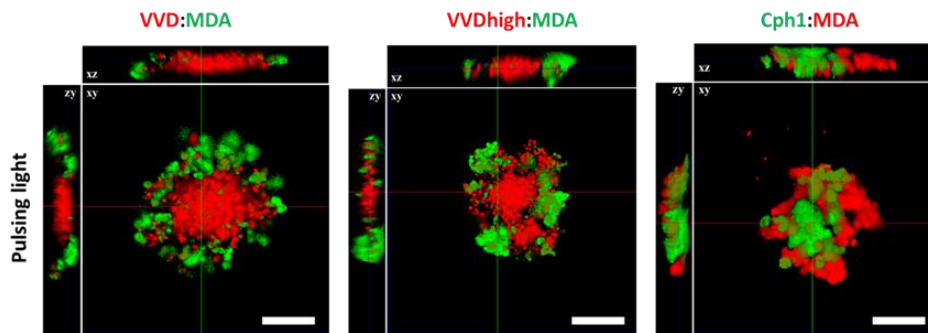


Figure 41: Confocal images of cell sorting of an initially intermixed of MDA-MB-231 and VVD-, VVDHigh and Cph1-MDA cell suspension. All the spheroid mixture illuminated by 5 min on 20 min off time by blue and red pulsing for VVD-, VVDHigh and Cph1-MDA, respectively from left to right. All scale bars are 100 μm .

These results clearly show that the dynamics of the cell-cell adhesions is essential for cells to self-sort into distinct groups. We showed this for three different cell types, which expressed different light dependent photoswitchable proteins on their surface. The cells organized into structures as predicted by the DAH. In the dark, the adhesions among the transfected cells (W_a), the adhesions among the MDA-MB-231 cells (W_b) and between each other (W_{ab}) are expected to be equally low, resulting in intermixed spheroids. Once the homophylic interaction between the transfected cells increased (W_a), more self-isolated ($W_a \geq W_b > W_{ab}$) and more enveloped ($(W_a + W_b)/2 > W_{ab}$) spheroids were observed compared to the dark, where the cells were intermixed ($W_{ab} > (W_a + W_b)/2 > W_b$). These findings show that the difference in adhesion between cells is enough and adhesion molecules do not need to be connected to the actin cytoskeleton for sorting out to take place.

Yet, these results show that the dynamics of the cell-cell adhesions are essential for self-sorting. Under continues illumination clearly, $W_a > W_{ab}$ and $W_a > W_b$, such that sorting would be expected. However, the lack of cell-cell adhesion dynamics prevents the self-sorting. Bringing concepts of dynamic interactions to bottom-up tissue engineering provides a new theoretical framework and will help in the design of more predictable

tissue-like structures. The DAH assumed; by minimizing the surface free energy, cell with strong adhesive molecules move toward the interior of cell population on the other hand the weaker one migrate toward the exterior.¹⁷⁴ The DAH has the predictive power based on minimizing the free energy proportional to the cell adhesion strength.

Finally, we combined different transfected cells to achieve various organization depending on the used light illumination. For this purpose, binary combinations of VVD-, VVDHigh-and Cph1-MDA cells were mixed in a 1:1 ratio and their sorting was examined in under blue or red light or coillumination with both colors of light after overnight incubation under 5 min on and 20 min off pulsed illumination.

For the mixture of VVD-MDA:VVDHigh-MDA cells, upon blue light illumination either self-isolated or enveloped structures with the VVDHigh cells at the center formed (Figure 39 A and B). As interaction between VVDHigh proteins is stronger than VVD proteins, it is expected that the more adhesive VVDHigh cells go to the center and are enveloped by the VVD-MDA cells ($W_a > W_b > W_{ab}$). As expected, similar results were obtained under coillumination with blue and red light because red light had no effect on VVD proteins. Overall, the combination of VVD and VVDHigh shows more than 50% out of 95% of total sorted cells are enveloped with VVDHigh interior structure.

The mixture of VVD:Cph1 and VVDHigh:Cph1 cells showed different arrangement depending on the illumination used. Under blue light illumination, the blue light responsive VVD and VVDHigh (labeled with red fluorescent dye) cells formed self-isolated (70% and 51% respectively for VVD:Cph1 and VVDHigh:Cph1) domains or moved to the center of the spheroid and were enveloped by the Cph1 cells (24% and 34% respectively for VVD:Cph1 and VVDHigh:Cph1) which labeled with green fluorescent dye (Figure 42A and B).

Under blue light illumination, the blue light VVD and VVDHigh cells (type a) are activated but the red light responsive Cph1-MDA cells (type b) are not. Therefore, the $W_a > W_b$ and W_{ab} . Under blue light illumination, 85% out of the whole VVDH:Cph1 spheroids

showed cell-sorting, of which around 34% were enveloped with red center, and 96% out of the whole VVD:Cph1 spheroids showed the cell-sorting of which around 26% were red centered enveloped.

In contrast under red light pulsing the organization of the VVD and Cph1 cells reversed. In these mixtures Cph1-MDA (green fluorescent labeled cell) cells were covered by VVD- or VVDHigh-MDA cells (red fluorescent labeled cells) forming green centered enveloped structures along side with self-isolated ones. Under red light activation Cph1-MDA (labeled in green) cells become more adhesive and as a consequence the work of adhesion for these cells increases. As a result the spheroids have more enveloped structure with the , green cells moving interior and red cells (VVD- or VVDHigh-MDA) moving exterior of the spheroid structure. Under the red illumination pulsing light, the quantitative analysis shows, 80% of the total spheroids sorted for the Cph1:VVDHigh mixtures and around 26% of these formed an enveloped shape with green labeled cells at the center. For the mixture of VVD:Cph1 cells 27% out of 94% of whole sorted cells formed an enveloped shape with green labeled cells at the center.. The quantitative analysis showed that under red light pulsing, in the VVD:Cph1 mixture less red centered enveloped (1%) spheroids formed than in the VVDHigh:Cph1 mixtures (6%), which can be justify by the higher strength binding of VVDHigh than VVD expressing cells (Figure 42B).

Finally, when mixtures of VVD:Cph1 and VVDHigh:Cph1 were simultaneously illuminated with pulsing blue and red light, the homophilic adhesions of both cell types were activated at the same time. As a result self-isolated and enveloped spheroids were obtained. The comparison between the final quantitative analysis of individual and coillumination showed similar percentage of red center envelope formation of VVD:Cph1 and VVDHigh:Cph1 on each experiments, as well similar percentage of green center envelope structure of spheroid under red or coilluminated light (Figure 42).

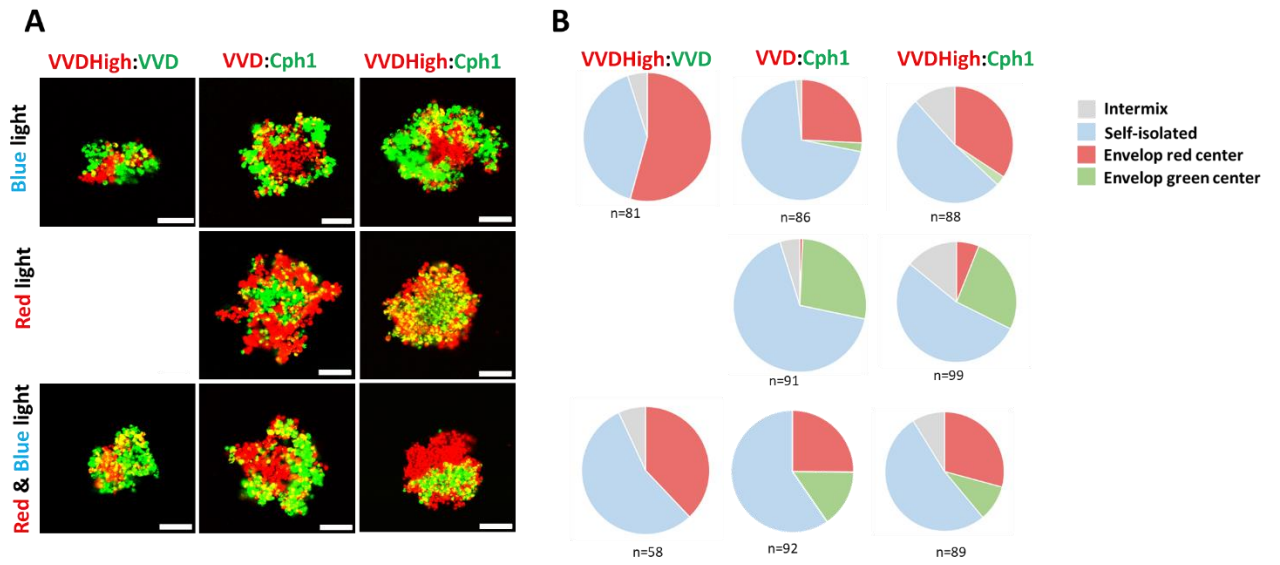


Figure 42: Cell sorting of an initially intermixed heterotypic cell suspension. A) The confocal images of co-culture of two systems with different adhesion activation. All spheroid illuminated under blue or red or coilluminated with blue and red light for 5 min on 20 min off. All scale bars are 100 μ m B) The distribution of co-culture spheroids formation structures under individual and coillumination pulsing light.

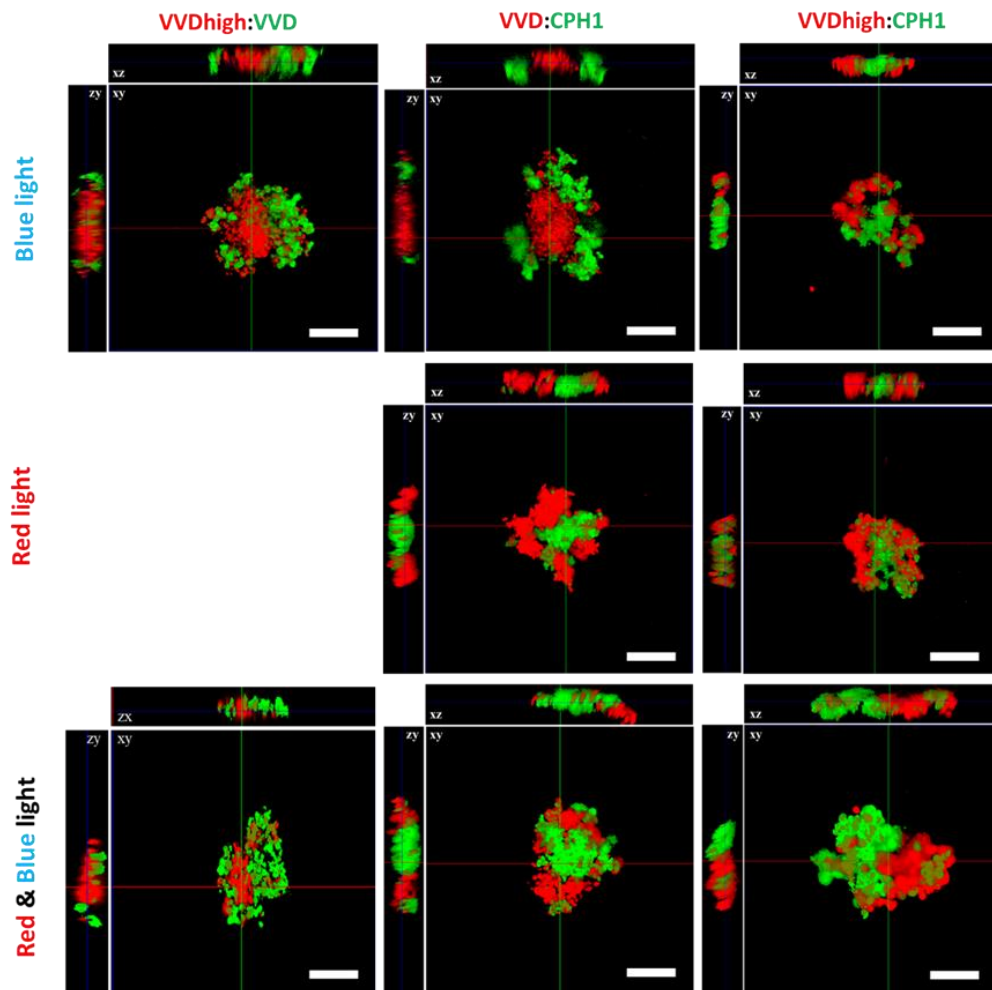


Figure 43: Confocal images of cell sorting of an initially intermixed heterotypic cell of VVD-, VVDHigh and Cph1-MDA in spheroids. All spheroid illuminated under blue, red and coillumination with both light for 5 min on 20 min off. All scale bars are 100 μm .

Overall, all the here obtained self-sorting behavior is in line with the thermodynamically controlled structures predicted by the DAH. As a key element of the DAH, the cell-cell adhesions have to be dynamic enough for the cells to sample their neighbors, move with respect to each other and position such that they maximize their adhesive interactions. In this respect, the photoswitchable cell-cell adhesions provide a unique tool to test this assumption of the DAH. Moreover, the cell sorting based on these artificial adhesion molecules that do not link to the actin cytoskeleton or intracellular signaling show that these aspect of cell adhesion are not required for cell sorting to take place.

Summary

Here, we developed cell types that form specific homophilic cell-cell interactions under visible light by presenting photoresponsive proteins as artificial adhesion molecules on their surface. Moreover, tuning dynamics of cell-cell interactions using pulsing light, cells sorted out into multicellular architectures based on specific self-recognition and differential adhesion hypothesis. The ability of these photoswitchable proteins to drive different structure formation illustrates the power of dynamic interactions in self-assembly. Bringing concepts of dynamic interactions to the differential adhesion hypothesis provides a new theoretical framework and will help in the design of more predictable tissue-like structures.

Chapter 4: Summary and Outlook

Cells interact with the neighbouring cells and form cell-cell contacts mainly mediated by cadherins. These processes are dynamic, spatially and temporally tightly regulated during many biological events including embryogenesis, wound healing and cancer development. Controlling cells interactions is important for both understanding the biochemical machinery and for several applications in biomedicine such as bottom-up tissue engineering and developing cell-cell based screening devices. Current approach for controlling cell-cell interaction are limited in terms of dynamicity, sustainability, high spatiotemporal resolution and reversibility. In this thesis, genetically expressing blue and red light photoswitchable cells contacts were developed to overcome the above-mentioned limitations.

In this thesis, blue and red light dependent switchable cell-cell interactions using the homodimerization of VVD, VVD^{High}, and Cph1 as well as the heterodimerization of Cry2 with CIBN were developed. The VVDs and Cph1 were suitable as adhesion receptors to form cell-cell interactions between cells of the same type and the Cry2/CIBN heterodimerization was suitable to form cell-cell interactions between cells of different types. Additionally, the blue and red light dependent cell-cell adhesions can be triggered independently from each other without interference. Moreover, the intrinsic properties of the photoswitchable proteins, such as the thermodynamic and mechanical stability of the dimerization and the protein–protein interaction dynamics was comparable to the E-cadherin based clustering of MCF7 cells, yet faster.

In mixtures of two cell populations cell-cell interactions could be triggered independently using different colors of visible light. Using this properly, I have demonstrated that how I can control the assembly and self-sorting of each cell type independently in the presence of another cell type relying on orthogonal triggers (i.e. blue and red light) and orthogonal

molecular interactions (VVD and Cph1). Therefore, this study highlights that self-sorting achieved with non-living colloidal particles can also be transferred to cells.

The concepts of using the photoswitchable proteins to control self-assembly of micron-sized objects is applicable to cellular and non-cellular systems. For example, Sentürk *et al.* showed that sorting out behaviour (known as narcissistic or asocial self-sorting in the colloidal self-assembly community) is achieved with mixtures of VVD^{High} and Cph1 coated polystyrene beads.¹⁶³ The extension of this to cells shows that not just concepts in colloidal self-assembly but self-sorting also apply to multicellular structures. Moreover, the parallels between colloidal and cellular self-assembly have also been witnessed in *in vitro* bead aggregation assays with cadherin coated beads.⁸¹

An important insight of this thesis is the importance of cell-cell interaction dynamics in the assembly and self-sorting of multicellular structures from cells as building blocks. Depending of the cell-cell adhesion dynamics structures under kinetic or thermodynamic control form. The earlier developed blue and red light triggered cell-cell interactions based on different homodimerizing photoswitchable protein interactions and their different reversion kinetics in the dark provide unique tools for modulating cell-cell interaction dynamics. Using the temporal control that light as a stimulus provides, I was able to assemble spheroids with different compactness's. As the cell-cell adhesion dynamics increased the spheroids transformed from loose and porous aggregates to compact and spherical structures. Moreover, the cell-cell adhesion dynamics were also pivotal in the outcome of the cells sorting out to control self-organizing in multicellular mixtures with different cell type and address different cell types within the mixture independently with blue and red light. Once cell-cell adhesions were dynamic enough spheroids with the arrangement of the two cell types as postulated by the DAH were obtained. These finding showed that adhesive molecules by themselves are not enough to obtain self-sorting in mixtures of cells but the dynamics of the cell adhesions have to be considered. While in previous studies cell-cell interactions have been controlled using chemical and genetic approaches, the importance of cell-cell interaction dynamics has not been considered.

In terms of dynamics, the photoswitchable mediated cell-cell interactions offer a wide range of interaction dynamics and strengths, which can be modulated to achieve both kinetically and thermodynamically driven multicellular assemblies. The possibility of triggering different cell-cell interactions within a multicellular assembly using different colours of light offers many opportunities in the bottom-up assembly of diverse cell types into tissue like structures and understanding the principles behind self-organization during development. The remarkable and innate ability of cells to self-assemble and sort themselves out into tissue like architectures reveal the high potential of bottom-up tissue engineering and make controlling cell-cell adhesions a very powerful tool to program synthetic tissues.^{19,163}

The photoswitchable cell-cell interactions further provide a unique chance of investigating the cell biology related to cell-cell interactions. Just like the native cadherin of cell-cell adhesions, the VVD and Cph1 mediated cell-cell adhesions also generate artificial adhesions between the same types of cells. Moreover, as with native cell-cell interactions they are switchable, dynamic, and can be spatiotemporally controlled as it is often the case during many biological processes. Differently from the cadherin based cell-cell interaction these photoswitchable cell-cell interactions do not link to the actin cytoskeleton and the associated signalling pathways. This fact provides a unique tool to dissect biochemical from biophysical signals transduced by cell-cell adhesions. More generally, these findings suggest that it is possible to assemble multicellular structures from cells and control parts of them with blue and a red light switchable cell-cell interaction pairs. Analogous to the sorting out of cells that express different cadherins types, cells expressing blue and red light-switchable proteins were able to replicate the same self-sorting behaviour. These cell-cell adhesions provide high control in multicellular structures assembled from two different cell types. Future studies that take advantage of the spatiotemporal control that photo-regulation provides will allow studying related questions in cell biology.

Additionally, having the spatial control using light allows to induce specific interaction limited to a certain region of interest. By using a microscope coupled to a digital mirror device, or a confocal microscope, it could be possible to illuminate a certain area and induce controlled cell-cell contacts in a specific place and observe the behaviour compare to the cells kept in the dark parallel.

The question of how synthetic cell-cell interactions influence the intracellular signalling pathways is another interesting aspect that needs to be addressed. The photoswitchable protein used here are only anchored in the membrane of the cell without any intracellular partner but in contrast the natural cell-cell adhesion proteins have an intracellular domain that connects them to the cytoskeleton and intracellular signalling networks. Yet, the photoswitchable proteins are not involved in direct biochemical signalling pathways of the cell, the biophysical contract to the neighbours still has the potential to influence cell behaviour. Thus, it would be interesting to study about the mechanical forces that are induced through the photoswitchable protein without a TM signal still change gene expression and cell behaviour. Moreover, another possibility would be to insert an intracellular domain to the photoswitchable proteins to link them to the actin cytoskeleton and study the natural signalling pathway and other biophysical behaviours.

Chapter 5: Appendix

Nucleotide and amino acid sequences, ORF

VVD-mCherry

DNA sequence 5' to 3'

ATGCACACACTATATGCTCCCGGAGGGTATGATATAATGGGATACCTACGTCAAATACGCAACCGTCC
GAACCCGCAAGTGGAGCTGGGCCCGGTGGACACCAGCTGCGCGCTGATCCTGTGCGACCTGAAGCA
GAAAGATACCCCGTTGTGTACGCGAGCGAGGCGTTCCTGTACATGACCGTTATAGCAACGCGGAA
GTTCTGGGCCGTAACCTGCCGTTTTCTGCAAAGCCCGGATGGTATGGTGAAGCCGAAAAGCACCCGTA
AGTATGTTGACAGCAACACCATCAACACCATGCGTAAAGCGATCGATCGTAACGCGGAAGTGCAGGT
TGAAGTGGTAACTTCAAGAAAAACGGCCAACGTTTCGTGAACTTTCTGACCATGATTCCGGTTCGTG
ATGAGACCGGCGAATATCGTTATAGCATGGGTTTTCAATGCGAGACCGAAGGCGGTAGC**AGATCTGT**
GAGCAAGGGCGAGGAGGATAACATGGCCATCATCAAGGAGTTCATGCGCTTCAAGGTGCACATGGA
GGGCTCCGTGAACGGCCACGAGTTCGAGATCGAGGGCGAGGGCGAGGGCCGCCCTACGAGGGCA
CCCAGACCGCCAAGCTGAAGGTGACCAAGGGTGGCCCCCTGCCCTTCGCCTGGGACATCCTGTCCC
CTCAGTTCATGTACGGCTCCAAGGCCTACGTGAAGCACCCCGCCGACATCCCGACTACTTGAAGCT
GTCCCTCCCGAGGGCTTCAAGTGGGAGCGCGTGATGAACTTCGAGGACGGCGGCGTGGTGACCGT
GACCCAGGACTCCTCCCTGCAGGACGGCGAGTTCATCTACAAGGTGAAGCTGCGCGGCACCAACTT
CCCCTCCGACGGCCCCGTAATGCAGAAGAAGACCATGGGCTGGGAGGCCTCCTCCGAGCGGATGTA
CCCGAGGACGGCGCCCTGAAGGGCGAGATCAAGCAGAGGCTGAAGCTGAAGGACGGCGGCCACT
ACGACGCTGAGGTCAAGACCACCTACAAGGCCAAGAAGCCCGTGCAGCTGCCCGGCGCCTACAACG
TCAACATCAAGTTGGACATCACCTCCACAACGAGGACTACACCATCGTGAACAGTACGAACGCGC
CGAGGGCCGCACTCCACCGGCGGCATGGACGAGCTGTACAAG

Amino acid sequence

MHTLYAPGGYDIMGYLRQIRNRPNPQVELGPVDTSCALILCDLKQKDTPVVYASEAFLYMTGYSNAEVLG
RNCRFLQSPDGMVKPKSTRKYVDSNTINTMRKAIDRNAEVQVEVVNFKKNQRFVNFMTMIPVRDETGEY
RYSMGFQCETEGGSRSVSKGEEDNMAIIEFMRFKVHMEGVSNGHEFEIEGEGEGRPYEGTQTAKLKVT
KGGPLPFAWDILSPQFMYGSKAYVKHPADIPDYLKLSFPEGFKWERVMNFEDGGVVTVTQDSSLQDGEFI

YKVKLRGTFNPSDGPVMQKKTMGWEASSERMYPEDGALKGEIKQRLKLDGGHYDAEVKTTYKAKKPV
QLPGAYNVNIKLDITSHNEDYTIVEQYERAEGRHSTGGMDELYK

VVDhigh-mCherry

DNA sequence 5' to 3'

ATGCACACACTATATGCTCCCGGAGGGTATGATATAATGGGATACCTAATTCAAATAATGAACCGTCC
GAACCCGCAAGTGGAGCTGGGCCCGGTGGACACCAGCTGCGCGCTGATCCTGTGCGACCTGAAGCA
GAAAGATACCCCGATTGTGTACGCGAGCGAGGCGTTCCTGTACATGACCGTTATAGCAACGCGGAA
GTTCTGGGCCGTAAGTCCGTTTTCTGCAAAGCCCGGATGGTATGGTGAAGCCGAAAAGCACCCGTA
AGTATGTTGACAGCAACACCATCAACACCATTTCGTAAGCGATCGATCGTAACGCGGAAGTGCAGGTT
GAAGTGGTTAACTTCAAGAAAAACGGCCAACGTTTCGTGAACTTTCTGACCATCATTCCGGTTCGTGA
TGAGACCGGCGAATATCGTTATAGCATGGGTTTTCAATGCGAGACCGAAGGCGGTAGC**AGATCTGTG**
AGCAAGGGCGAGGAGGATAACATGGCCATCATCAAGGAGTTCATGCGCTTCAAGGTGCACATGGAG
GGCTCCGTGAACGGCCACGAGTTCGAGATCGAGGGCGAGGGCGAGGGCCGCCCTACGAGGGCAC
CCAGACCGCCAAGCTGAAGGTGACCAAGGGTGGCCCCCTGCCCTTCGCCTGGGACATCCTGTCCCC
TCAGTTCATGTACGGCTCCAAGGCCTACGTGAAGCACCCCGCCGACATCCCCGACTACTTGAAGCTG
TCCTTCCCCGAGGGCTTCAAGTGGGAGCGCGTGATGAACTTCGAGGACGGCGGCGTGGTGACCGTG
ACCCAGGACTCCTCCCTGCAGGACGGCGAGTTCATCTACAAGGTGAAGCTGCGCGGCACCAACTTC
CCCTCCGACGGCCCCGTAATGCAGAAGAAGACCATGGGCTGGGAGGCCTCCTCCGAGCGGATGTAC
CCCGAGGACGGCGCCCTGAAGGGCGAGATCAAGCAGAGGCTGAAGCTGAAGGACGGCGGCCACTA
CGACGCTGAGGTCAAGACCACCTACAAGGCCAAGAAGCCCGTGCAGCTGCCCGGCGCCTACAACGT
CAACATCAAGTTGGACATCACCTCCACAACGAGGACTACACCATCGTGGAACAGTACGAACGCGCC
GAGGGCCGCCACTCCACCGCGGCATGGACGAGCTGTACAAG

Amino acid sequence

MHTLYAPGGYDIMGYLIQIMNRPNPQVELGPVDTSCALILCDLKQKDTPIVYASEAFLYMTGYSNAEVLGR
NCRFLQSPDGMVKPKSTRKYVDSNTINTIRKAIDRNAEVQVEVNFKKNQRFVNFLLTIIPVRDETGEYRYS
MGFQCETEGGSRSVSKGEEDNMAIIEFMRFKVHMEGSVNGHEFEIEGEGEGRPYEGTQTAKLKVTKGG
PLPFAWDILSPQFMYGSKAYVKHPADIPDYLLKSFPEGFKWERVMNFEDGGVVTVTQDSSLQDGEFIYKV
KLRGTFNPSDGPVMQKKTMGWEASSERMYPEDGALKGEIKQRLKLDGGHYDAEVKTTYKAKKPVQLP
GAYNVNIKLDITSHNEDYTIVEQYERAEGRHSTGGMDELYK

Cph1-GFP

DNA sequence 5' to 3'

CATATGCACCATCACCACCACGAGAATCTGTACTTTCAAGGCGGATCCGAATTCGAGCTCGCAAC
CACCGTTCAACTGAGCGACCAAAGCCTGCGTCAGCTGAAAACCCTGGCTATCCACACCGCTCACCTG
ATTCAGCCGCATGGCCTGGTGGTGGTGTGCTGCAGGAACCGGACCTGACCATCAGCCAGATTAGCGCC
AACTGCACCGGCATCCTGGGTCTAGCCCGGAGGATCTGCTGGGTGCGACCCTGGGCGAAGTGTTT
GACAGCTTTCAGATCGATCCAATCCAGAGCCGCCTGACCGCCGGTCAGATCAGCAGCCTGAACCCGA
GCAAGCTGTGGGCTCGTGTGATGGGTGACGATTTTCGTGATTTTTGACGGCGTGTTCACCGCAACAG
CGATGGTCTGCTGGTGTGCGAGCTGGAACCGCGTACACCAGCGACAACCTGCCGTTCTGGGTTT
TTATCACATGGCTAATGCCGCGCTGAACCGTCTGCGTCAGCAGGCGAACCTGCGTGACTTTTACGAT
GTGATCGTGGAGGAAGTGCCTCGCATGACCGGCTTCGACCGTGTGATGCTGTATCGCTTTGATGAGA
ACAACCACGGTGACGTGATTGCGGAGGATAAACGTGACGATATGGAACCGTACCTGGGCCTGACTA
TCCGAAAAGCGACATCCCACAGCCAGCTCGTCCGCTGTTTATTACAACCCGATCCGCGTGATTCCG
GACGTGTACGGTGTGGCTGTGCCACTGACCCCGGCTGTGAACCCGAGCACCAACCGTGCTGTGGAC
CTGACCGAGAGCATCCTGCGCAGCGCTACCACTGCCACCTGACCTATCTGAAGAACATGGGCGTG
GGTGCTAGCCTGACCATCAGCCTGATCAAGGATGGTACCTGTGGGGCCTGATTGCTTGCCACCACC
AGACCCCGAAAGTGATCCCGTTTGAGCTGCGTAAAGCCTGCGAGTTCTTCGGCCGCGTGGTGTTCAG
CAACATCAGCGCGCAGGAAGACACCGAAACCTTTGATTATCGTGTGCAGCTGGCGGAGCACGAAGCT
GTGCTGCTGGACAAGATGACCACCGTCCGATTTTCGTGGAGGGTCTGACCAATCATCCAGACCGTC
TGCTGGGCCTGACCGGTAGCCAGGGCGCGGCTATCTGCTTTGGTGAAGGCTGATTCTGGTGGGCG
AAACCCCGGATGAAAAAGCCGTGCAGTACCTGCTGCAGTGGCTGGAGAACCGTGAAGTGCAGGACG
TGTTCTTTACCAGCAGCCTGAGCCAGATCTATCCGGATGCGGTGAACTTCAAAGCGTGGCTAGCGG
CCTGCTGGCTATCCAATTGCCCGTCAAACTTCTGCTGTGGTTTCGCCCGAAGTGCTGCAGACC
GTGAACTGGGGCGGTGACCCGAACCATGCCTACGAGGCGACCCAGGAAGATGGCAAGATTGAGCTG
CACCCGCGTCAGAGCTTTGACCTGTGAAAGAAATCGTGCCTGCAGAGCCTGCCATGGCAGAGC
GTGGAGATTCAATCCGCGCTGGCACTGAAAAGGCTATCGTGAACCTGATTCTGCGTCAAGCTGAGT
AAGTCGAC**AGATCTGTGAGCAAGGGCGAGGAGCTGTTACCGGGGTGGTGCCATCCTGGT**CGAGC
TGGACGGCGACGTAAACGGCCACAAGTTCAGCGTGTCCGGCGAGGGCGAGGGCGATGCCACCTAC
GGCAAGCTGACCCTGAAGTTCATCTGCACCACCGGCAAGCTGCCCGTGCCCTGGCCACCCTCGTG
ACCACCCTGACCTACGGCGTGCAGTGCTTCAGCCGCTACCCCGACCACATGAAGCAGCAGACTTCT
TCAAGTCCGCCATGCCCGAAGGCTACGTCCAGGAGCGCACCATCTTCTTCAAGGACGACGGCAACTA

CAAGACCCGCGCCGAGGTGAAGTTCGAGGGCGACACCCTGGTGAACCGCATCGAGCTGAAGGGCAT
CGACTTCAAGGAGGACGGCAACATCCTGGGGCACAAGCTGGAGTACAACAGCCACAACGTC
TATATCATGGCCGACAAGCAGAAGAACGGCATCAAGGTGAACTTCAAGATCCGCCACAACATCGAGG
ACGGCAGCGTGCAGCTCGCCGACCACTACCAGCAGAACACCCCATCGGGCAGCGCCCGTGCTG
CTGCCCGACAACCACTACCTGAGCACCCAGTCCGCCCTGAGCAAAGACCCCAACGAGAAGCGCGAT
CACATGGTCCTGCTGGAGTTCGTGACCGCCGCGGGATCACTCTCGGCATGGACGAGCTGTATAAG
GGTAAAAAGAAGAAAAGAAGTCAAAGACAAAGTGTGTAATTATG

Amino acid sequence

HMHHHHHENLYFQGGSEFELATTVQLSDQSLRQLETLAIHTAHLIQPHGLVWVLQEPDLTISQISANCTGI
LGRSPEDLLGRTLGEVDFSQIDPIQSRLTAGQISSLNPSKLWARVMGDDFVFDGVFHRNSDGLLVELE
PAYTSDNLPFLGFYHMANAALNRLRQQANLRDFYDVIVEEVRMTGFDRVMLYRFDENNHGDVIAEDKRD
DMEPYLGLHYPESDIPQPARRLFIHNPIRVIPDVYGVAVPLTPAVNPSTNRAVDLTESILRSAYHCHLTYLKN
MGVGASLTISLIKDGHLWGLIACHHQTPKVIPFELRKACEFFGRVVFNSISAQEDTETFDYRVQLAEHEAVL
LDKMTTAADFVEGLTNHPDRLLGLTGSQGAICFGEKLILVGETPDEKAVQYLLQWLENREVQDVFFTSSL
SQIYPDAVNFKSVASGLLAIPIARHNFLWFRPEVLQTVNWGGDPNHAYEATQEDGKIELHPRQSFDLWKE
IVRLQSLPWQSVEIQSALALKKAIVNLILRQAE-VD

References

1. Liu, J. S. & Gartner, Z. J. Directing the assembly of spatially organized multicomponent tissues from the bottom up. *Trends Cell Biol.* **22**, 683–691 (2012).
2. Steinberg, M. S. & Poole, T. J. Strategies for specifying form and pattern: adhesion-guided multicellular assembly. *Philos Trans R Soc L. B Biol Sci* **295**, 451–460 (1981).
3. Steinberg, M. S. Goal-directedness in embryonic development. *Integr. Biol. Issues, News, Rev.* **1**, 49–59 (1998).
4. Breuls, R. G. M., Jiya, T. U. & Smit, T. H. Scaffold stiffness influences cell behavior: opportunities for skeletal tissue engineering. *Open Orthop. J.* **2**, 103–109 (2008).
5. Harrison, S. E., Sozen, B., Christodoulou, N., Kyprianou, C. & Zernicka-Goetz, M. Assembly of embryonic and extraembryonic stem cells to mimic embryogenesis in vitro. *Science (80-)*. **356**, (2017).
6. Rivron, N. C. *et al.* Blastocyst-like structures generated solely from stem cells. *Nature* **557**, 106–111 (2018).
7. Langer, R. & Vacanti, J. P. Tissue engineering. *Science (80-)*. **260**, 920 LP – 926 (1993).
8. Rosso, F., Giordano, A., Barbarisi, M. & Barbarisi, A. From cell-ECM interactions to tissue engineering. *J. Cell. Physiol.* **199**, 174–180 (2004).
9. Liaudanskaya, V., Gasperini, L., Maniglio, D., Motta, A. & Migliaresi, C. Assessing the Impact of Electrohydrodynamic Jetting on Encapsulated Cell Viability, Proliferation, and Ability to Self-Assemble in Three-Dimensional Structures. *Tissue Eng. Part C Methods* **21**, 631–638 (2014).
10. Guillotin, B. & Guillemot, F. Cell patterning technologies for organotypic tissue

References

- fabrication. *Trends Biotechnol.* **29**, 183–190 (2011).
11. Tiruvannamalai-Annamalai, R., Armant, D. R. & Matthew, H. W. T. A Glycosaminoglycan Based, Modular Tissue Scaffold System for Rapid Assembly of Perfusable, High Cell Density, Engineered Tissues. *PLoS One* **9**, e84287 (2014).
 12. Tasoglu, S. *et al.* Guided and magnetic self-assembly of tunable magnetoceptive gels. *Nat. Commun.* **5**, 4702 (2014).
 13. Tasoglu, S., Diller, E., Guven, S., Sitti, M. & Demirci, U. Untethered micro-robotic coding of three-dimensional material composition. *Nat. Commun.* **5**, 3124 (2014).
 14. Chen, P. *et al.* Microscale Assembly Directed by Liquid-Based Template. *Adv. Mater.* **26**, 5936–5941 (2014).
 15. Murphy, S. V & Atala, A. 3D bioprinting of tissues and organs. *Nat. Biotechnol.* **32**, 773–785 (2014).
 16. Atala, A. Tissue engineering of human bladder. *Br. Med. Bull.* **97**, 81–104 (2011).
 17. Nichol, J. W. & Khademhosseini, A. Modular Tissue Engineering: Engineering Biological Tissues from the Bottom Up. *Soft Matter* **5**, 1312–1319 (2009).
 18. Smith, L. A., Liu, X. & Ma, P. X. Tissue Engineering with Nano-Fibrous Scaffolds. *Soft Matter* **4**, 2144–2149 (2008).
 19. Mueller, M., Rasoulinejad, S., Garg, S. & Wegner, S. V. The Importance of Cell–Cell Interaction Dynamics in Bottom-Up Tissue Engineering: Concepts of Colloidal Self-Assembly in the Fabrication of Multicellular Architectures. *Nano Lett.* (2019) doi:10.1021/acs.nanolett.9b04160.
 20. Haraguchi, Y. *et al.* Fabrication of functional three-dimensional tissues by stacking cell sheets in vitro. *Nat. Protoc.* **7**, 850–858 (2012).

References

21. Elbert, D. L. Bottom-up tissue engineering. *Curr. Opin. Biotechnol.* **22**, 674–680 (2011).
22. Fedorovich, N. E., Wijnberg, H. M., Dhert, W. J. A. & Alblas, J. Distinct tissue formation by heterogeneous printing of osteo- and endothelial progenitor cells. *Tissue Eng. Part A* **17**, 2113–2121 (2011).
23. Mironov, V., Boland, T., Trusk, T., Forgacs, G. & Markwald, R. R. Organ printing: computer-aided jet-based 3D tissue engineering. *Trends Biotechnol.* **21**, 157–161 (2003).
24. Jakab, K. *et al.* Tissue engineering by self-assembly and bio-printing of living cells. *Biofabrication* **2**, 22001 (2010).
25. Gartner, Z. J. & Bertozzi, C. R. Programmed assembly of 3-dimensional microtissues with defined cellular connectivity. *Proc. Natl. Acad. Sci.* **106**, 4606–4610 (2009).
26. Philp, D. & Stoddart, J. F. Self-Assembly in Natural and Unnatural Systems. *Angew. Chemie Int. Ed. English* **35**, 1154–1196 (1996).
27. Hartgerink, J. D., Beniash, E. & Stupp, S. I. Self-assembly and mineralization of peptide-amphiphile nanofibers. *Science* **294**, 1684–1688 (2001).
28. Liu, X. & Ma, P. X. Polymeric Scaffolds for Bone Tissue Engineering. *Ann. Biomed. Eng.* **32**, 477–486 (2004).
29. Athanasiou, K. A., Eswaramoorthy, R., Hadidi, P. & Hu, J. C. Self-organization and the self-assembling process in tissue engineering. *Annu. Rev. Biomed. Eng.* **15**, 115–136 (2013).
30. Lovett, M., Lee, K., Edwards, A. & Kaplan, D. L. Vascularization strategies for tissue engineering. *Tissue Eng. Part B. Rev.* **15**, 353–370 (2009).
31. Vunjak-Novakovic, G. *et al.* Bioreactor cultivation conditions modulate the composition and mechanical properties of tissue-engineered cartilage. *J.*

References

- Orthop. Res. Off. Publ. Orthop. Res. Soc.* **17**, 130–138 (1999).
32. Foty, R. A. & Steinberg, M. S. Cadherin-mediated cell-cell adhesion and tissue segregation in relation to malignancy. *Int. J. Dev. Biol.* **48**, 397–409 (2004).
33. Armstrong, P. B. & Parenti, D. CELL SORTING IN THE PRESENCE OF CYTOCHALASIN B. *J. Cell Biol.* **55**, 542–553 (1972).
34. Steinberg, M. S. & Wiseman, L. L. Do morphogenetic tissue rearrangements require active cell movements? The reversible inhibition of cell sorting and tissue spreading by cytochalasin B. *J. Cell Biol.* **55**, 606–615 (1972).
35. Sasai, Y. Cytosystems dynamics in self-organization of tissue architecture. *Nature* **493**, 318–326 (2013).
36. Sato, T. *et al.* Single Lgr5 stem cells build crypt-villus structures in vitro without a mesenchymal niche. *Nature* **459**, 262–265 (2009).
37. Song, W. *et al.* Dynamic self-organization of microwell-aggregated cellular mixtures. *Soft Matter* **12**, 5739–5746 (2016).
38. Winklbauer, R. & Parent, S. E. Forces driving cell sorting in the amphibian embryo. *Mech. Dev.* **144**, 81–91 (2017).
39. Townes, P. L. & Holtfreter, J. Directed movements and selective adhesion of embryonic amphibian cells. *J. Exp. Zool.* **128**, 53–120 (1955).
40. Green, J. B. A. Sophistications of cell sorting. *Nat. Cell Biol.* **10**, 375–377 (2008).
41. Steinberg, M. S. Reconstruction of tissues by dissociated cells. Some morphogenetic tissue movements and the sorting out of embryonic cells may have a common explanation. *Science (80-.)*. **141**, 401–408 (1963).
42. Foty, R. A. & Steinberg, M. S. The differential adhesion hypothesis: a direct evaluation. *Dev. Biol.* **278**, 255–263 (2005).
43. Duguay, D., Foty, R. A. & Steinberg, M. S. Cadherin-mediated cell adhesion and tissue segregation: qualitative and quantitative determinants. *Dev. Biol.* **253**,

References

- 309–323 (2003).
44. Steinberg, M. S. & Takeichi, M. Experimental specification of cell sorting, tissue spreading, and specific spatial patterning by quantitative differences in cadherin expression. *Proc. Natl. Acad. Sci. U. S. A.* **91**, 206–209 (1994).
 45. Brodland, G. W. The Differential Interfacial Tension Hypothesis (DITH): a comprehensive theory for the self-rearrangement of embryonic cells and tissues. *J. Biomech. Eng.* **124**, 188–197 (2002).
 46. Nose, A., Nagafuchi, A. & Takeichi, M. Expressed recombinant cadherins mediate cell sorting in model systems. *Cell* **54**, 993–1001 (1988).
 47. Godt, D. & Tepass, U. Drosophila oocyte localization is mediated by differential cadherin-based adhesion. *Nature* **395**, 387–391 (1998).
 48. Moore, R., Tao, W., Meng, Y., Smith, E. R. & Xu, X.-X. Cell adhesion and sorting in embryoid bodies derived from N-or E-cadherin deficient murine embryonic stem cells. *Biol. Open* **3**, 121–128 (2014).
 49. Maître, J.-L. *et al.* Adhesion functions in cell sorting by mechanically coupling the cortices of adhering cells. *Science* **338**, 253–256 (2012).
 50. Manning, M. L., Foty, R. A., Steinberg, M. S. & Schoetz, E.-M. Coaction of intercellular adhesion and cortical tension specifies tissue surface tension. *Proc. Natl. Acad. Sci.* **107**, 12517 LP – 12522 (2010).
 51. Winklbauer, R. Cell adhesion strength from cortical tension – an integration of concepts. *J. Cell Sci.* **128**, 3687 LP – 3693 (2015).
 52. Evans, E. & Yeung, A. Apparent viscosity and cortical tension of blood granulocytes determined by micropipet aspiration. *Biophys. J.* **56**, 151–160 (1989).
 53. Maître, J.-L. & Heisenberg, C.-P. Three functions of cadherins in cell adhesion. *Curr. Biol.* **23**, R626-33 (2013).

References

54. Lecuit, T. & Yap, A. S. E-cadherin junctions as active mechanical integrators in tissue dynamics. *Nat. Cell Biol.* **17**, 533–539 (2015).
55. Borghi, N. *et al.* E-cadherin is under constitutive actomyosin-generated tension that is increased at cell-cell contacts upon externally applied stretch. *Proc. Natl. Acad. Sci. U. S. A.* **109**, 12568–12573 (2012).
56. Ng, M. R., Besser, A., Brugge, J. S. & Danuser, G. Mapping the dynamics of force transduction at cell-cell junctions of epithelial clusters. *Elife* **3**, e03282 (2014).
57. Anastasiadis, P. Z. p120-ctn: A nexus for contextual signaling via Rho GTPases. *Biochim. Biophys. Acta - Mol. Cell Res.* **1773**, 34–46 (2007).
58. Harris, A. K. Is cell sorting caused by differences in the work of intercellular adhesion? A critique of the Steinberg hypothesis. *J. Theor. Biol.* **61**, 267–285 (1976).
59. Friedlander, D. R., Mège, R. M., Cunningham, B. A. & Edelman, G. M. Cell sorting-out is modulated by both the specificity and amount of different cell adhesion molecules (CAMs) expressed on cell surfaces. *Proc. Natl. Acad. Sci.* **86**, 7043 LP – 7047 (1989).
60. Odell, G. M., Oster, G., Alberch, P. & Burnside, B. The mechanical basis of morphogenesis: I. Epithelial folding and invagination. *Dev. Biol.* **85**, 446–462 (1981).
61. Lecuit, T. Cell adhesion: sorting out cell mixing with echinoid? *Curr. Biol.* **15**, R505-7 (2005).
62. Lecuit, T. & Le Goff, L. Orchestrating size and shape during morphogenesis. *Nature* **450**, 189–192 (2007).
63. Lecuit, T. “Developmental mechanics”: Cellular patterns controlled by adhesion, cortical tension and cell division. *HFSP J.* **2**, 72–78 (2008).

References

64. Jones, B. M., Evans, P. M. & Lee, D. A. Relation between the rate of cell movement under agarose and the positioning of cells in heterotypic aggregates. *Exp. Cell Res.* **180**, 287–296 (1989).
65. Maslow, D. E. & Mayhew, E. Cytochalasin B prevents specific sorting of reaggregating embryonic cells. *Science* **177**, 281–282 (1972).
66. Sanger, J. W. & Holtzer, H. Cytochalasin B: Effects on Cell Morphology, Cell Adhesion, and Mucopolysaccharide Synthesis. *Proc. Natl. Acad. Sci.* **69**, 253 LP – 257 (1972).
67. Overton, J. & Kapmarski. Hybrid desmosomes in aggregated chick and mouse cells. *J. Exp. Zool.* **192**, 33–41 (1975).
68. Armstrong, P. B. & Armstrong, M. T. A role for fibronectin in cell sorting. *J. Cell Sci.* **69**, 179 LP – 197 (1984).
69. Foty, R. A. & Steinberg, M. S. Differential adhesion in model systems. *WIREs Dev. Biol.* **2**, 631–645 (2013).
70. Tepass, U., Godt, D. & Winklbauer, R. Cell sorting in animal development: signalling and adhesive mechanisms in the formation of tissue boundaries. *Curr. Opin. Genet. Dev.* **12**, 572–582 (2002).
71. Gumbiner, B. M. Regulation of cadherin-mediated adhesion in morphogenesis. *Nat. Rev. Mol. Cell Biol.* **6**, 622–634 (2005).
72. Geng, F., Shi, B. Z., Yuan, Y. F. & Wu, X. Z. The expression of core fucosylated E-cadherin in cancer cells and lung cancer patients: prognostic implications. *Cell Res.* **14**, 423–433 (2004).
73. Hulpiau, P. & van Roy, F. Molecular evolution of the cadherin superfamily. *Int. J. Biochem. Cell Biol.* **41**, 349–369 (2009).
74. Hulpiau, P. & Van Roy, F. New insights into the evolution of metazoan cadherins. *Mol. Biol. Evol.* **28**, 647–657 (2011).

References

75. Nagafuchi, A. & Takeichi, M. Cell binding function of E-cadherin is regulated by the cytoplasmic domain. *EMBO J.* **7**, 3679–3684 (1988).
76. Fukata, M. & Kaibuchi, K. Rho-family GTPases in cadherin-mediated cell-cell adhesion. *Nat. Rev. Mol. Cell Biol.* **2**, 887–897 (2001).
77. Halbleib, J. M. & Nelson, W. J. Cadherins in development: cell adhesion, sorting, and tissue morphogenesis. *Genes Dev.* **20**, 3199–3214 (2006).
78. Yap, A. S., Briehner, W. M., Pruschy, M. & Gumbiner, B. M. Lateral clustering of the adhesive ectodomain: a fundamental determinant of cadherin function. *Curr. Biol.* **7**, 308–315 (1997).
79. Liu, X. & Chu, K.-M. E-Cadherin and Gastric Cancer: Cause, Consequence, and Applications. *Biomed Res. Int.* **2014**, 637308 (2014).
80. Niessen, C. M. & Gumbiner, B. M. Cadherin-mediated cell sorting not determined by binding or adhesion specificity. *J. Cell Biol.* **156**, 389–399 (2002).
81. Emond, M. R., Biswas, S., Blevins, C. J. & Jontes, J. D. A complex of Protocadherin-19 and N-cadherin mediates a novel mechanism of cell adhesion(1) Emond, M. R.; Biswas, S.; Blevins, C. J.; Jontes, J. D. A Complex of Protocadherin-19 and N-Cadherin Mediates a Novel Mechanism of Cell Adhesion. *J. Cell Biol.* **201**. *J. Cell Biol.* **195**, 1115–1121 (2011).
82. Toda, S., Blauch, L. R., Tang, S. K. Y., Morsut, L. & Lim, W. A. Programming self-organizing multicellular structures with synthetic cell-cell signaling. *Science (80-.)*. **361**, 156–162 (2018).
83. Stephan, M. T. & Irvine, D. J. Enhancing Cell therapies from the Outside In: Cell Surface Engineering Using Synthetic Nanomaterials. *Nano Today* **6**, 309–325 (2011).
84. Dutta, D., Pulsipher, A., Luo, W. & Yousaf, M. N. Synthetic Chemoselective Rewiring of Cell Surfaces: Generation of Three-Dimensional Tissue Structures. *J. Am. Chem. Soc.* **133**, 8704–8713 (2011).

References

85. O'Brien, P. J., Luo, W., Rogozhnikov, D., Chen, J. & Yousaf, M. N. Spheroid and Tissue Assembly via Click Chemistry in Microfluidic Flow. *Bioconjug. Chem.* **26**, 1939–1949 (2015).
86. Koo, H. *et al.* Bioorthogonal Click Chemistry-Based Synthetic Cell Glue. *Small* **11**, 6458–6466 (2015).
87. De Bank, P. A. *et al.* Accelerated formation of multicellular 3-D structures by cell-to-cell cross-linking. *Biotechnol. Bioeng.* **97**, 1617–1625 (2007).
88. Wang, B. *et al.* Multicellular assembly and light-regulation of cell-cell communication by conjugated polymer materials. *Adv. Mater.* **26**, 2371–2375 (2014).
89. Teramura, Y., Chen, H., Kawamoto, T. & Iwata, H. Control of cell attachment through polyDNA hybridization. *Biomaterials* **31**, 2229–2235 (2010).
90. Todhunter, M. E. *et al.* Programmed synthesis of three-dimensional tissues. *Nat. Methods* **12**, 975 (2015).
91. Shi, P. *et al.* Host–guest recognition on photo-responsive cell surfaces directs cell–cell contacts. *Mater. Today* **20**, 16–21 (2017).
92. Shi, P. *et al.* Spatiotemporal control of cell–cell reversible interactions using molecular engineering. *Nat. Commun.* **7**, 13088 (2016).
93. Luo, W., Pulsipher, A., Dutta, D., Lamb, B. M. & Yousaf, M. N. Remote Control of Tissue Interactions via Engineered Photo-switchable Cell Surfaces. *Sci. Rep.* **4**, 6313 (2014).
94. Cachat, E. *et al.* 2- and 3-dimensional synthetic large-scale de novo patterning by mammalian cells through phase separation. *Sci. Rep.* **6**, 20664 (2016).
95. Spudich, J. L. & Luecke, H. Sensory rhodopsin II: functional insights from structure. *Curr. Opin. Struct. Biol.* **12**, 540–546 (2002).
96. Franklin, K. A. & Quail, P. H. Phytochrome functions in Arabidopsis

References

- development. *J. Exp. Bot.* **61**, 11–24 (2010).
97. Chen, M. & Chory, J. Phytochrome signaling mechanisms and the control of plant development. *Trends Cell Biol.* **21**, 664–671 (2011).
98. Arinkin, V. *et al.* Structure of a LOV protein in apo-state and implications for construction of LOV-based optical tools. *Sci. Rep.* **7**, 42971 (2017).
99. Glantz, S. T. *et al.* Functional and topological diversity of LOV domain photoreceptors. *Proc. Natl. Acad. Sci.* **113**, E1442 LP-E1451 (2016).
100. Müller, K. & Weber, W. Optogenetic tools for mammalian systems. *Mol. Biosyst.* **9**, 596–608 (2013).
101. Mühlhäuser, W. W. D., Fischer, A., Weber, W. & Radziwill, G. Optogenetics - Bringing light into the darkness of mammalian signal transduction. *Biochim. Biophys. acta. Mol. cell Res.* **1864**, 280–292 (2017).
102. Niopek, D. *et al.* Engineering light-inducible nuclear localization signals for precise spatiotemporal control of protein dynamics in living cells. *Nat. Commun.* **5**, 4404 (2014).
103. Quejada, J. R. *et al.* Optimized light-inducible transcription in mammalian cells using Flavin Kelch-repeat F-box1/GIGANTEA and CRY2/CIB1. *Nucleic Acids Res.* **45**, e172 (2017).
104. Guntas, G. *et al.* Engineering an improved light-induced dimer (iLID) for controlling the localization and activity of signaling proteins. *Proc. Natl. Acad. Sci.* **112**, 112 LP – 117 (2015).
105. Liao, Z., Kasirer-Friede, A. & Shattil, S. J. Optogenetic interrogation of integrin α V β 3 function in endothelial cells. *J. Cell Sci.* **130**, 3532 LP – 3541 (2017).
106. Zoltowski, B. D., Vaccaro, B. & Crane, B. R. Mechanism-based tuning of a LOV domain photoreceptor. *Nat. Chem. Biol.* **5**, 827–834 (2009).
107. Kawano, F., Suzuki, H., Furuya, A. & Sato, M. Engineered pairs of distinct

References

- photoswitches for optogenetic control of cellular proteins. *Nat Commun* **6**, 6256 (2015).
108. Muller, K. *et al.* Multi-chromatic control of mammalian gene expression and signaling. *Nucleic Acids Res.* **41**, e124 (2013).
109. Müller, K., Engesser, R., Timmer, J., Zurbriggen, M. D. & Weber, W. Orthogonal Optogenetic Triple-Gene Control in Mammalian Cells. *ACS Synth. Biol.* **3**, 796–801 (2014).
110. Wang, X., Chen, X. & Yang, Y. Spatiotemporal control of gene expression by a light-switchable transgene system. *Nat. Methods* **9**, 266–269 (2012).
111. Han, T., Chen, Q. & Liu, H. Engineered Photoactivatable Genetic Switches Based on the Bacterium Phage T7 RNA Polymerase. *ACS Synth. Biol.* **6**, 357–366 (2017).
112. Kim, K.-T. & Song, M.-R. Light-induced Notch activity controls neurogenic and gliogenic potential of neural progenitors. *Biochem. Biophys. Res. Commun.* **479**, 820–826 (2016).
113. Liu, H., Liu, B., Zhao, C., Pepper, M. & Lin, C. The action mechanisms of plant cryptochromes. *Trends Plant Sci.* **16**, 684–691 (2011).
114. Tischer, D. & Weiner, O. D. Illuminating cell signalling with optogenetic tools. *Nat. Rev. Mol. Cell Biol.* **15**, 551–558 (2014).
115. Duan, L. *et al.* Optogenetic control of molecular motors and organelle distributions in cells. *Chem. Biol.* **22**, 671–682 (2015).
116. Idevall-Hagren, O., Dickson, E. J., Hille, B., Toomre, D. K. & De Camilli, P. Optogenetic control of phosphoinositide metabolism. *Proc. Natl. Acad. Sci.* **109**, 13894 LP – 13895 (2012).
117. Polstein, L. R. & Gersbach, C. A. A light-inducible CRISPR-Cas9 system for control of endogenous gene activation. *Nat. Chem. Biol.* **11**, 198–200 (2015).

References

118. Wilde, A., Fiedler, B. & Börner, T. The cyanobacterial phytochrome Cph2 inhibits phototaxis towards blue light. *Mol. Microbiol.* **44**, 981–988 (2002).
119. Davis, S. J., Vener, A. V & Vierstra, R. D. Bacteriophytochromes: Phytochrome-Like Photoreceptors from Nonphotosynthetic Eubacteria. *Science (80-)*. **286**, 2517 LP – 2520 (1999).
120. Griffith, G. W., Jenkins, G. I., Milner-White, E. J. & Clutterbuck, A. J. HOMOLOGU AT THE AMINO ACID LEVEL BETWEEN PLANT PHYTOCHROMES AND A REGULATOR OF ASEXUAL SPORULATION IN *Emericella (=Aspergillus) nidulans*. *Photochem. Photobiol.* **59**, 252–256 (1994).
121. Blumenstein, A. *et al.* The *Aspergillus nidulans* phytochrome FphA represses sexual development in red light. *Curr. Biol.* **15**, 1833–1838 (2005).
122. Hughes, J. *et al.* A prokaryotic phytochrome. *Nature* **386**, 663 (1997).
123. Yeh, K.-C., Wu, S.-H., Murphy, J. T. & Lagarias, J. C. A Cyanobacterial Phytochrome Two-Component Light Sensory System. *Science (80-)*. **277**, 1505 LP – 1508 (1997).
124. De Riso, V. *et al.* Gene silencing in the marine diatom *Phaeodactylum tricorutum*. *Nucleic Acids Res.* **37**, e96–e96 (2009).
125. Müller, K., Zurbriggen, M. D. & Weber, W. Control of gene expression using a red- and far-red light-responsive bi-stable toggle switch. *Nat. Protoc.* **9**, 622 (2014).
126. Shearn, J. T. *et al.* Tendon tissue engineering: progress, challenges, and translation to the clinic. *J. Musculoskelet. Neuronal Interact.* **11**, 163–173 (2011).
127. Essen, L.-O., Mailliet, J. & Hughes, J. The structure of a complete phytochrome sensory module in the Pr ground state. *Proc. Natl. Acad. Sci.* **105**, 14709–14714 (2008).
128. Reichhart, E., Ingles-Prieto, A., Tichy, A. M., McKenzie, C. & Janovjak, H. A

References

- Phytochrome Sensory Domain Permits Receptor Activation by Red Light. *Angew Chem Int Ed Engl* **55**, 6339–6342 (2016).
129. Levskaya, A. *et al.* Engineering *Escherichia coli* to see light. *Nature* **438**, 441–442 (2005).
130. Fernandez-Rodriguez, J., Moser, F., Song, M. & Voigt, C. A. Engineering RGB color vision into *Escherichia coli*. *Nat. Chem. Biol.* **13**, 706–708 (2017).
131. Schmidl, S. R., Sheth, R. U., Wu, A. & Tabor, J. J. Refactoring and Optimization of Light-Switchable *Escherichia coli* Two-Component Systems. *ACS Synth. Biol.* **3**, 820–831 (2014).
132. Ma, S., Luo, S., Wu, L. I., Liang, Z. & Wu, J.-R. Re-engineering the two-component systems as light-regulated in *Escherichia coli*. *J. Biosci.* **42**, 565–573 (2017).
133. Yüz, S. G., Rasoulinejad, S., Mueller, M., Wegner, A. E. & Wegner, S. V. Blue Light Switchable Cell–Cell Interactions Provide Reversible and Spatiotemporal Control Towards Bottom-Up Tissue Engineering. *Adv. Biosyst.* **3**, 1800310 (2019).
134. Stauffer, W., Sheng, H. & Lim, H. N. EzColocalization: An ImageJ plugin for visualizing and measuring colocalization in cells and organisms. *Sci. Rep.* **8**, 15764 (2018).
135. Sheng, H., Stauffer, W. & Lim, H. N. Systematic and general method for quantifying localization in microscopy images. *Biol. Open* **5**, 1882 LP – 1893 (2016).
136. Schneider, C. A., Rasband, W. S. & Eliceiri, K. W. NIH Image to ImageJ: 25 years of image analysis. *Nat. Methods* **9**, 671–675 (2012).
137. Preibisch, S., Saalfeld, S. & Tomancak, P. Globally optimal stitching of tiled 3D microscopic image acquisitions. *Bioinformatics* **25**, 1463–1465 (2009).

References

138. Chen, W. *et al.* High-throughput image analysis of tumor spheroids: a user-friendly software application to measure the size of spheroids automatically and accurately. *J. Vis. Exp.* 51639 (2014) doi:10.3791/51639.
139. Moreno-Bueno, G. *et al.* The morphological and molecular features of the epithelial-to-mesenchymal transition. *Nat. Protoc.* **4**, 1591–1613 (2009).
140. Kalluri, R. & Weinberg, R. A. The basics of epithelial-mesenchymal transition. *J. Clin. Invest.* **119**, 1420–1428 (2009).
141. Place, E. S., Evans, N. D. & Stevens, M. M. Complexity in biomaterials for tissue engineering. *Nat. Mater.* **8**, 457–470 (2009).
142. Gabrielse, K. *et al.* Reversible Re-programing of Cell–Cell Interactions. *Angew. Chemie Int. Ed.* **53**, 5112–5116 (2014).
143. Wang, J. *et al.* Chemical Remodeling of Cell-Surface Sialic Acids through a Palladium-Triggered Bioorthogonal Elimination Reaction. *Angew. Chemie Int. Ed.* **54**, 5364–5368 (2015).
144. Shi, P. *et al.* Polyvalent Display of Biomolecules on Live Cells. *Angew. Chemie Int. Ed.* **57**, 6800–6804 (2018).
145. Kennedy, M. J. *et al.* Rapid blue-light–mediated induction of protein interactions in living cells. *Nat. Methods* **7**, 973–975 (2010).
146. Guglielmi, G., Falk, H. J. & De Renzis, S. Optogenetic Control of Protein Function: From Intracellular Processes to Tissue Morphogenesis. *Trends Cell Biol.* **26**, 864–874 (2016).
147. Bugaj, L. J., Choksi, A. T., Mesuda, C. K., Kane, R. S. & Schaffer, D. V. Optogenetic protein clustering and signaling activation in mammalian cells. *Nat. Methods* **10**, 249 (2013).
148. Krishnamurthy, V. V *et al.* Reversible optogenetic control of kinase activity during differentiation and embryonic development. *Development* **143**, 4085 LP – 4094

References

- (2016).
149. Valon, L., Marín-Llauradó, A., Wyatt, T., Charras, G. & Trepát, X. Optogenetic control of cellular forces and mechanotransduction. *Nat. Commun.* **8**, 14396 (2017).
150. Yüz, S. G., Ricken, J. & Wegner, S. V. Independent Control over Multiple Cell Types in Space and Time Using Orthogonal Blue and Red Light Switchable Cell Interactions. *Adv. Sci.* **5**, 1800446 (2018).
151. Nieman, M. T., Prudoff, R. S., Johnson, K. R. & Wheelock, M. J. N-cadherin promotes motility in human breast cancer cells regardless of their E-cadherin expression. *J. Cell Biol.* **147**, 631–644 (1999).
152. Ripley, B. D. The second-order analysis of stationary point processes. *J. Appl. Probab.* **13**, 255–266 (1976).
153. Thu, C. A. *et al.* Single-cell identity generated by combinatorial homophilic interactions between alpha, beta, and gamma protocadherins. *Cell* **158**, 1045–1059 (2014).
154. Hui, E. E. & Bhatia, S. N. Micromechanical control of cell–cell interactions. *Proc. Natl. Acad. Sci.* **104**, 5722–5726 (2007).
155. Wei, Q. & Huang, H. Chapter Five - Insights into the Role of Cell–Cell Junctions in Physiology and Disease. in *International Review of Cell and Molecular Biology* (ed. Jeon, K. W. B. T.-I. R. of C. and M. B.) vol. 306 187–221 (Academic Press, 2013).
156. Ryan, P. L., Foty, R. A., Kohn, J. & Steinberg, M. S. Tissue spreading on implantable substrates is a competitive outcome of cell-cell vs. cell-substratum adhesivity. *Proc Natl Acad Sci U S A* **98**, 4323–4327 (2001).
157. Ovsianikov, A., Khademhosseini, A. & Mironov, V. The Synergy of Scaffold-Based and Scaffold-Free Tissue Engineering Strategies. *Trends Biotechnol.* **36**, 348–357 (2018).

References

158. Selden, N. S. *et al.* Chemically programmed cell adhesion with membrane-anchored oligonucleotides. *J. Am. Chem. Soc.* **134**, 765–768 (2012).
159. Katsamba, P. *et al.* Linking molecular affinity and cellular specificity in cadherin-mediated adhesion. *Proc. Natl. Acad. Sci.* **106**, 11594–11599 (2009).
160. Han, K. *et al.* Social Self-Sorting of Colloidal Families in Co-Assembling Microgel Systems. *Angew. Chemie - Int. Ed.* (2017) doi:10.1002/anie.201612196.
161. Shi, Q., Chien, Y.-H. & Leckband, D. Biophysical properties of cadherin bonds do not predict cell sorting. *J. Biol. Chem.* **283**, 28454–28463 (2008).
162. Sato, K., Hosokawa, K. & Maeda, M. Rapid Aggregation of Gold Nanoparticles Induced by Non-Cross-Linking DNA Hybridization. *J. Am. Chem. Soc.* **125**, 8102–8103 (2003).
163. Sentürk, O. I., Chervyachkova, E., Ji, Y. & Wegner, S. V. Independent Blue and Red Light Triggered Narcissistic Self-Sorting Self-Assembly of Colloidal Particles. *Small* **0**, 1901801 (2019).
164. Vaidya, A. T., Chen, C.-H., Dunlap, J. C., Loros, J. J. & Crane, B. R. Structure of a Light-Activated LOV Protein Dimer That Regulates Transcription. *Sci. Signal.* **4**, ra50–ra50 (2011).
165. Zhou, X. X. *et al.* A Single-Chain Photoswitchable CRISPR-Cas9 Architecture for Light-Inducible Gene Editing and Transcription. *ACS Chem Biol* **13**, 443–448 (2018).
166. Friedl, P. & Zallen, J. A. Dynamics of cell-cell and cell-matrix interactions in morphogenesis, regeneration and cancer. *Curr. Opin. Cell Biol.* **22**, 557–559 (2010).
167. McMillen, P. & Holley, S. A. Integration of cell-cell and cell-ECM adhesion in vertebrate morphogenesis. *Curr. Opin. Cell Biol.* **36**, 48–53 (2015).
168. Yamada, S., Pokutta, S., Drees, F., Weis, W. I. & Nelson, W. J. Deconstructing

References

- the cadherin-catenin-actin complex. *Cell* **123**, 889–901 (2005).
169. Rasoulinejad, S., Mueller, M., Nzigou Mombo, B. & Wegner, S. V. Orthogonal Blue and Red Light Controlled Cell–Cell Adhesions Enable Sorting-out in Multicellular Structures. *ACS Synth. Biol.* (2020)
doi:10.1021/acssynbio.0c00150.
170. Graner & Glazier. Simulation of biological cell sorting using a two-dimensional extended Potts model. *Phys. Rev. Lett.* **69**, 2013–2016 (1992).
171. Glazier, J. A. & Graner, F. Simulation of the differential adhesion driven rearrangement of biological cells. *Phys. Rev. E* **47**, 2128–2154 (1993).
172. Kafer, J., Hogeweg, P. & Maree, A. F. M. Moving forward moving backward: directional sorting of chemotactic cells due to size and adhesion differences. *PLoS Comput. Biol.* **2**, e56 (2006).
173. Buffle, J. & Leppard, G. G. Characterization of Aquatic Colloids and Macromolecules. 1. Structure and Behavior of Colloidal Material. *Environ. Sci. Technol.* **29**, 2169–2175 (1995).
174. Steinberg, M. S. Does differential adhesion govern self-assembly processes in histogenesis? Equilibrium configurations and the emergence of a hierarchy among populations of embryonic cells. *J. Exp. Zool.* **173**, 395–433 (1970).

Curriculum vitae

Samaneh Rasoulinejad

LucyHillebrandstrasse 4, 55128 Mainz,

Email: rasoulinejad@mpip-mainz.mpg.de

Experience & Educations

2017 – 2020	Scientist at Max Planck Institute of Polymer Research <ul style="list-style-type: none">• Responsibility for chemical, biochemical and microscopy laboratories (chemical and technical inventory, cleanness, safety etc.)• Maintenance of laboratory equipment (Confocal Microscopy, PCR, Cell culture, etc.)• Supervision of fellow Ph.D. students and internship students
2017 – 2020	Aimed degree Dr. rer. nat. in biotechnology at Max Planck Institute of Polymer Research under Prof. Katharina Landfester, supervised by Prof. Seraphine Wegner. Subject: "Light Controlled Cell-Cell Adhesions and Self-sorting in Multicellular Structures"
2016 – 2018	Research assistance at Shahed University <ul style="list-style-type: none">• Supervision of Master thesis
2016	Coordinator at South Korea Embassy and South Korean Media Group <ul style="list-style-type: none">• Coordinator of intercultural events• Translator (English to Persian)• Member of organization committee for a Korean theater in Tehran central hall
2013 – 2016	Lecturer at Shahed University <ul style="list-style-type: none">• Molecular & Cellular Biology for bachelor students Research assistance at Shahed University <ul style="list-style-type: none">• Developing clinical diagnostics (Microbial) M.Sc. in Microbial Biotechnology (Grade 1.7) Thesis: "Aptamer-nanobody based ELASA for specific detection of Acinetobacter baumannii isolates" (Grade 1.0) <ul style="list-style-type: none">• Modules included: biotechnology (biology molecular assays) and biochemistry
2009 - 2013	B.Sc. Biotechnology (Grade 1.7) <ul style="list-style-type: none">• Ranked 1st in "Cumulative GPA" among all molecular biology B.Sc. students

Achievements

Workshops	<ul style="list-style-type: none">• Scientific presentation workshop, Max-Planck-Institute for Polymer Research, Mainz, 2019• Quality assurance system with a focus on GMP given by Dr.Norbet Egger, Max-Planck-Institute for Polymer Research, Mainz, 2018
------------------	--

Publication

- **Samaneh Rasoulinejad**, Seraphine Wegner. The dynamic differential adhesion hypothesis: The role of cell-cell adhesion dynamics in cell sorting. **2020**.
- Brice Nzigou, Bijonowski, B.t M., **Samaneh Rasoulinejad**, Mark Mueller, Seraphine Wegner. Spatiotemporal control over multicellular migration using green light reversible cell-cell interactions. Submitted **2020**.
- **Samaneh Rasoulinejad**, Zahra Nosaz, Seyed Latif MousaviGargari. Characterization of ssDNA aptamer for detection of predominant Brucella. **J VET RES. 2020**.
- **Samaneh Rasoulinejad**, Marc Mueller, Brice Nzigou, Seraphine Wegner. Orthogonal Blue and Red Light Controlled Cell-Cell Adhesions enable Sorting-out in Multicellular Structures. **ACS Synth. Biol. 2020**; 9, 2076–2086.
- Marc Mueller, **Samaneh Rasoulinejad**, Sukant GargSukant Garg and Seraphine V. Wegner. The Importance of Cell–Cell Interaction Dynamics in Bottom-Up Tissue Engineering: Concepts of Colloidal Self-Assembly in the Fabrication of Multicellular Architectures. **Nano Lett. 2020**; 20, 2257–2263.
- **Samaneh Rasoulineja***, **Simge Yüz***, **Marc Mueller**, **Seraphine Wegner**. Blue Light Switchable Cell–Cell Interactions Provide Reversible and Spatiotemporal Control Towards Bottom-Up Tissue Engineering. **Adv. Biosyst. 2019**; 3, 1800310.
- Dongdong Xu, Solveig M. Bartelt, **Samaneh Rasoulinejad**, Fei Chena and Seraphine V. Wegner. Green light lithography: a general strategy to create active protein and cell micropatterns. **Mater. Horizons 2019**; 6, 1222–1229.
- Kimia Mirzakhani, Seyed Latif Mousavi Gargari, Iraj Rasooli, **Samaneh Rasoulinejad**. Development of a DNA Aptamer for Screening Neisseria meningitidis Serogroup B by Cell SELEX. **Iran Biomed J 2017**; 24;22(3):193-201.
- Hanif Alfavian, Seyed Latif Mousavi Gargari, **Samaneh Rasoulinejad**, Arvin Medhat. Development of a DNA aptamer that binds specifically to group A Streptococcus serotype M3. **Can J Microbiol 2017**;63(2):160-168.
- Faezeh Almasi, Seyed Latif Mousavi Gargari, Fatemeh Bitaraf, **Samaneh Rasoulinejad**. Development of a Single Stranded DNA Aptamer as a Molecular Probe for LNCap Cells Using Cell-SELEX. **Avicenna J Med Biotechnol, 2016**;8(3):104-11.
- **Samaneh Rasoulinejad**, Seyed Latif Mousavi Gargari. Aptamer-nanobody based ELASA for specific detection of Acinetobacter baumannii isolates. **J Biotechnol 2016**;10; 231:46-54.

Skills

Language

- Persian
- English
- German
- Korean

Curriculum vitae

Computer

- **MS Office**
- **Origin, Prism**
- **Photoshop, InDesign, Image J**

Mainz, 2020